Synthesis and biological activity of squaramido-tethered bisbenzimidazoles as synthetic anion transporters

Zhong-Kun Wang [a], Xiao-Qiao Hong [b], Jinhui Hu [a], Yuan-Yuan Xing [a] and Wen-Hua Chen*[,a,c]

[a] *School of Biotechnology and Health Sciences, Wuyi University, Jiangmen 529020, P. R. China*

[b] *School of Pharmaceutical Sciences, Tsinghua University, Haidian District, Beijing 100084, P. R. China*

[c] *State Key Laboratory of Chemical Oncogenomics, Key Laboratory of Chemical Genomics, Peking University Shenzhen Graduate School, Shenzhen 518055, P. R. China*

Supporting Information

Experimental procedures

Preparation of EYPC vesicles

Vesicles for chloride efflux were prepared completely according to the reported protocols, [1] except that they were formed in 25 mM HEPES buffer (500 mM NaCl, pH 7.0), whereas the external solution was 25 mM HEPES buffer (500 mM $NaNO_3$, pH 7.0).

Vesicles for calcein leakage experiments were prepared in a similar fashion, except that they were formed in a 100 mM calcein solution in 25 mM HEPES buffer (500 mM NaCl, pH 7.0); and 25 mM HEPES buffer (500 mM NaCl, pH 7.0) was used to elute the Sephadex G-25 column to remove the non-entrapped calcein.

Measurement of anionophoric activity

Literature protocols described by us [2-4] and others [5-7] were used to conduct the chloride efflux, cation and anion selective transport, and calcein leakage experiments of each compound.

^{1}H NMR titrations [8]

^{1}H NMR titrations were performed by keeping the concentrations of each compound constant, while gradually increasing the concentration of TBACl. Typically, to a solution of each compound (1 mM) in 4:1 CD_3CN-DMSO-d_6 were added aliquots of each compound (1 mM) and TBACl (4-50 mM) in the same solvent. The association constants (K_a's) were derived from nonlinear least-square fit of the experimental data according to a 1 : 1 binding model, $\delta = \delta_0+((\delta_\infty-\delta_0)/2[C]_0)\{([N]_0+[C]_0+1/K_a)-(([N]_0+[C]_0+1/K_a)^2-4[N]_0[C]_0)^{1/2}\}$, wherein $[N]_0$ and $[C]_0$ are the initial analytical concentrations of TBACl and each compound, respectively; δ and δ_0 represent the chemical shifts of the sample and compound alone, respectively, and δ_∞ is the chemical shift when compound is totally bound.

MTT-based cytotoxicity assay [2,7]

The cytotoxicity was measured in standard DMEM/high glucose media. Specifically, cells were dispersed in a 96-well flat bottom tissue culture treated plates (Corning) at density of 3000 cells/well (per 100 μL) and incubated at 37 ^{o}C in a 5% CO_2 incubator for 24 h. Then, they were treated for 48 h with each compound (50 μM). A solution of MTT (Amresco) in

PBS buffer (5 mg MTT/mL) was added to each well and incubation continued for an additional 4 h. Then, the MTT solution was removed and DMSO (100 μL) was added in each well to dissolve the formed formazan crystals. The absorbance at 570 nm was recorded in a microplate reader (Tecan Infinite M1000 PRO). For each condition, at least three independent experiments were performed and the mean value was taken. DMSO (1%) was used as a control. Cell viability was expressed as a percentage of control cells, and the data are reported as the mean value ± S.D. The concentration of each compound resulting in 50% inhibition in cell growth (IC_{50} value) was calculated from the dose-cell viability curves, by using GraphPad Prism v8.0 software.

References

1. W.-H. Chen and S. L. Regen, *J. Am. Chem. Soc.*, **2005**, *127*, 6538-6539.
2. X.-H. Yu, C.-C. Peng, X.-X. Sun and W.-H. Chen, *Eur. J. Med. Chem.*, **2018**, *152*, 115-125.
3. Z. Li, X.-H. Yu, Y. Chen, D.-Q. Yuan and W.-H. Chen, *J. Org. Chem.*, **2017**, *82*, 13368-13375.
4. C.-C. Peng, M.-J. Zhang, X.-X. Sun, X.-J. Cai, Y. Chen and W.-H. Chen, *Org. Biomol. Chem.*, **2016**, *14*, 8232-8236.
5. N. Busschaert, S. H. Park, K. H. Baek, Y. P. Choi, J. Park, E. N. W. Howe, J. R. Hiscock, L. E. Karagiannidis, I. Marques, V. Felix, W. Namkung, J. L. Sessler, P. A. Gale and I. Shin, *Nat. Chem.*, **2017**, *9*, 667-675.
6. W. Van Rossom, D. J. Asby, A. Tavassoli and P. A. Gale, *Org. Biomol. Chem.*, **2016**, *14*, 2645-2650.
7. T. Saha, M. S. Hossain, D. Saha, M. Lahiri and P. Talukdar, *J. Am. Chem. Soc.*, **2016**, *138*, 7558-7567.
8. X. Bao, X. Wu, S. N. Berry, E. N. W. Howe, Y. T. Chang and P. A. Gale, *Chem. Commun.*, **2018**, *54*, 1363-1366.

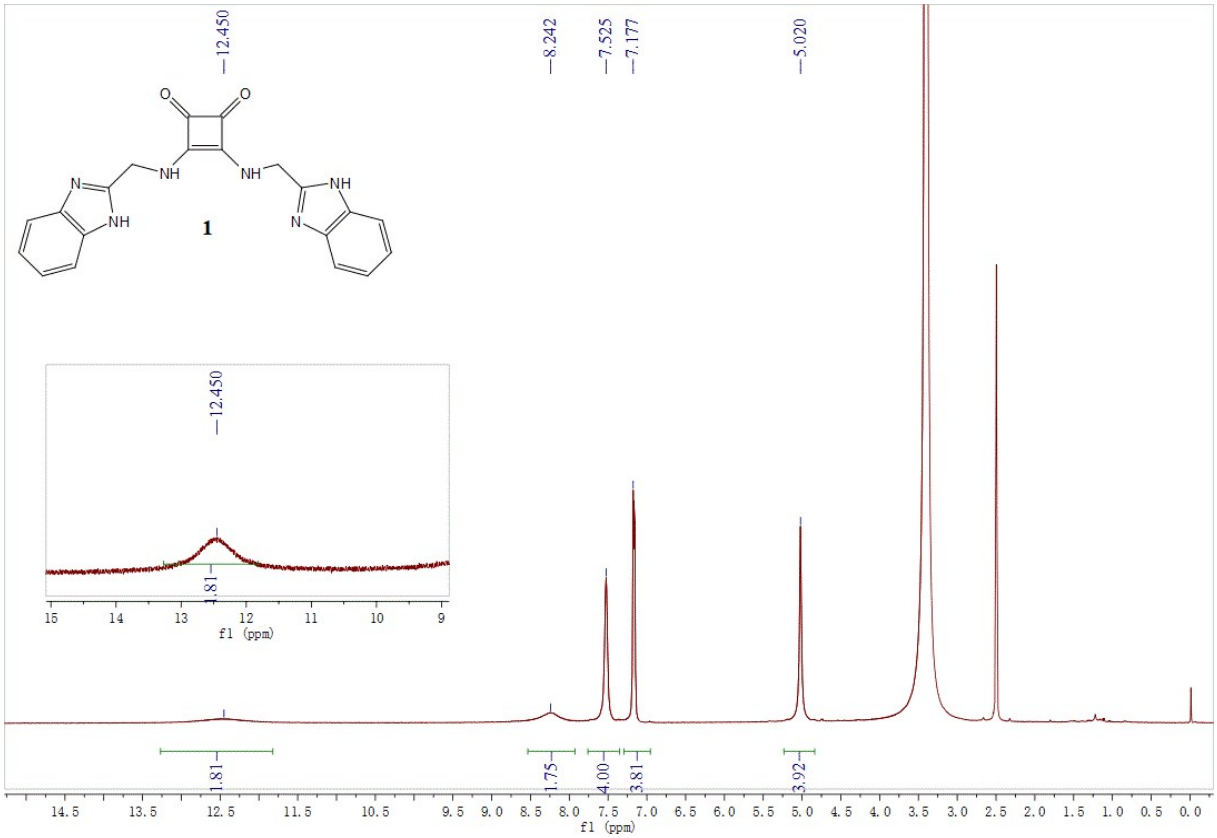

Fig. S1. ^{1}H NMR (DMSO-d_6, 400 MHz) of compound **1**.

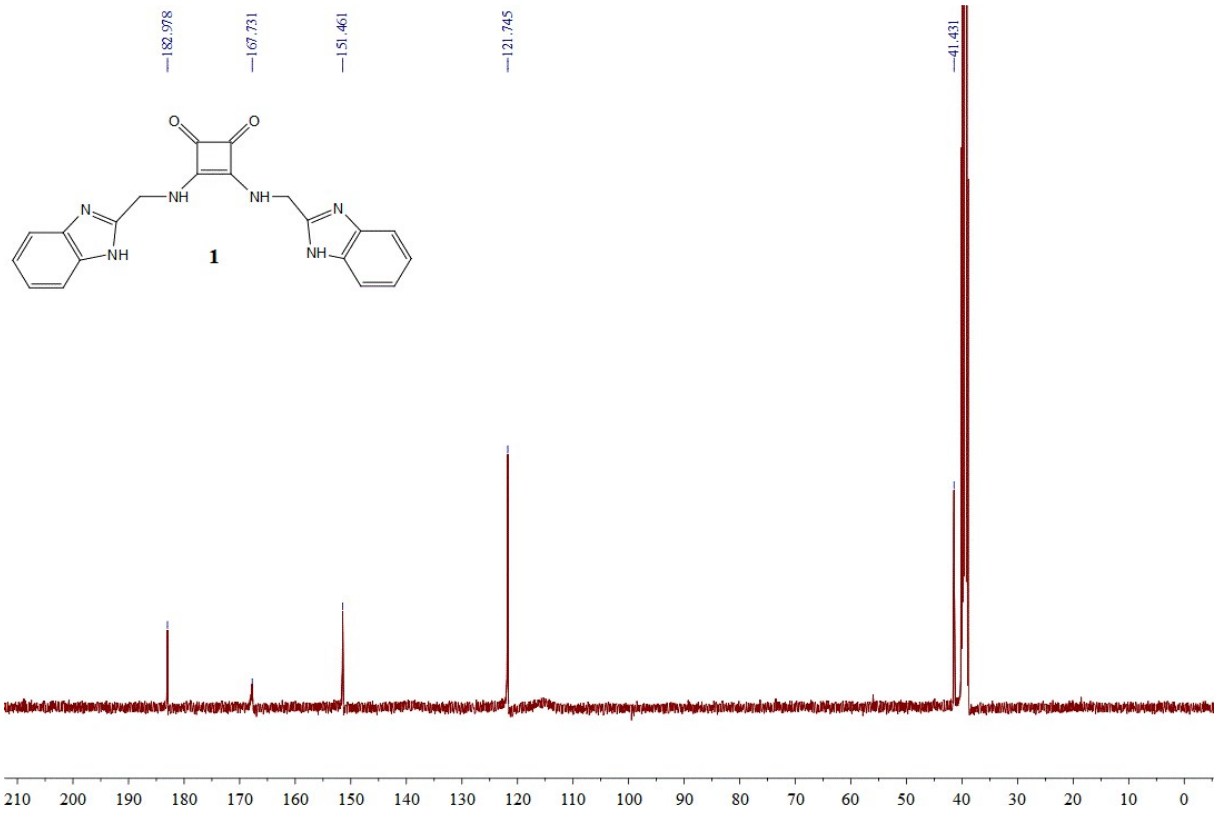

Fig. S2. ^{13}C NMR (DMSO-d_6, 125 MHz) of compound **1**.

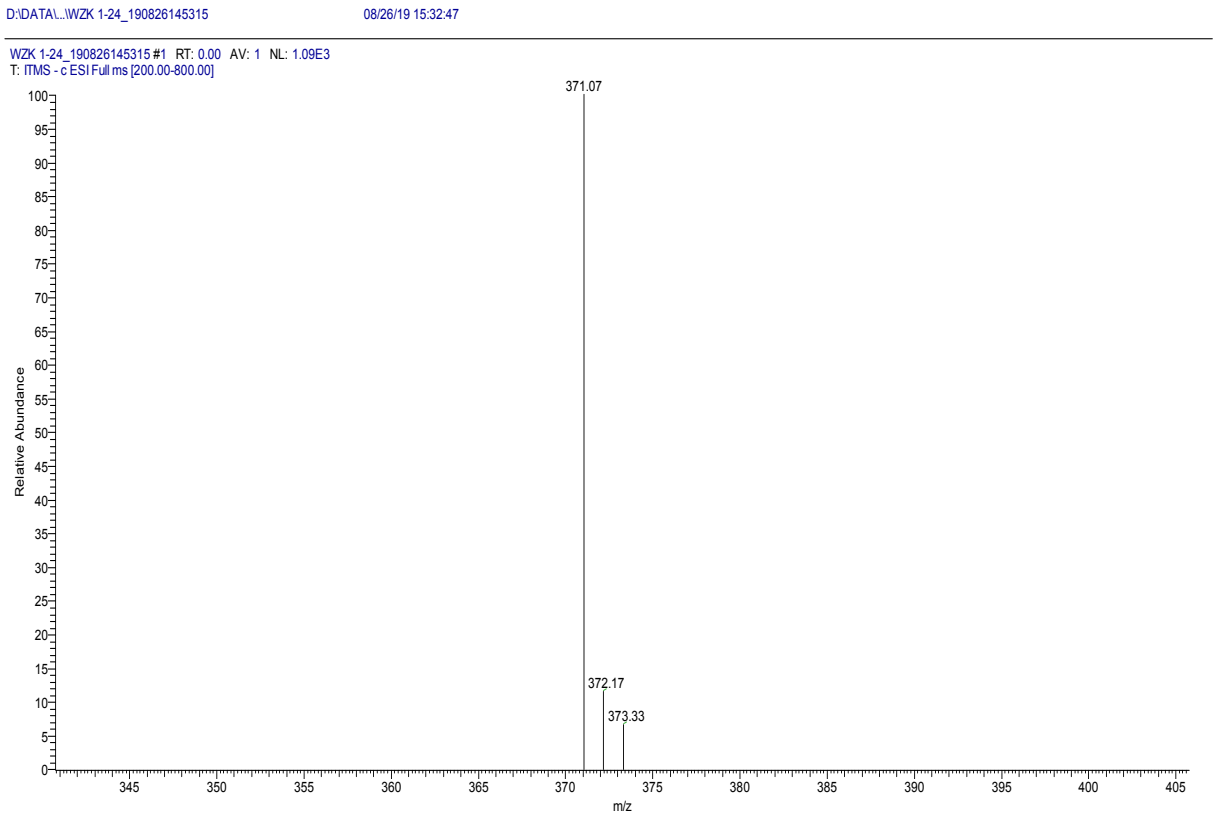

Fig. S3. Negative ESI-MS of compound **1**.

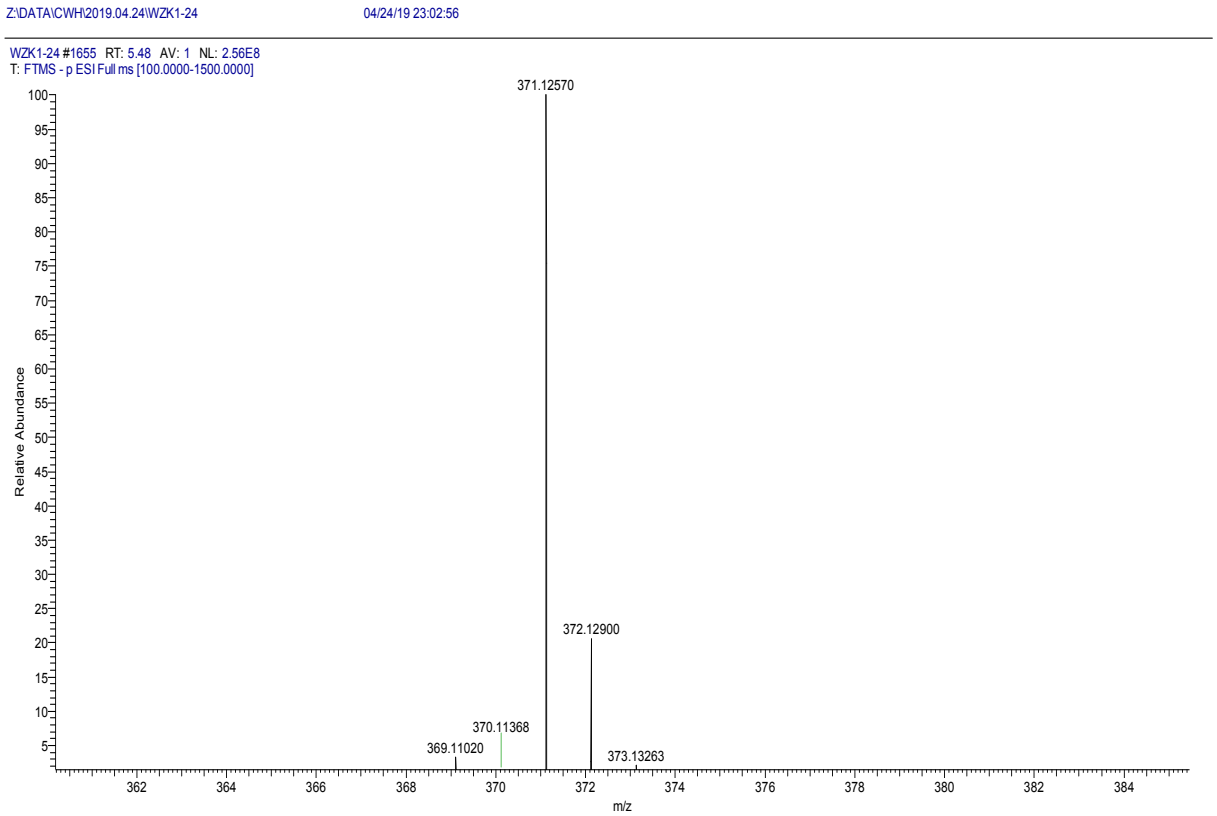

Fig. S4. Negative HR-ESI-MS of compound **1**.

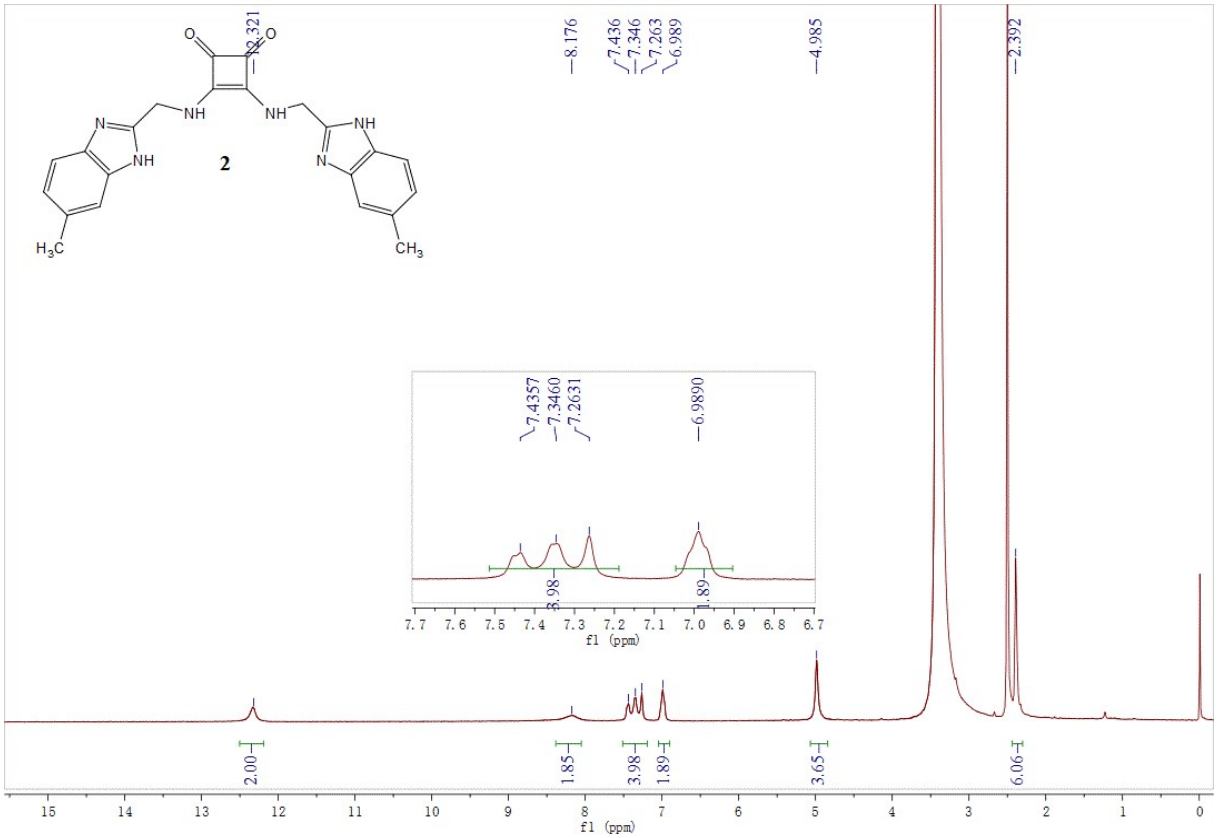

Fig. **S5.** [1]H NMR (DMSO-d_6, 400 MHz) of compound **2**.

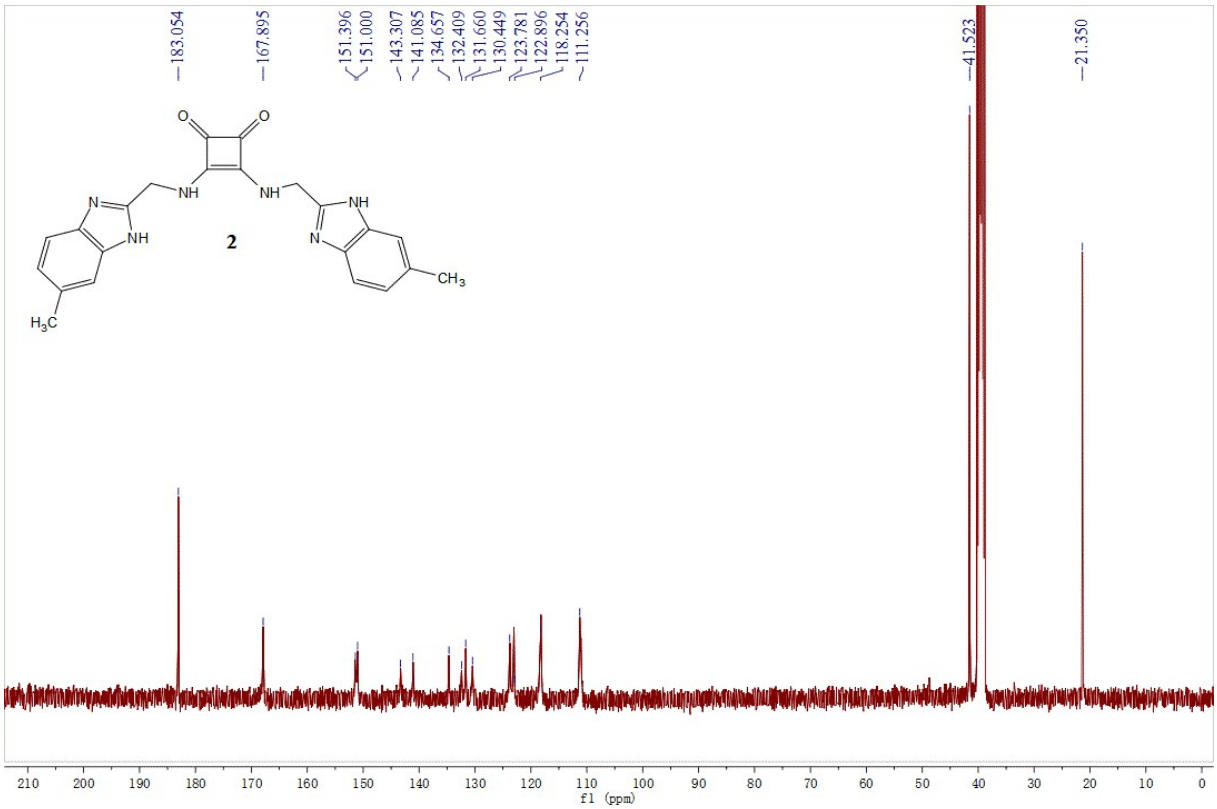

Fig. **S6**. [13]C NMR (DMSO-d_6, 100 MHz) of compound **2**.

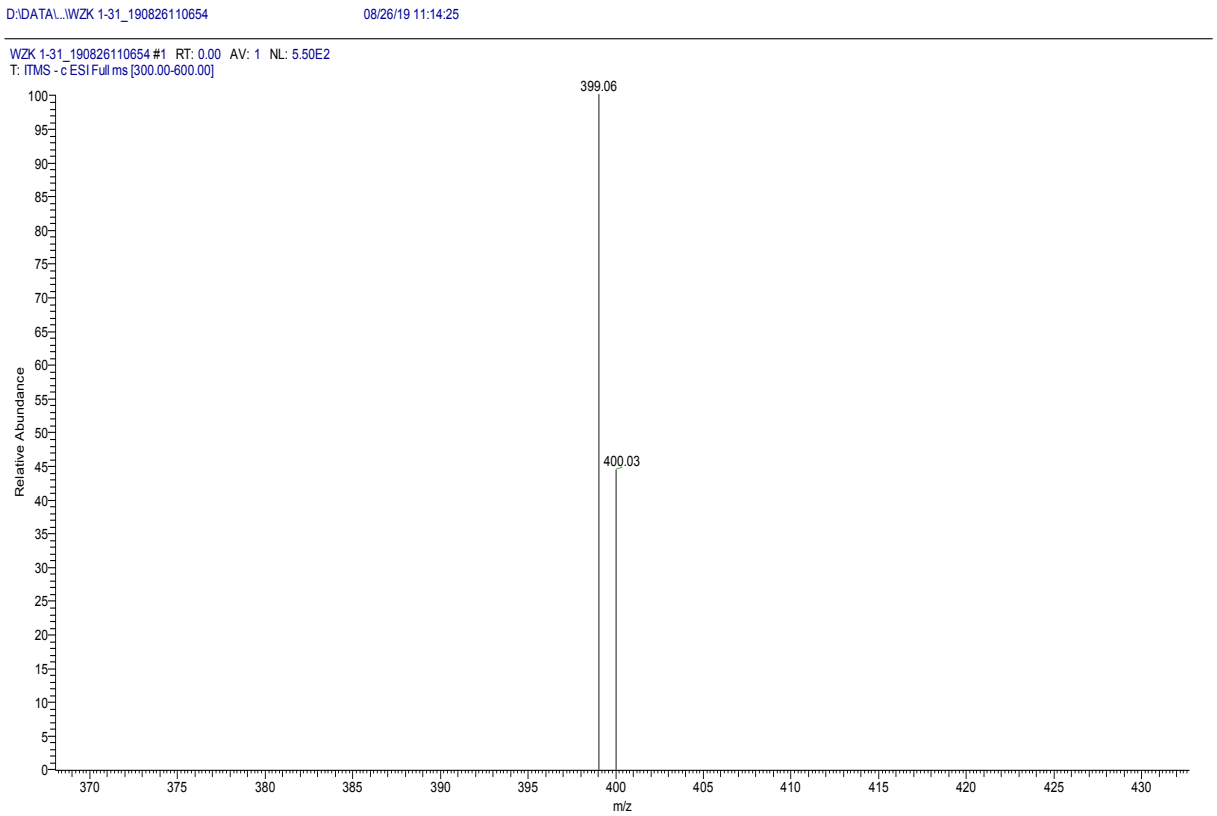

Fig. S7. Negative ESI-MS of compound **2**.

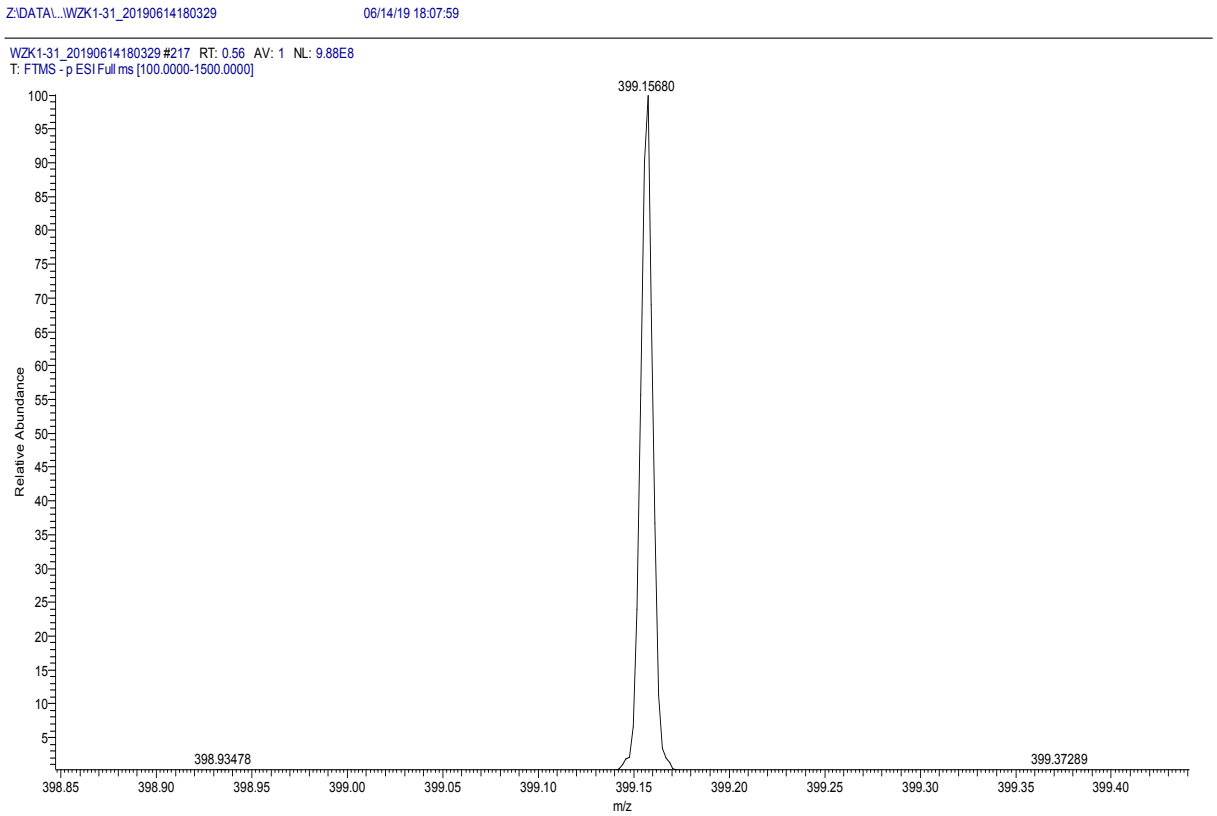

Fig. **S8**. Negative HR-ESI-MS of compound **2**.

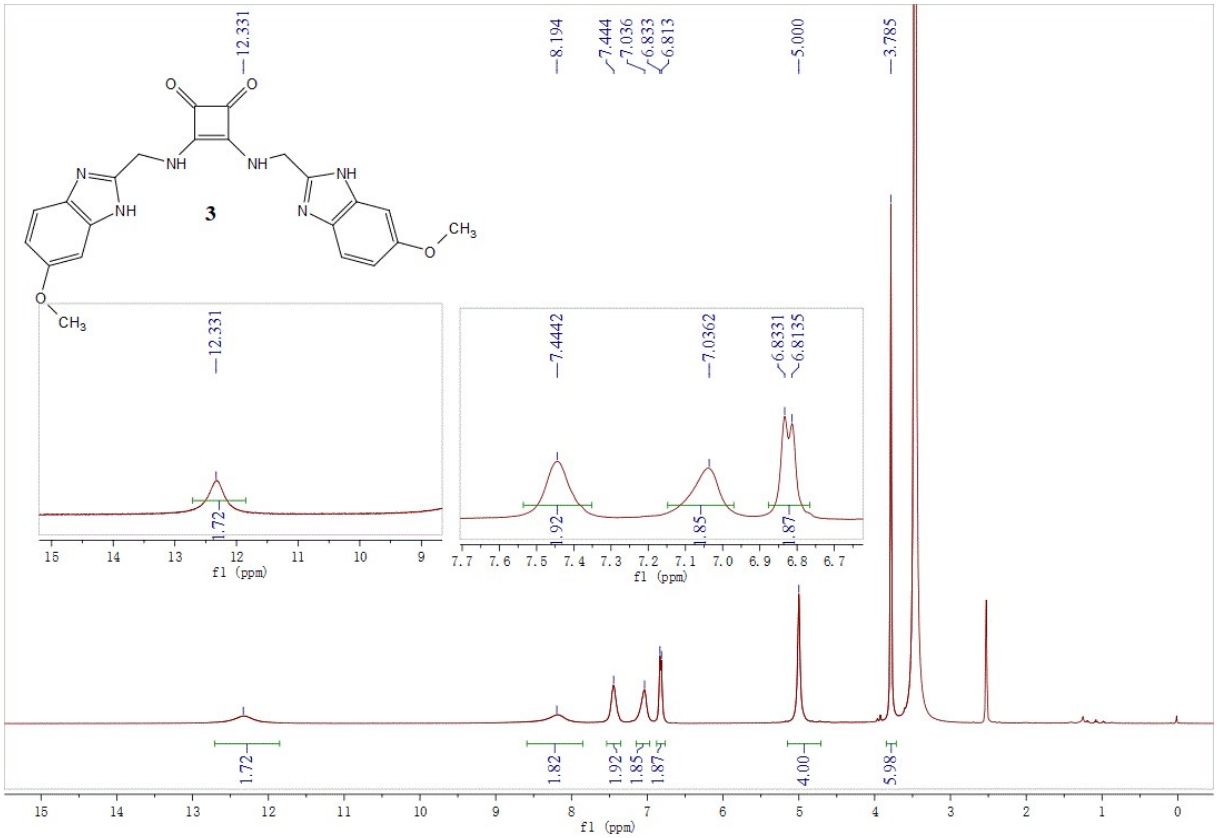

Fig. S9. ^{1}H NMR (DMSO-d_6, 400 MHz) of compound **3**.

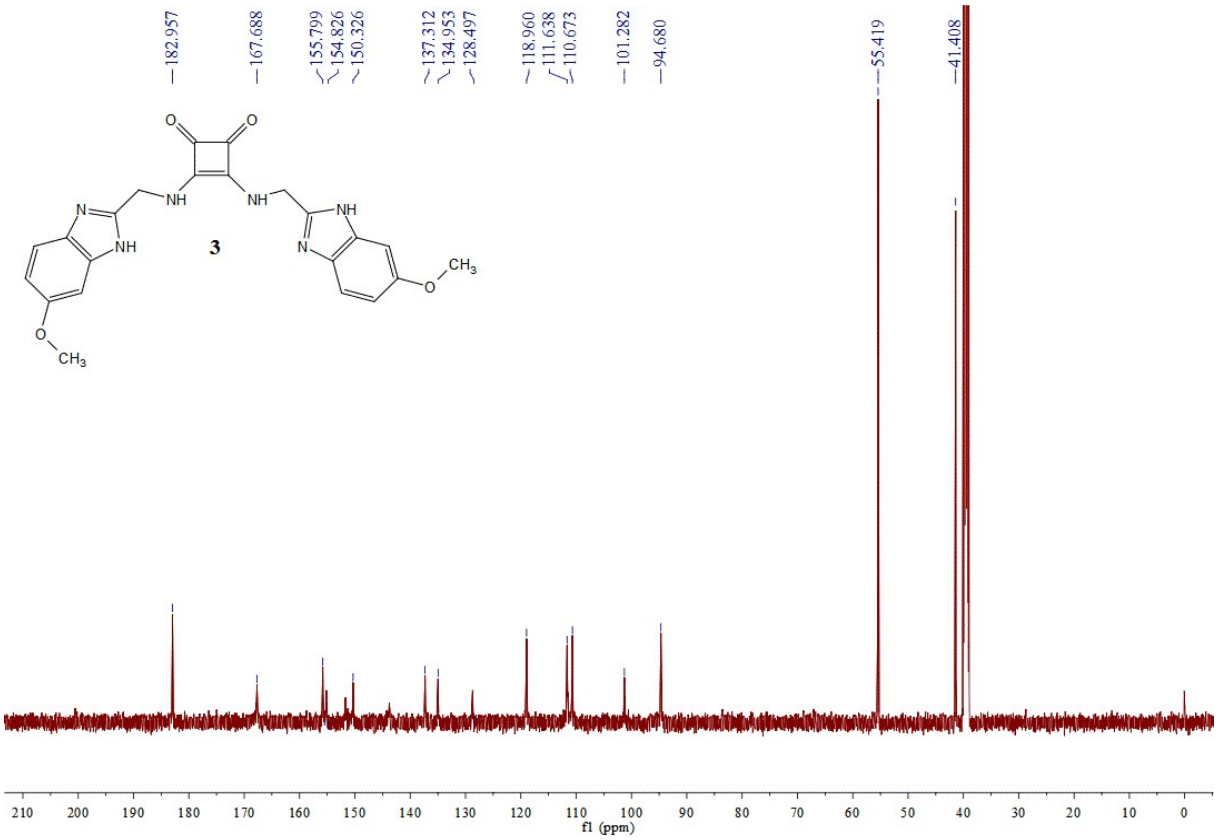

Fig. S10. ^{13}C NMR (DMSO-d_6, 125 MHz) of compound **3**.

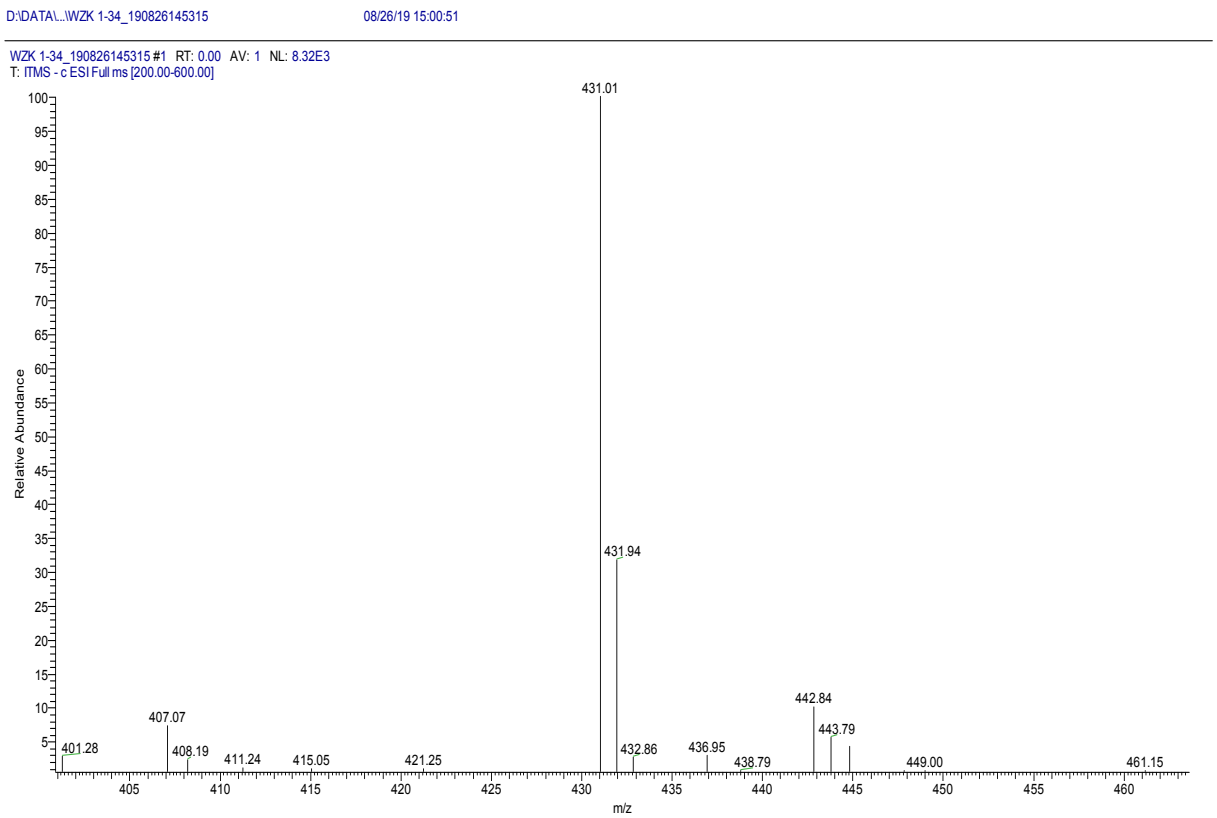

Fig. S11. Negative ESI-MS of compound **3**.

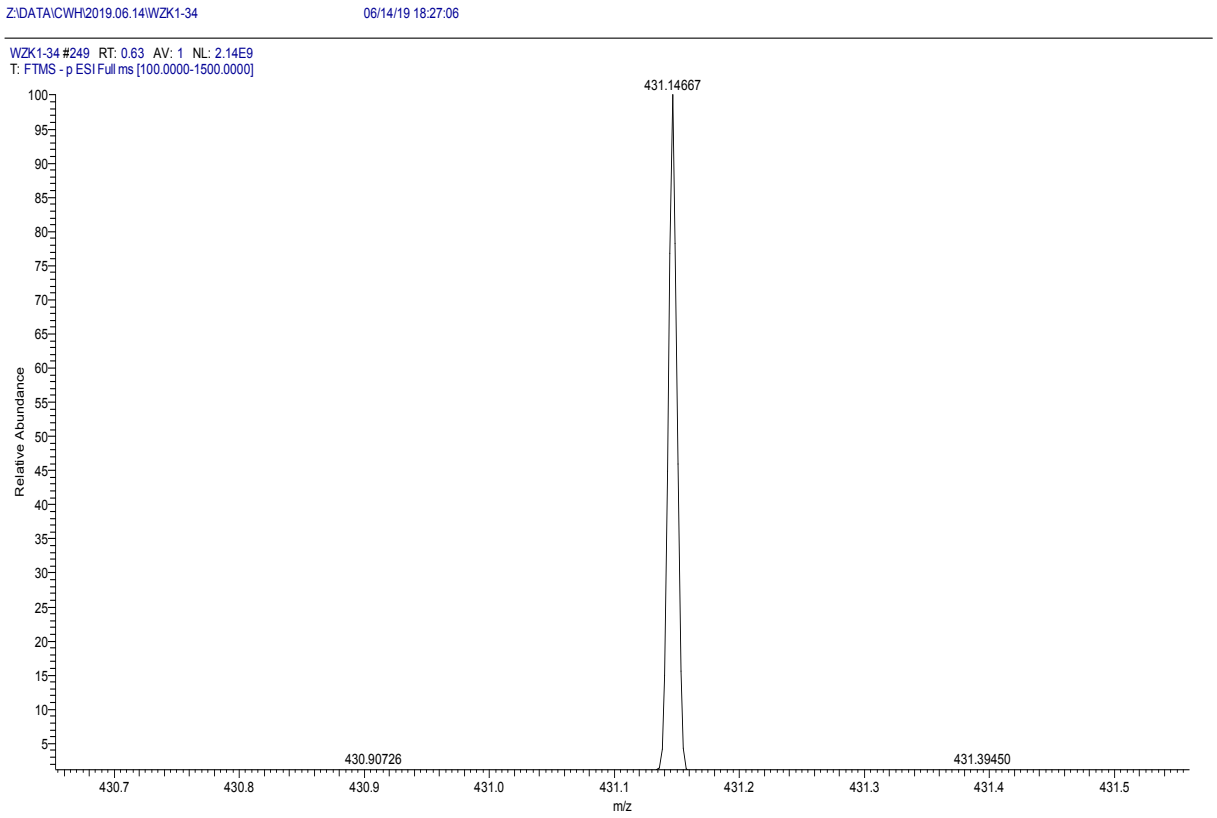

Fig. S12. Negative HR-ESI-MS of compound **3**.

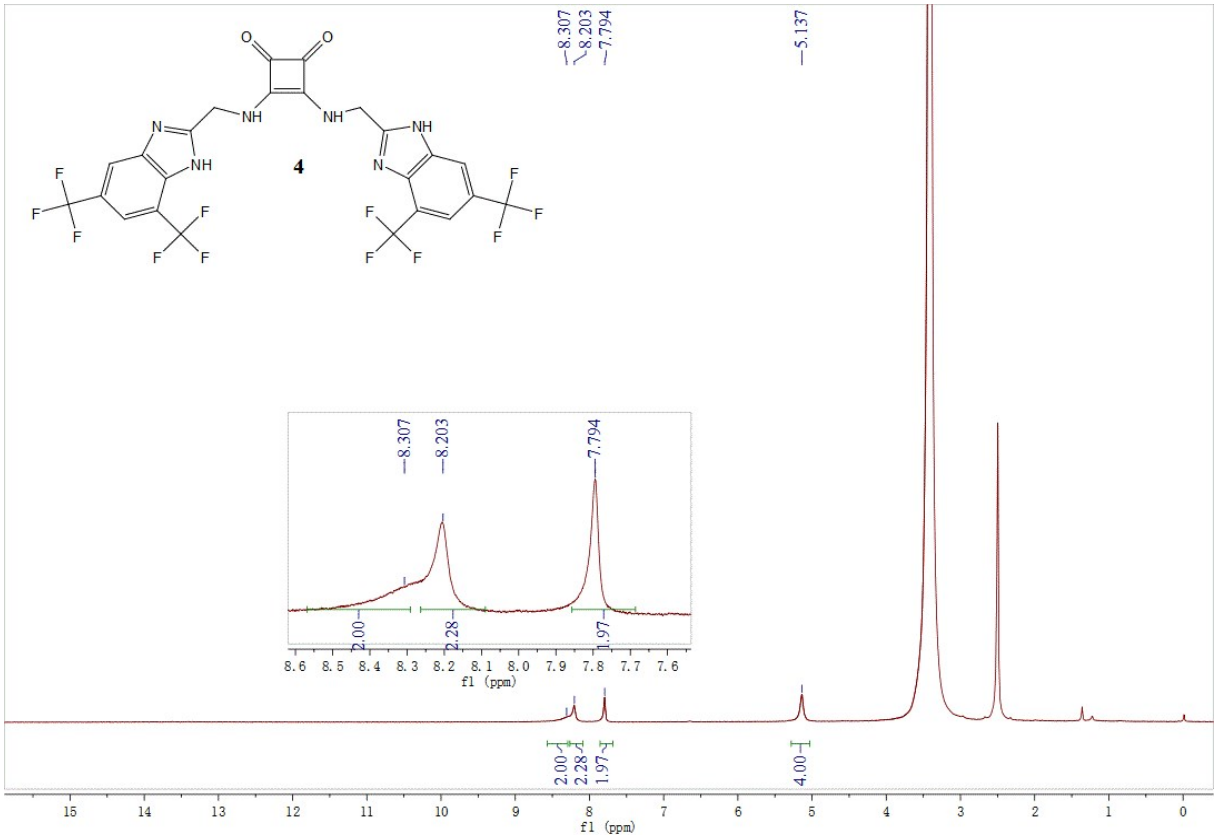

Fig. S13. ^{1}H NMR (DMSO-d_6, 400 MHz) of compound **4**.

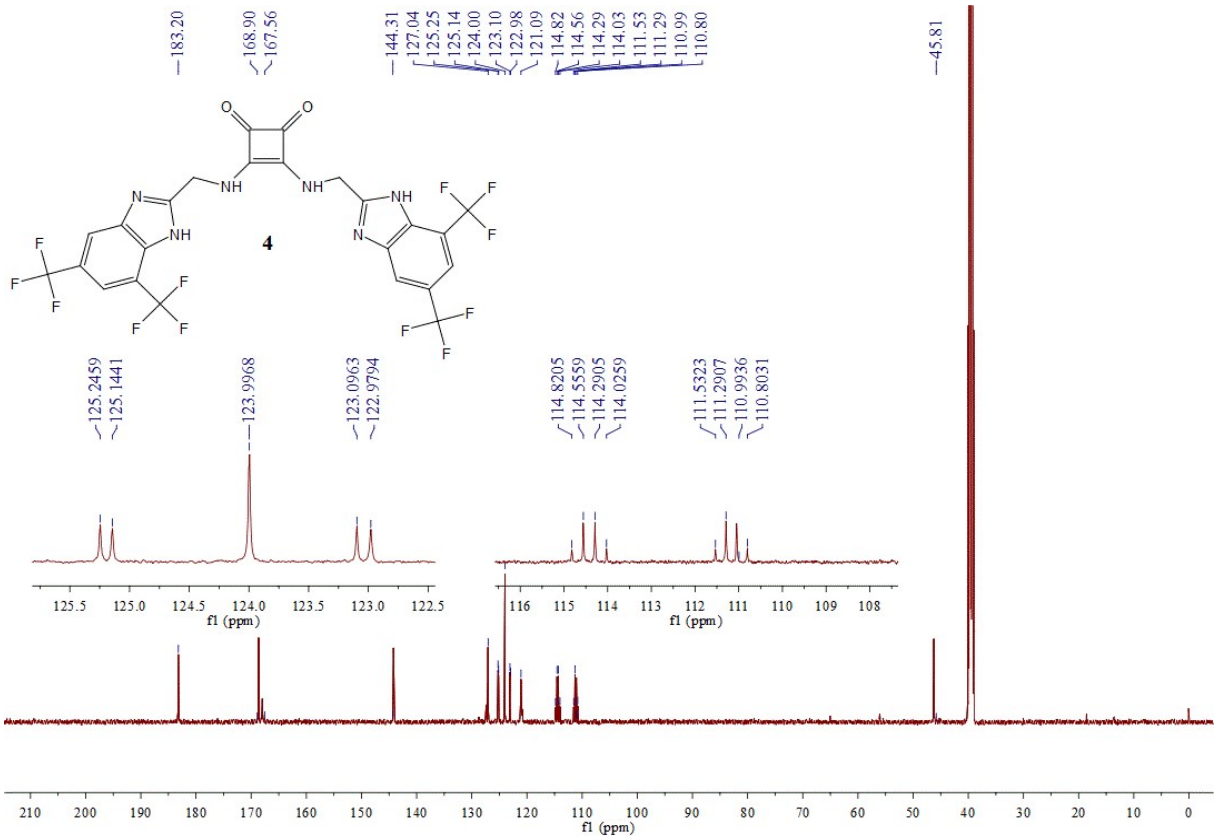

Fig. S14. ^{13}C NMR (DMSO-d_6, 125 MHz) of compound **4**.

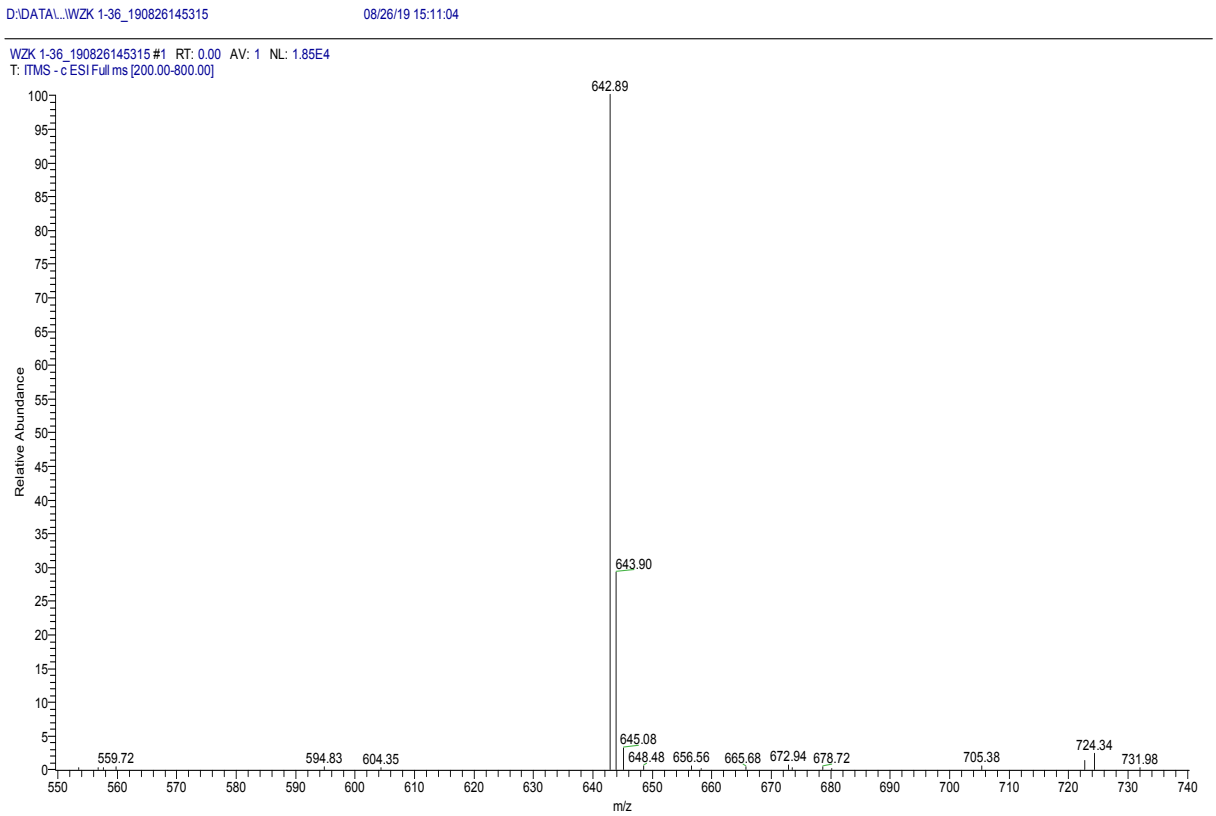

Fig. S15. Negative ESI-MS of compound **4**.

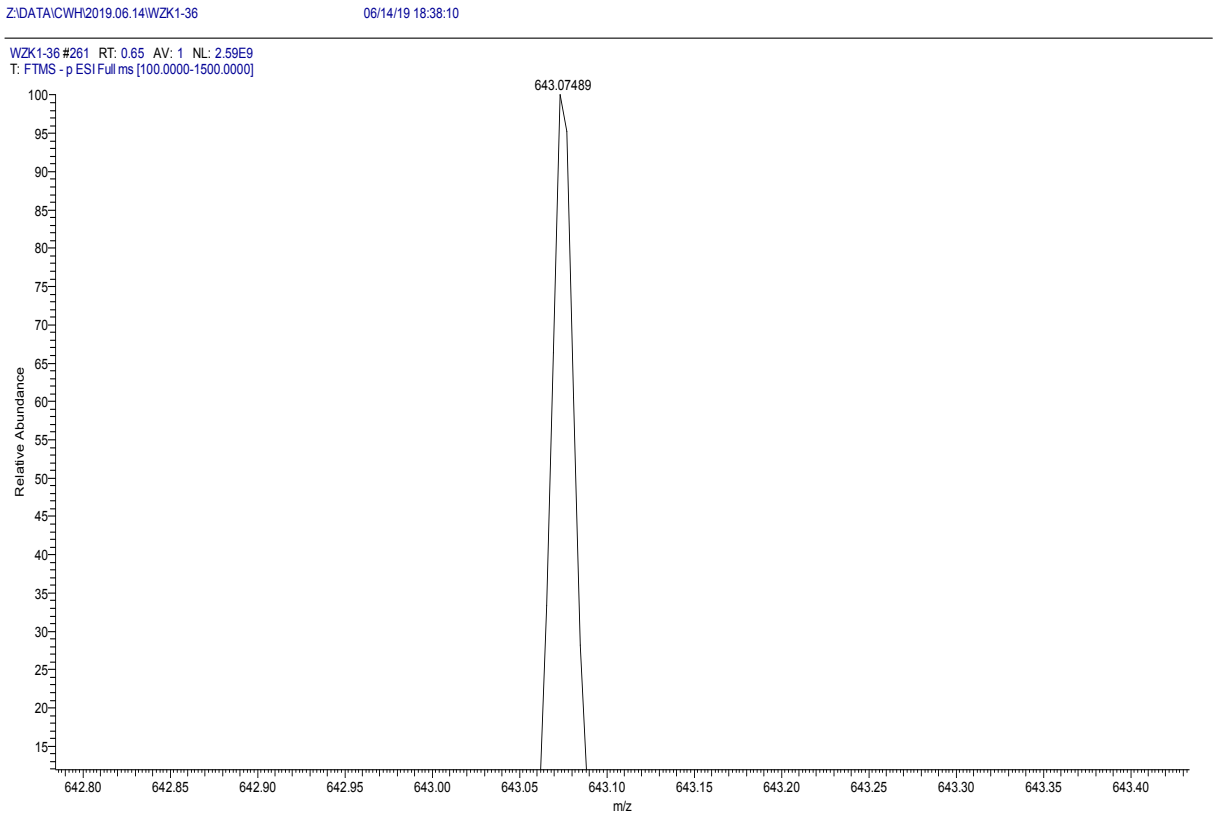

Fig. S16. Negative HR-ESI-MS of compound **4**.

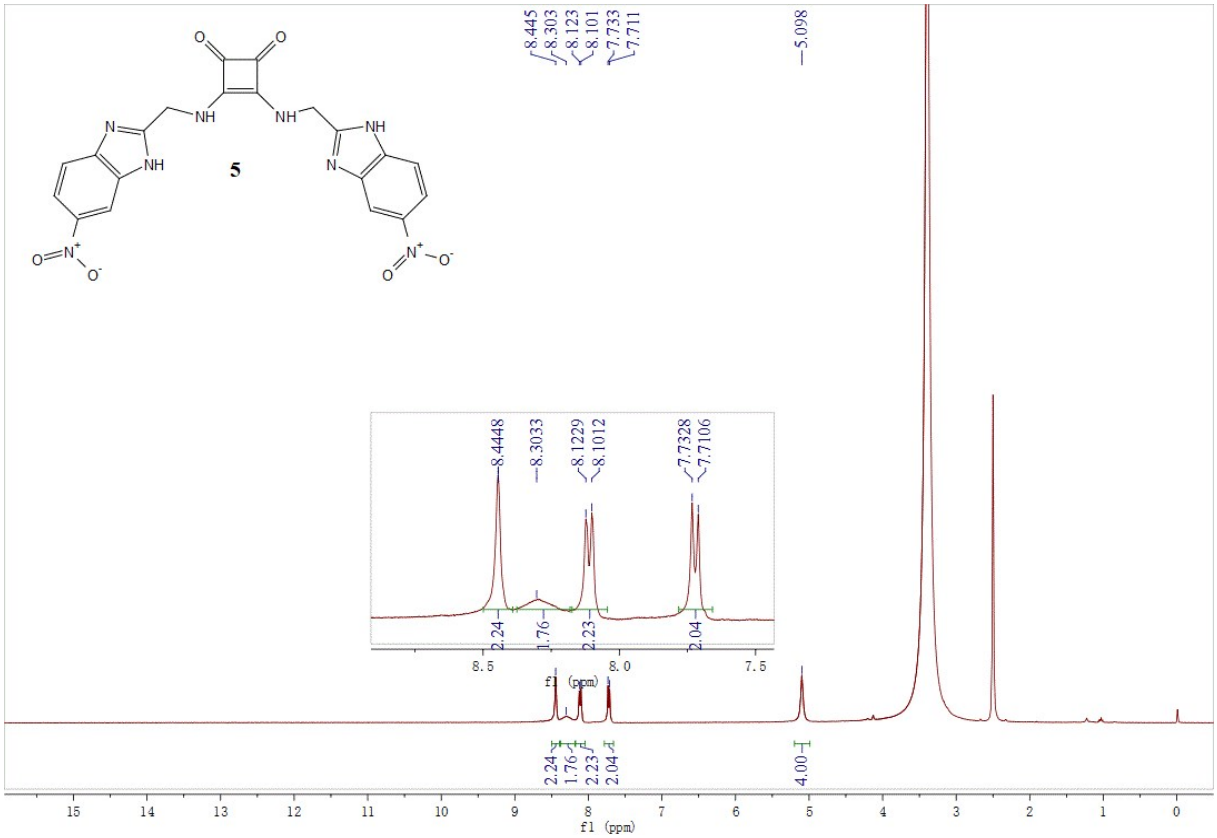

Fig. S17. ^{1}H NMR (DMSO-d_6, 400 MHz) of compound **5**.

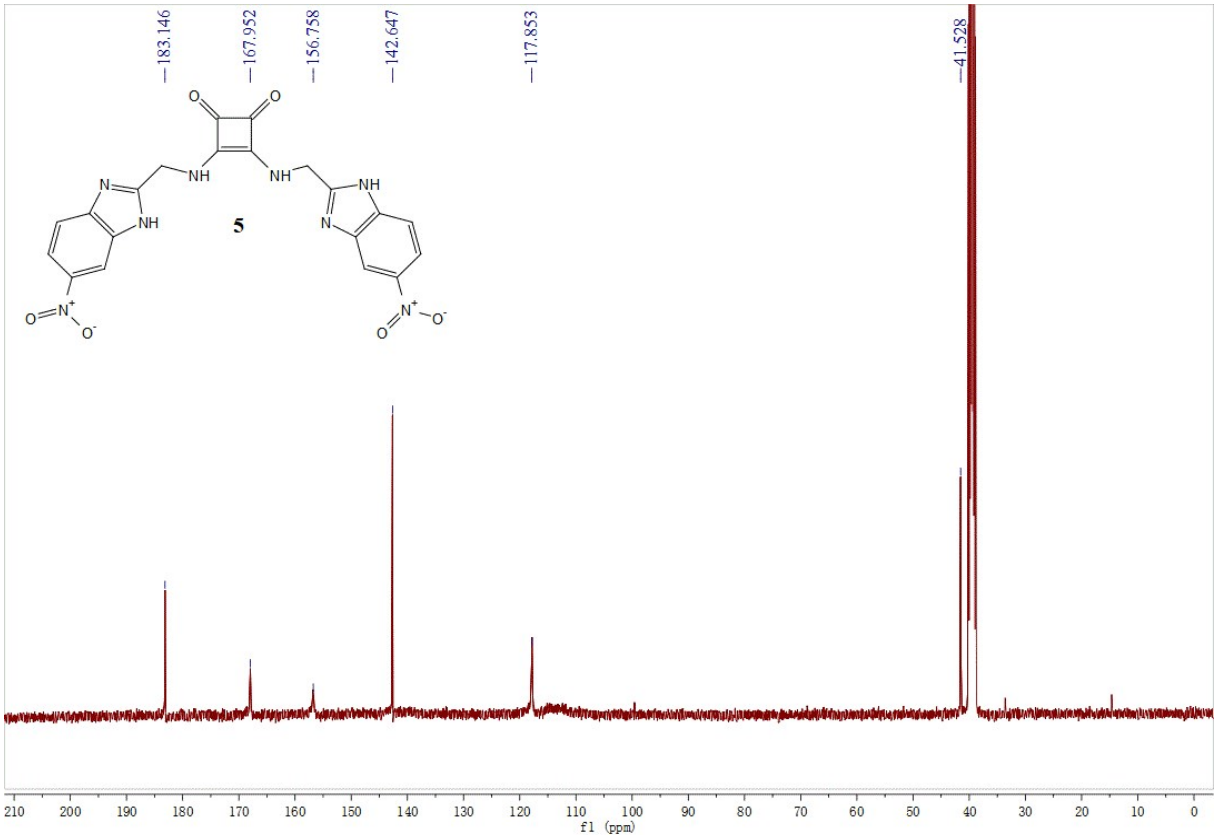

Fig. S18. ^{13}C NMR (DMSO-d_6, 125 MHz) of compound **5**.

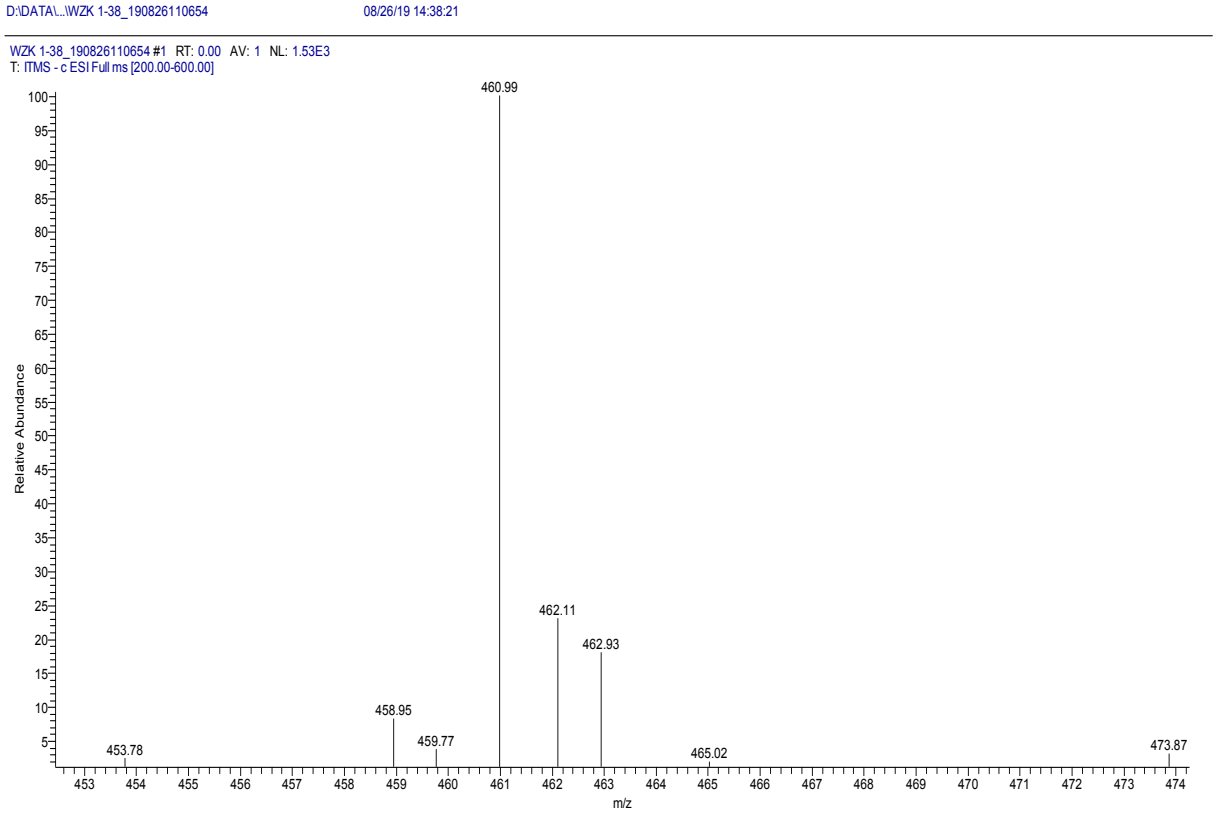

Fig. S19. Negative ESI-MS of compound **5**.

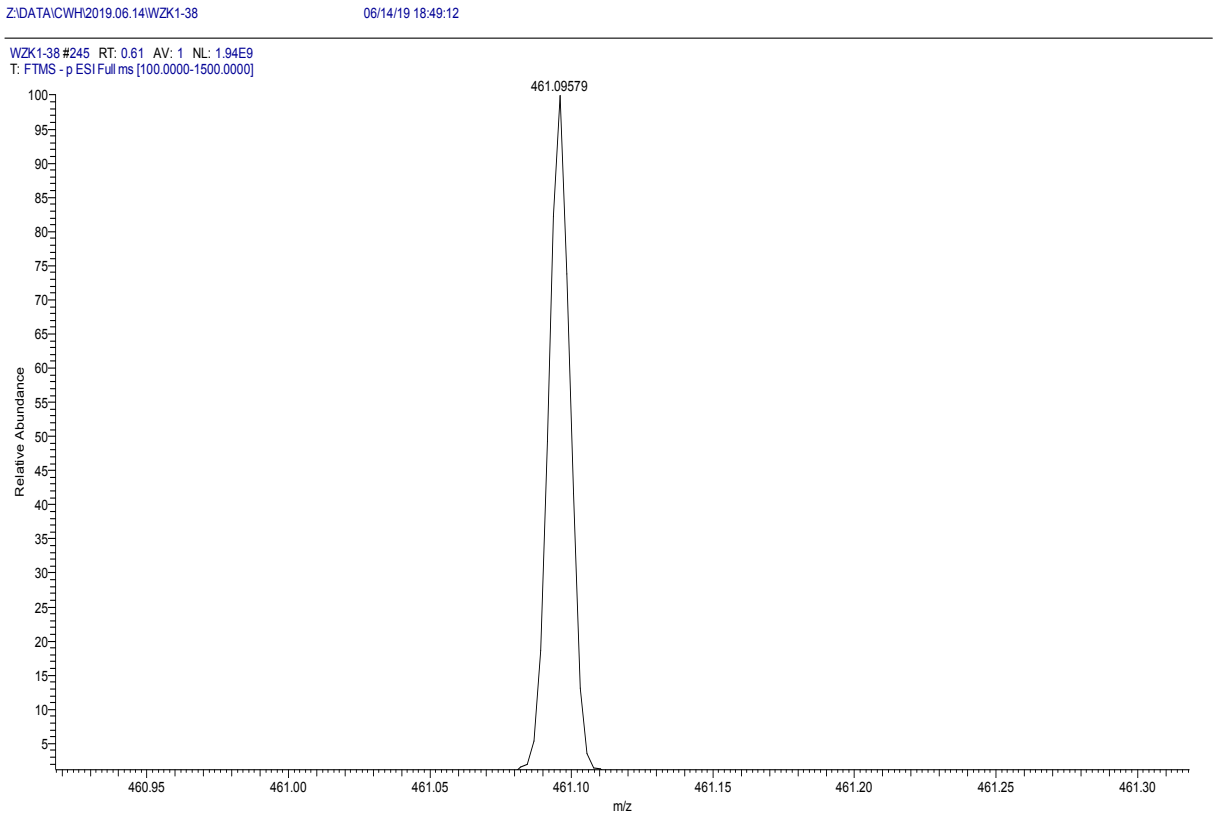

Fig. S20. Negative HR-ESI-MS of compound **5**.

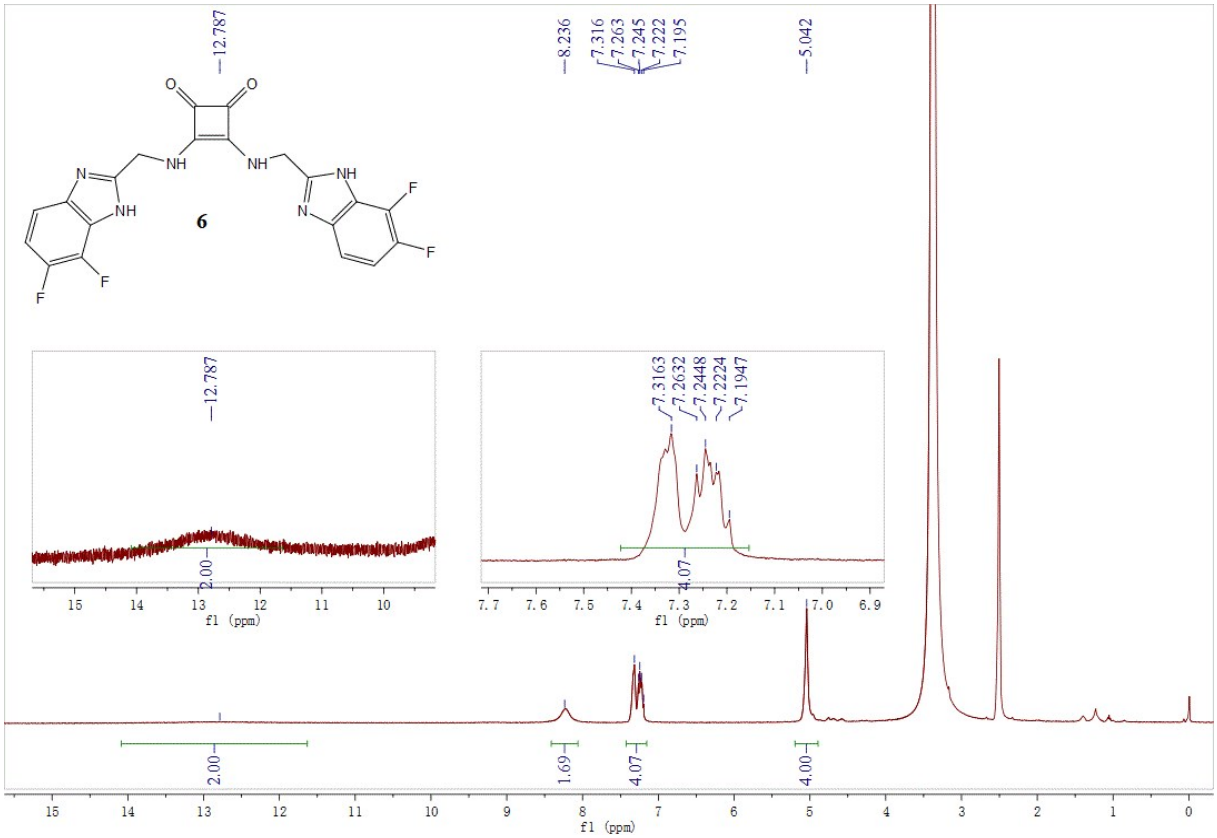

Fig. S21. ^{1}H NMR (DMSO-d_6, 400 MHz) of compound **6**.

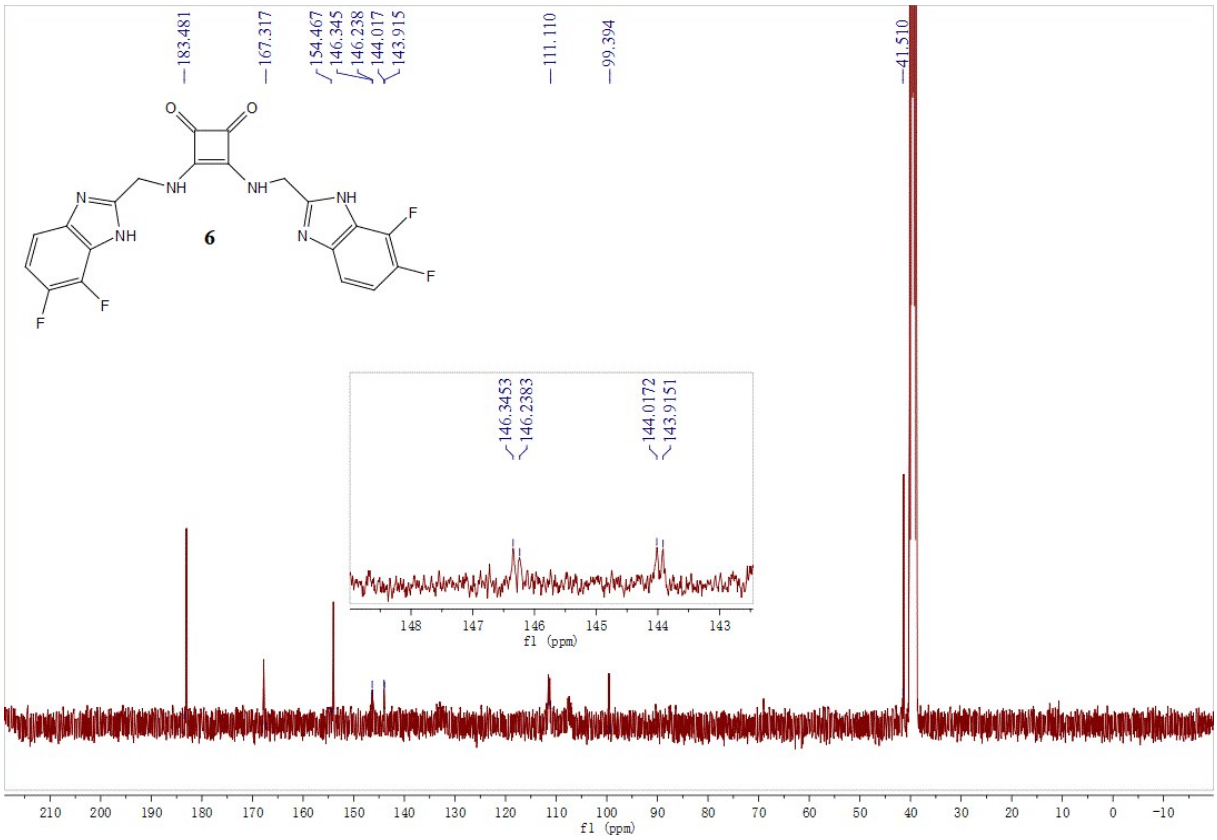

Fig. S22. ^{13}C NMR (DMSO-d_6, 100 MHz) of compound **6**.

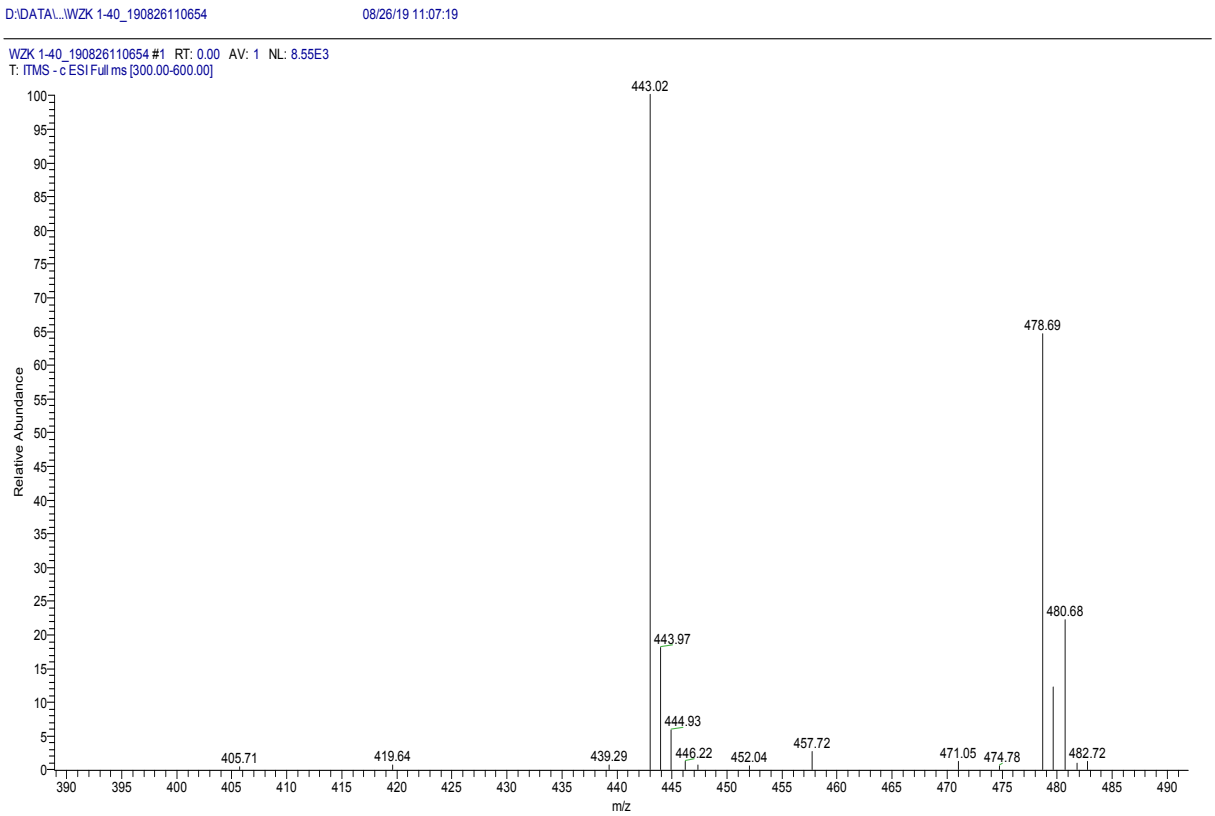

Fig. S23. Negative ESI-MS of compound **6**.

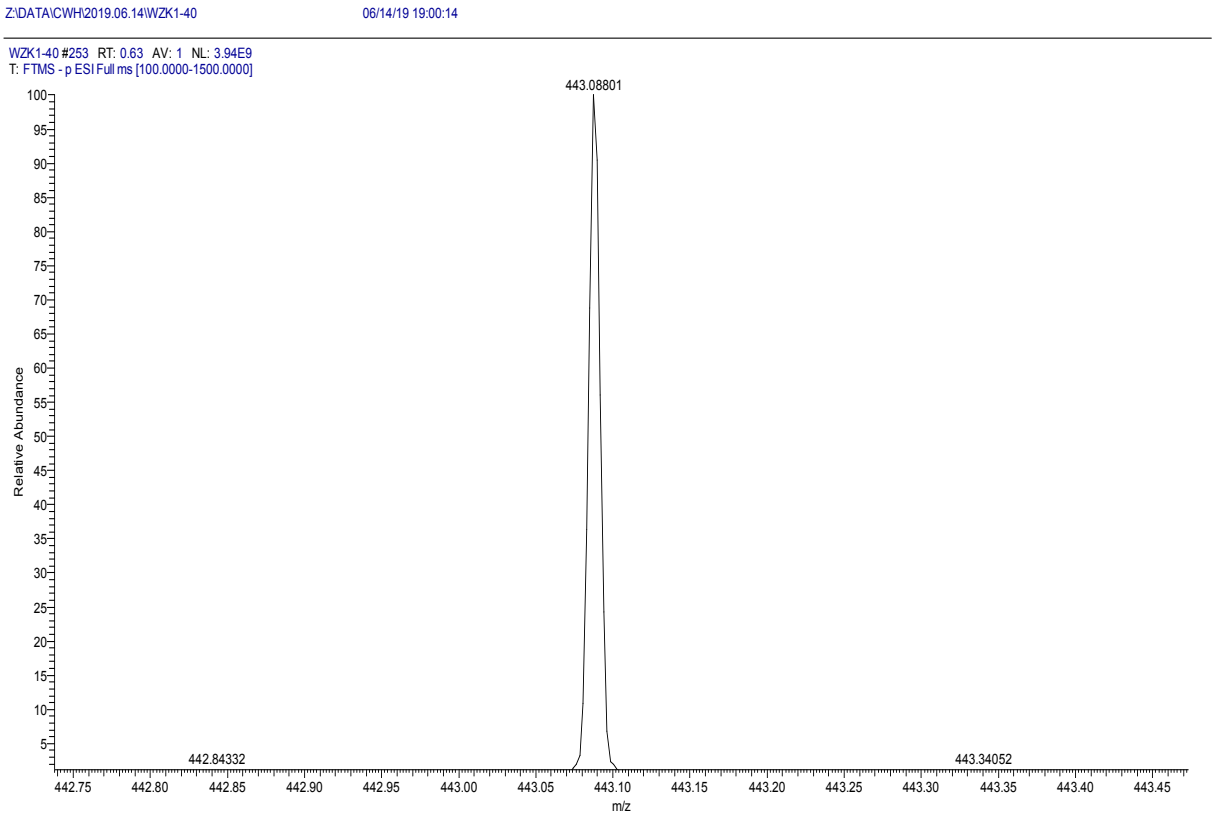

Fig. S24. Negative HR-ESI-MS of compound **6**.

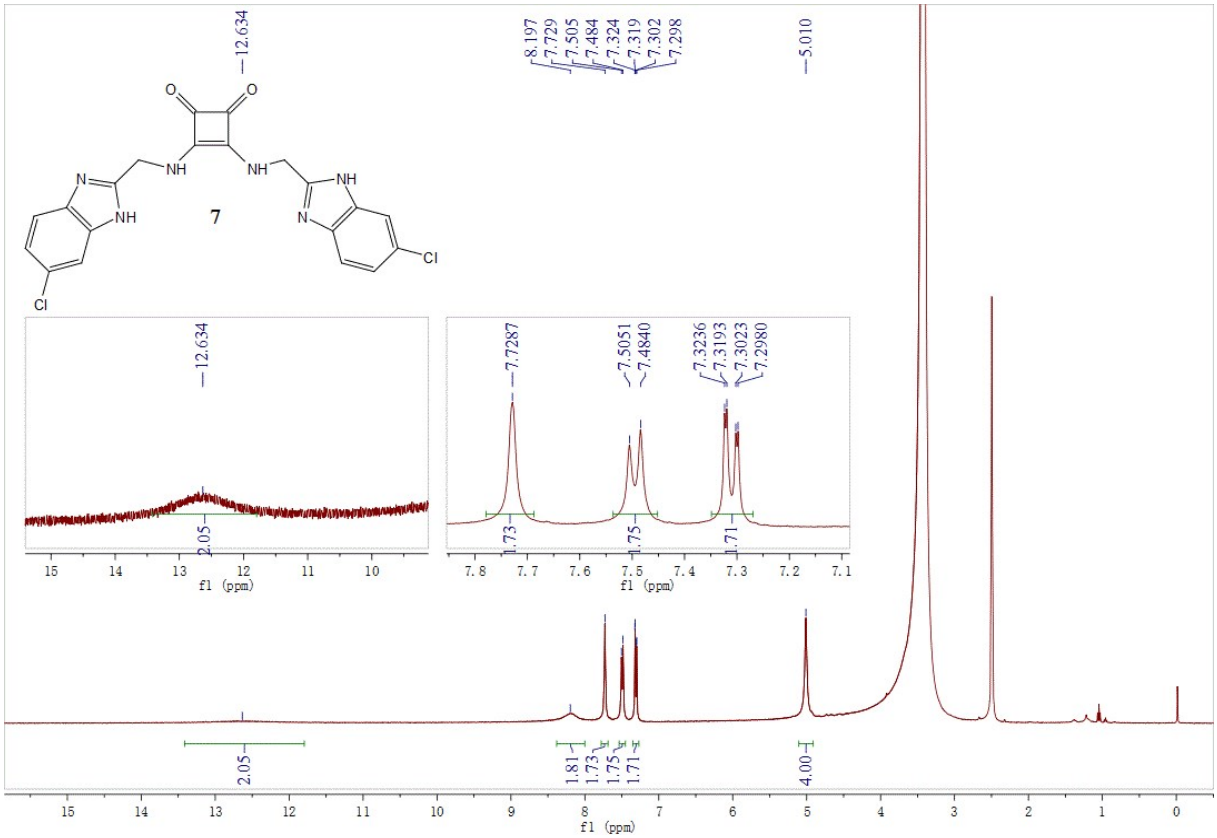

Fig. S25. ^{1}H NMR (DMSO-d_6, 400 MHz) of compound **7**.

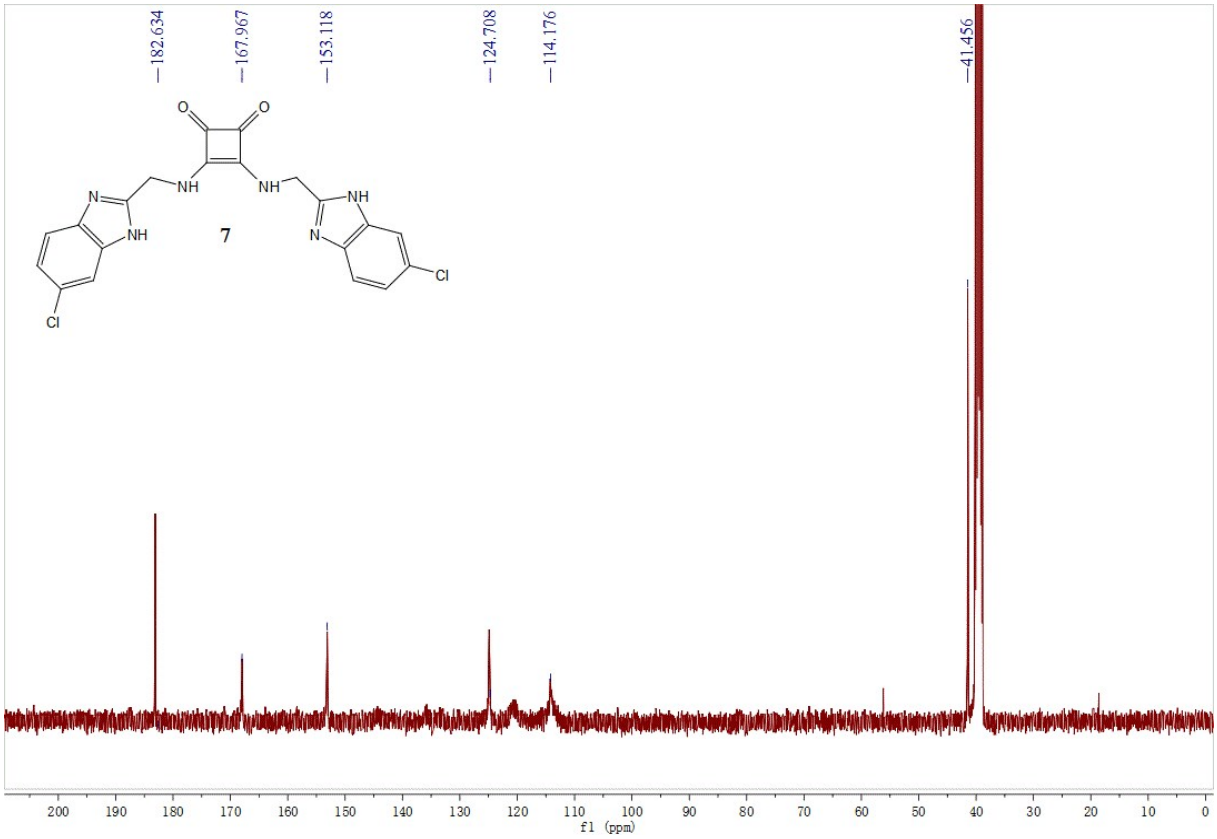

Fig. S26. ^{13}C NMR (DMSO-d_6, 100 MHz) of compound **7**.

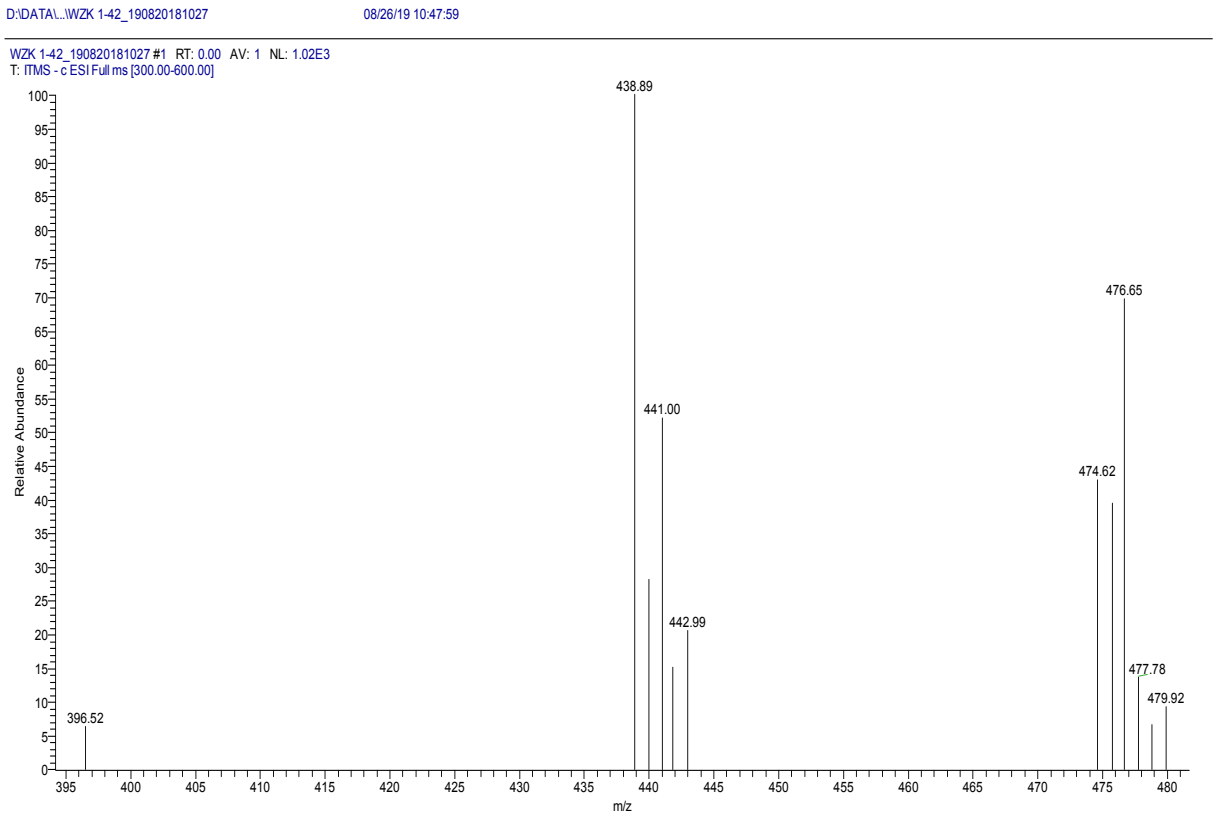

Fig. S27. Negative ESI-MS of compound **7**.

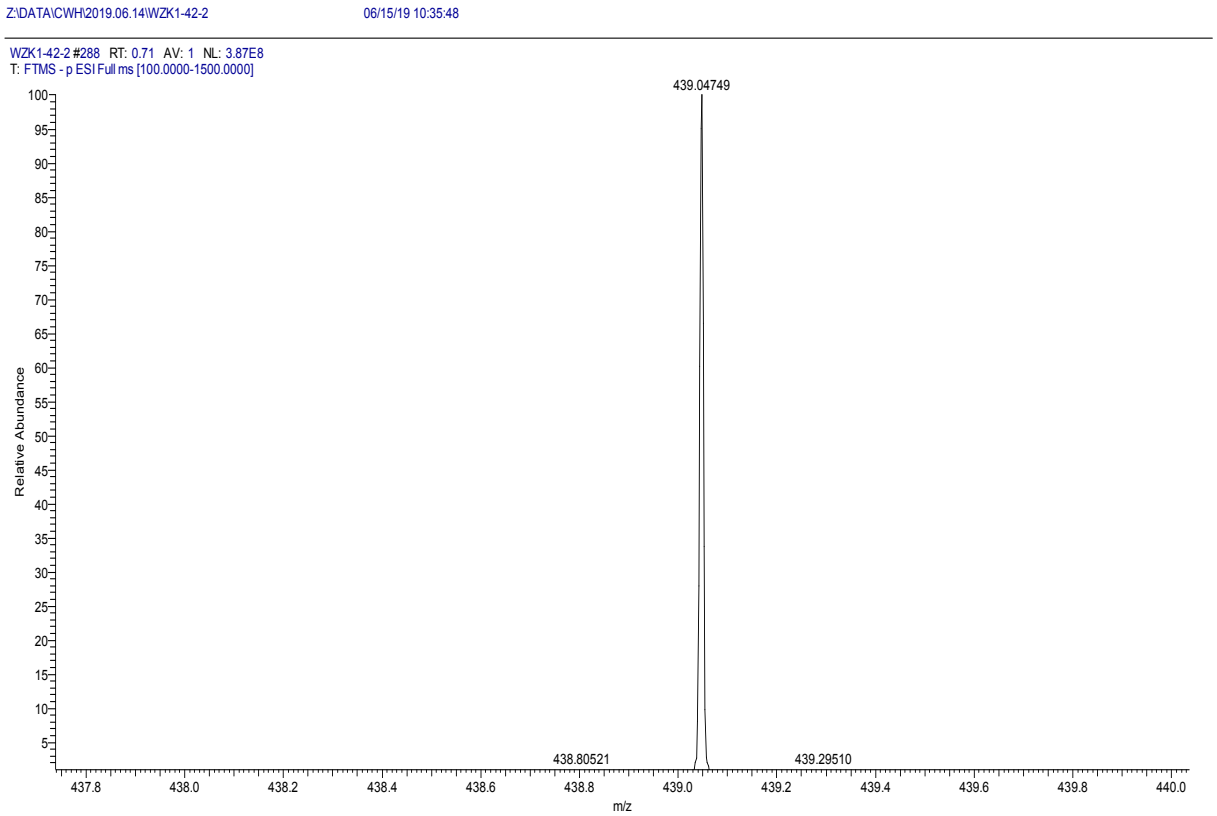

Fig. S28. Negative HR-ESI-MS of compound **7**.

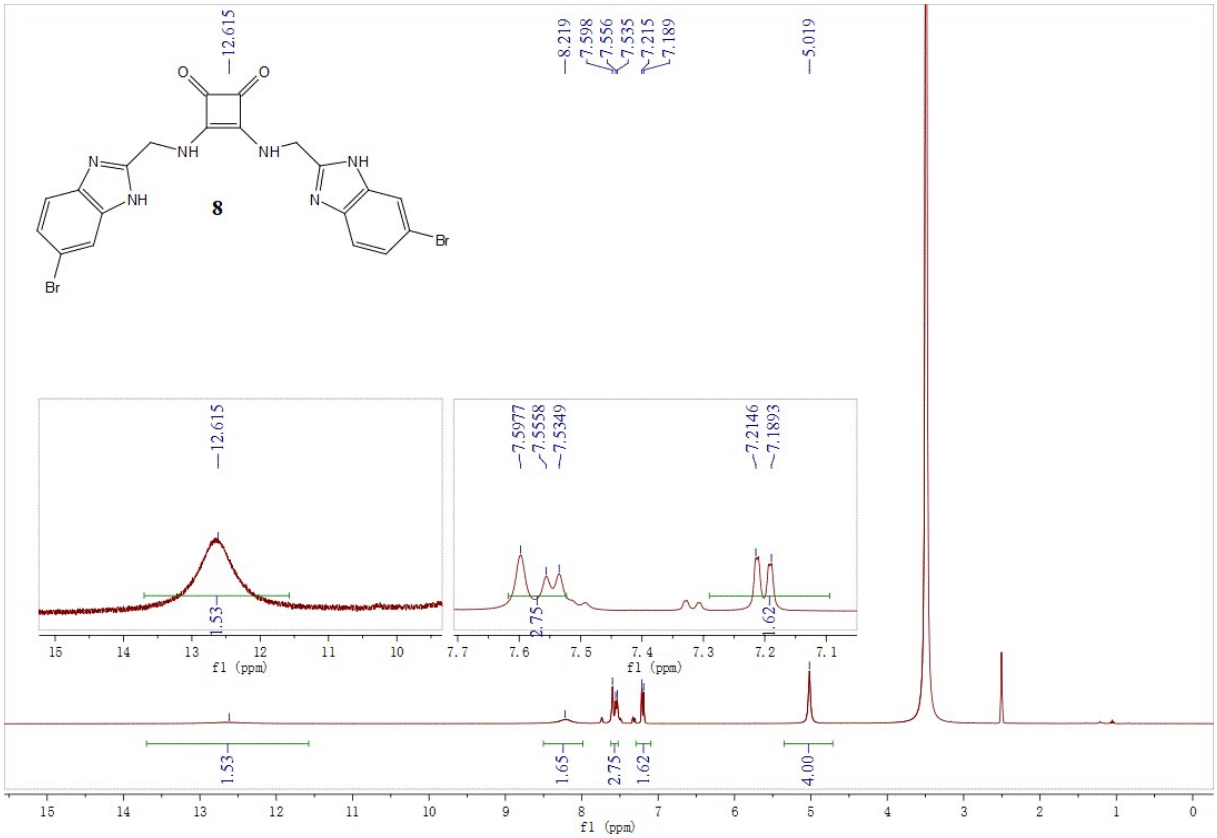

Fig. S29. ^{1}H NMR (DMSO-d_6, 400 MHz) of compound **8**.

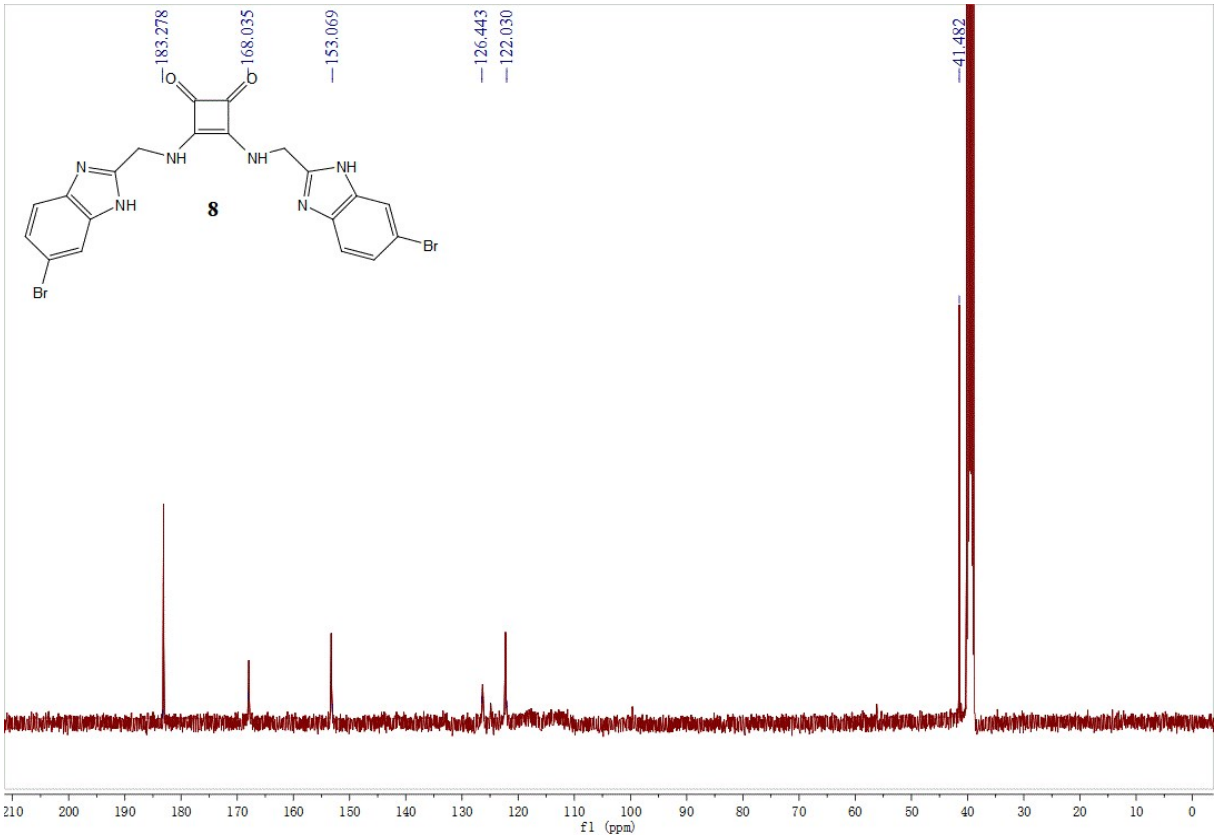

Fig. S30. ^{13}C NMR (DMSO-d_6, 100 MHz) of compound **8**.

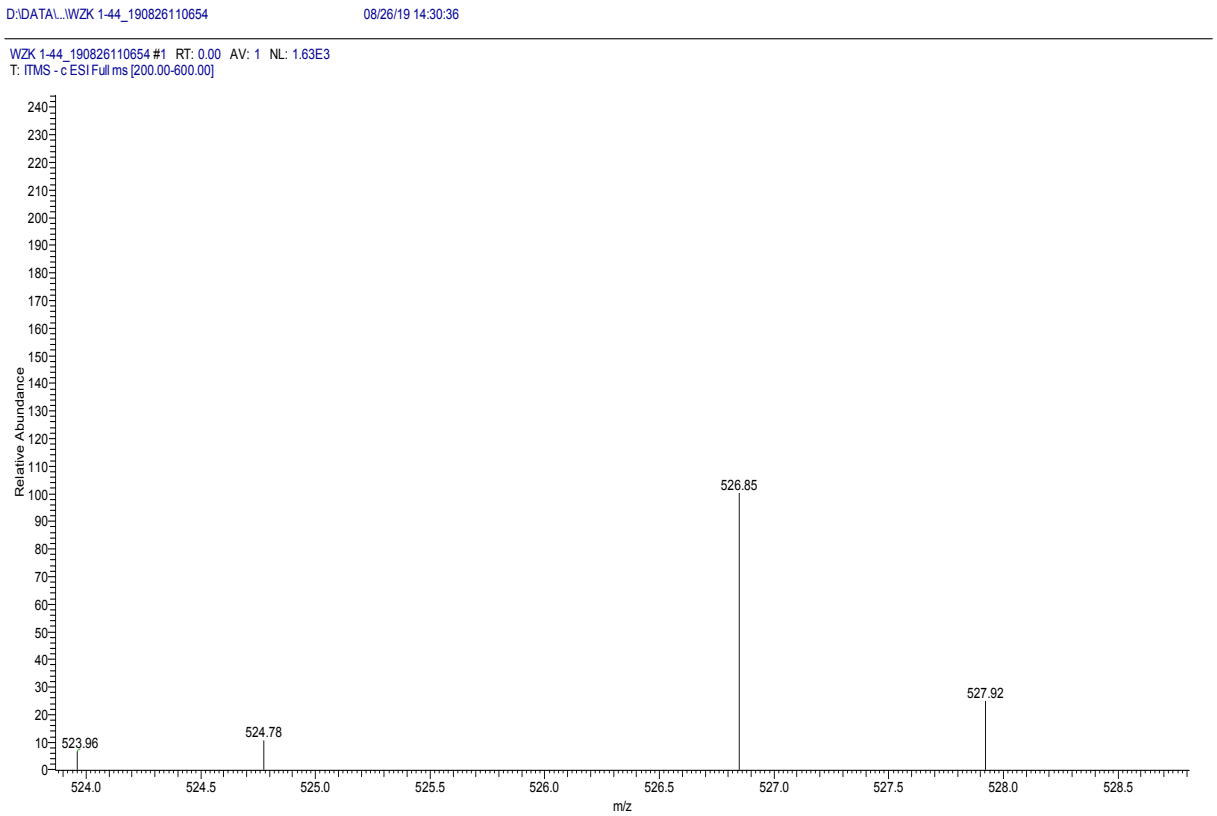

Fig. S31. Negative ESI-MS of compound **8**.

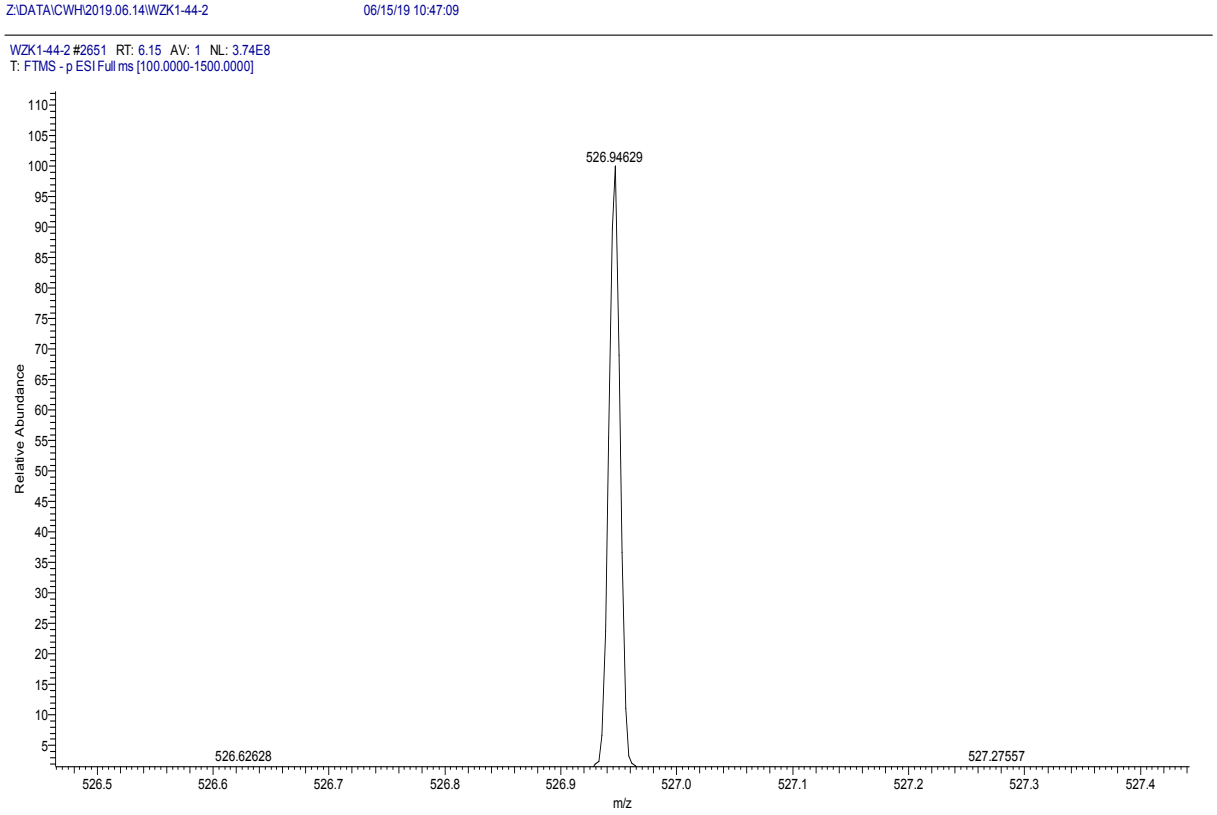

Fig. S32. Negative HR-ESI-MS of compound **8**.

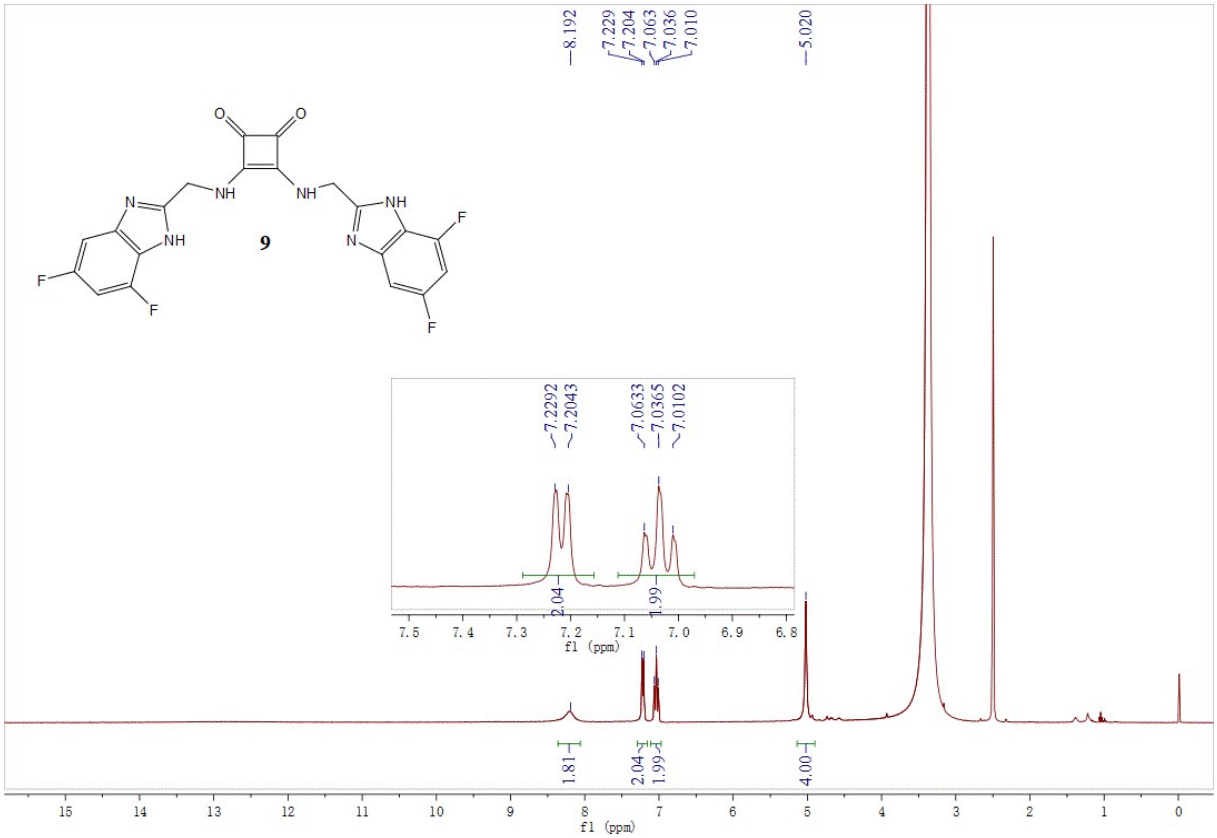

Fig. S33. ^{1}H NMR (DMSO-d_6, 400 MHz) of compound **9**.

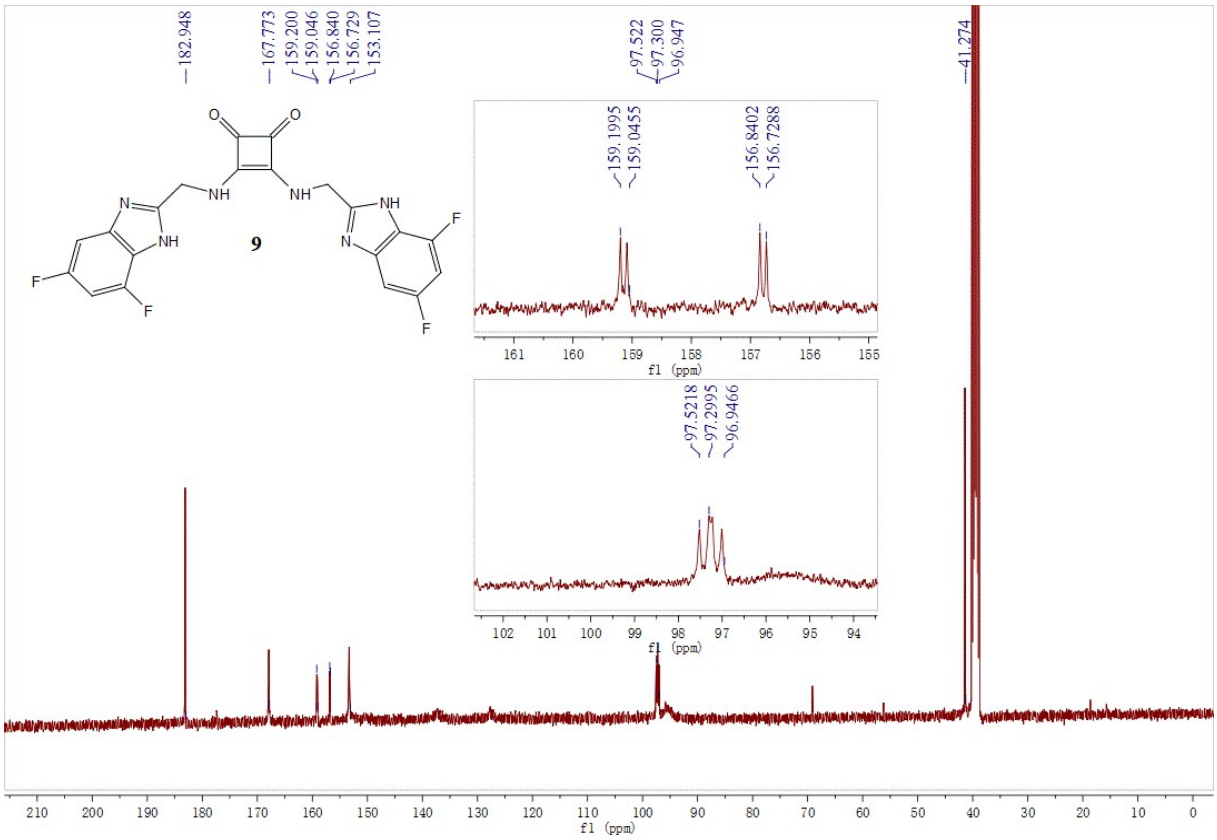

Fig. S34. ^{13}C NMR (DMSO-d_6, 125 MHz) of compound **9**.

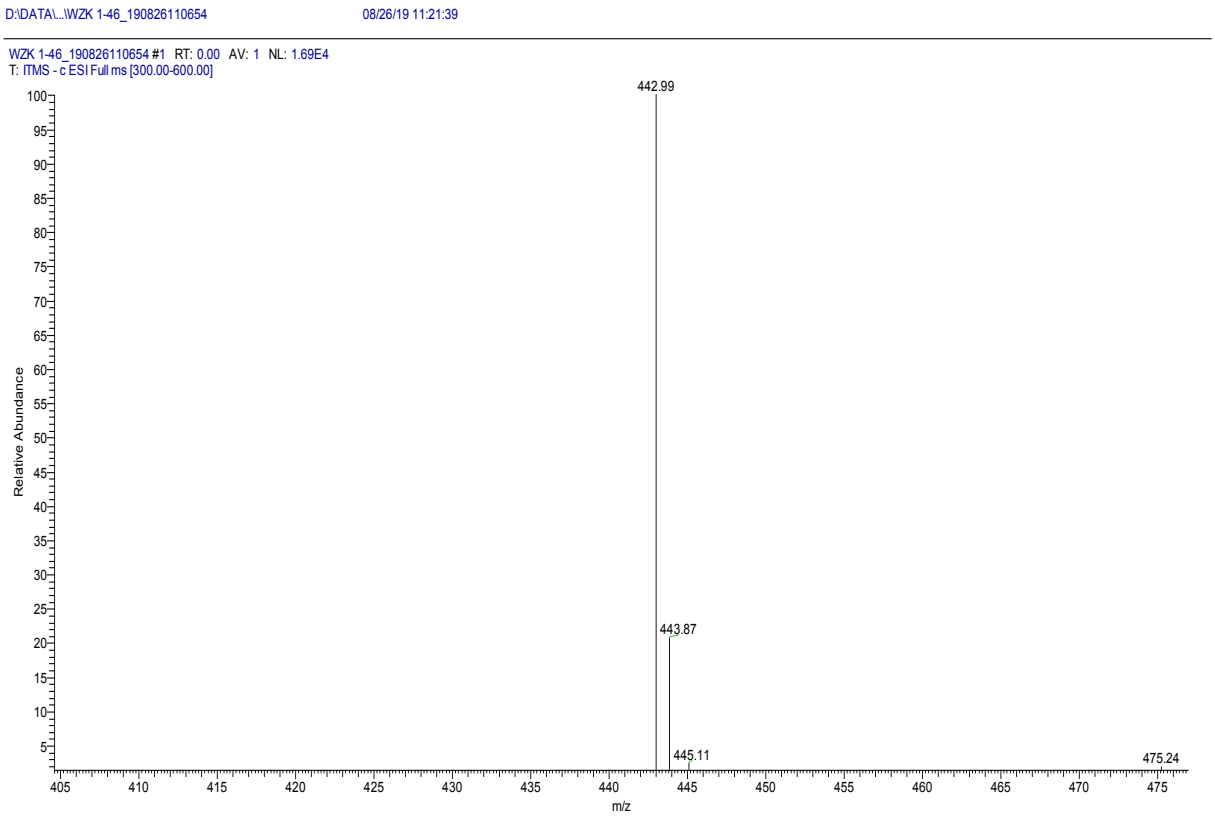

Fig. S35. Negative ESI-MS of compound **9**.

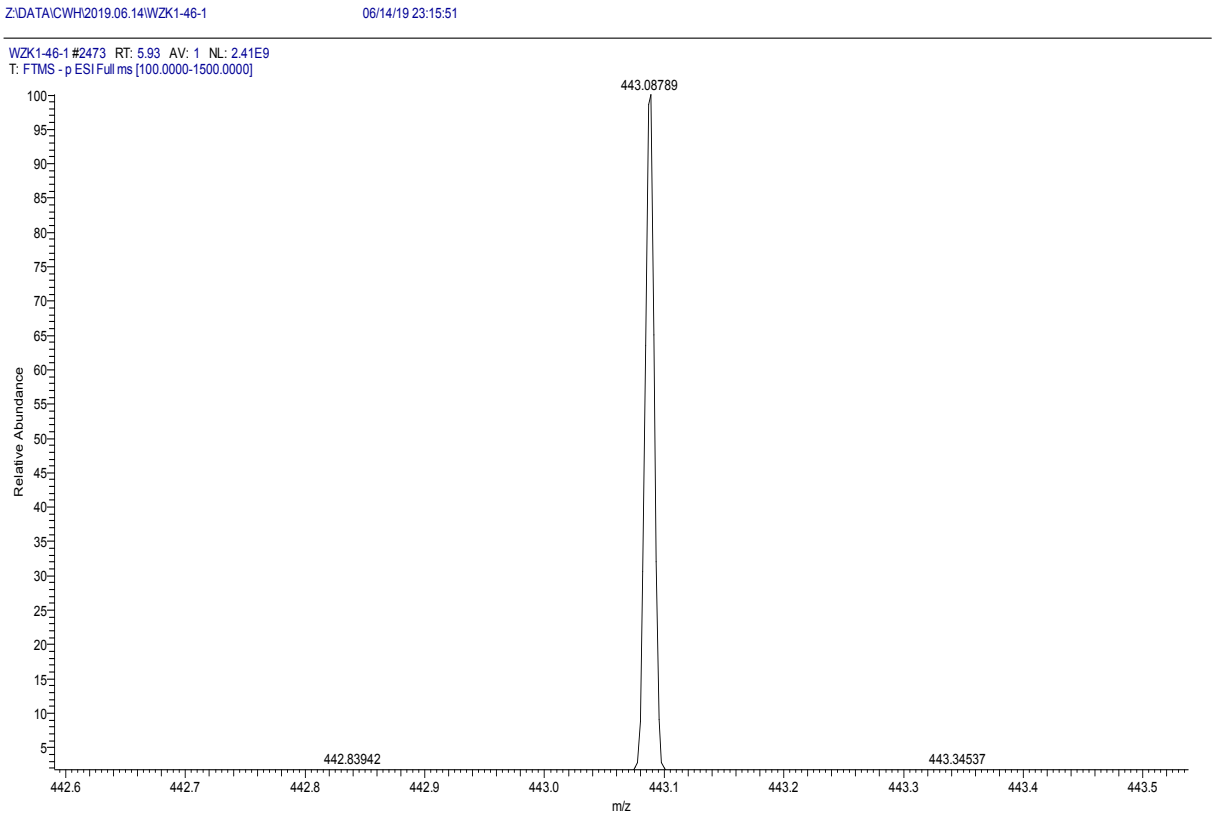

Fig. S36. Negative HR-ESI-MS of compound **9**.

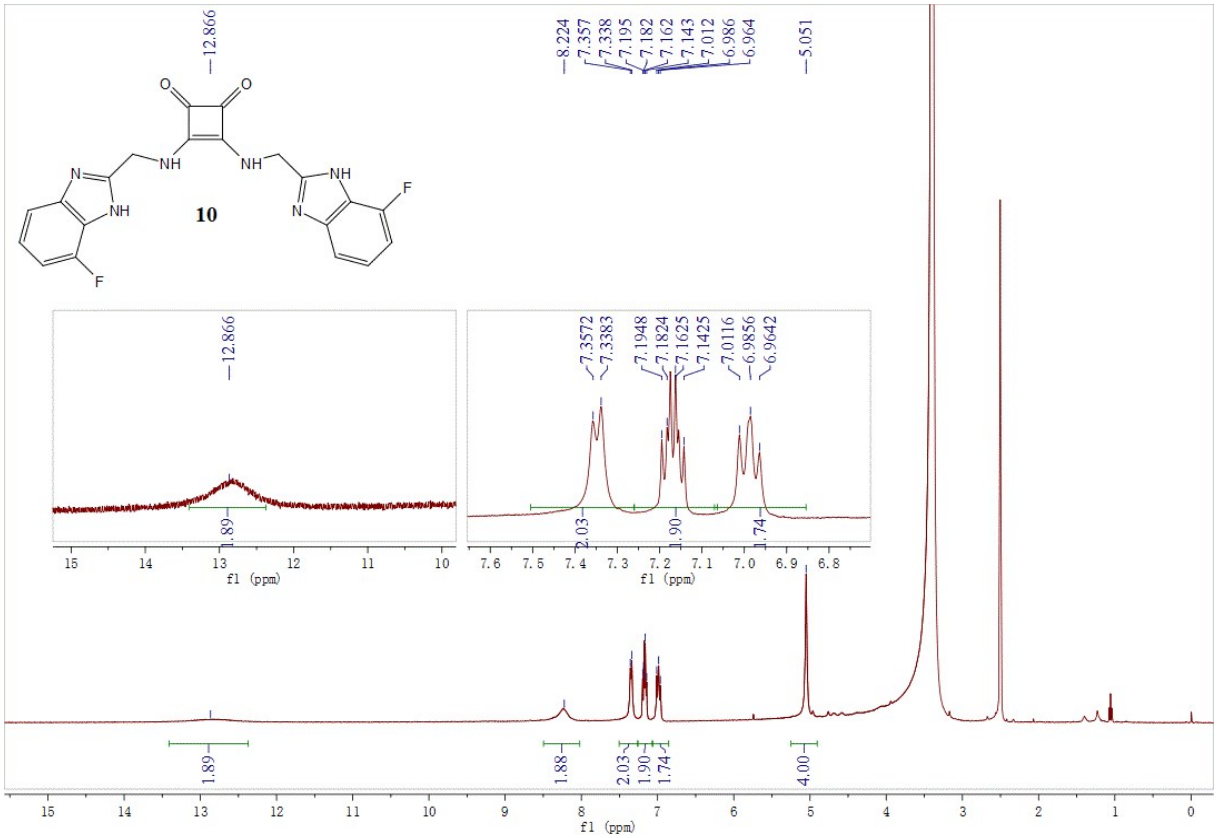

Fig. S37. ^{1}H NMR (DMSO-d_6, 400 MHz) of compound **10**.

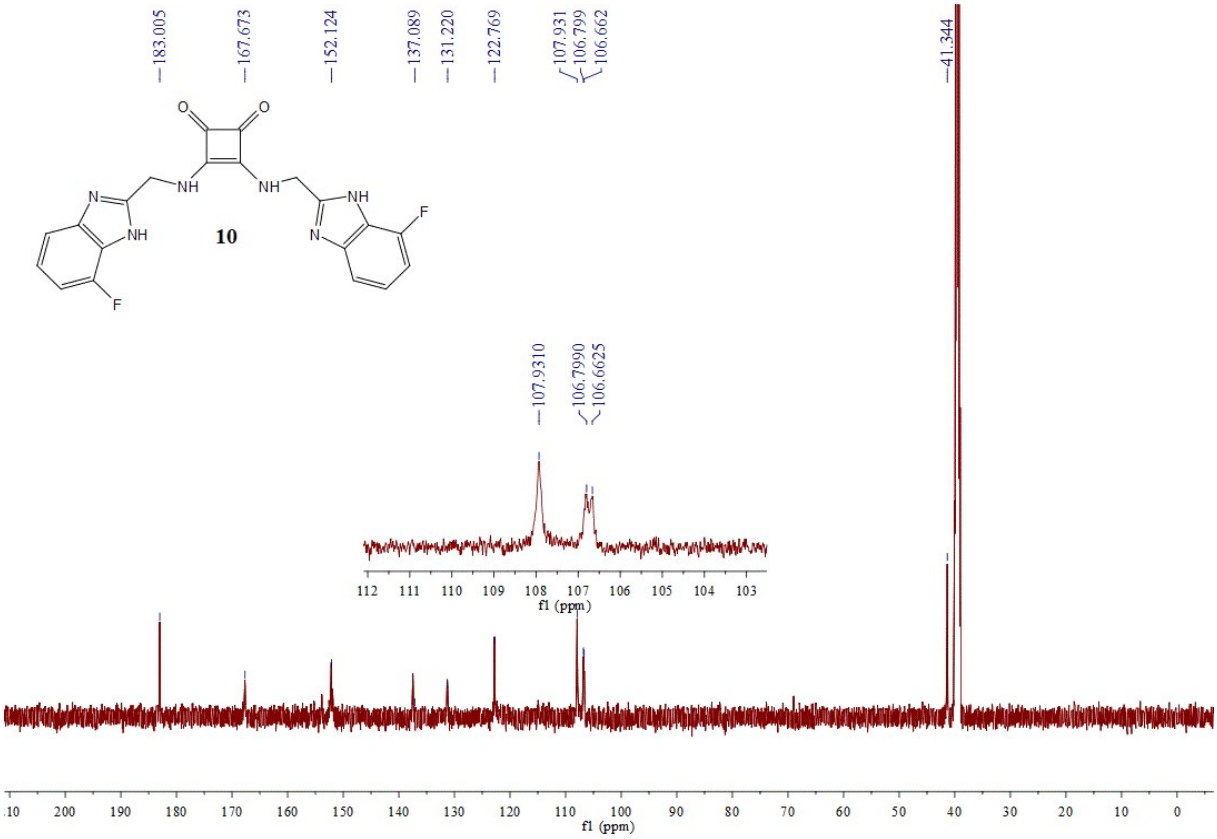

Fig. S38. ^{13}C NMR (DMSO-d_6, 125 MHz) of compound **10**.

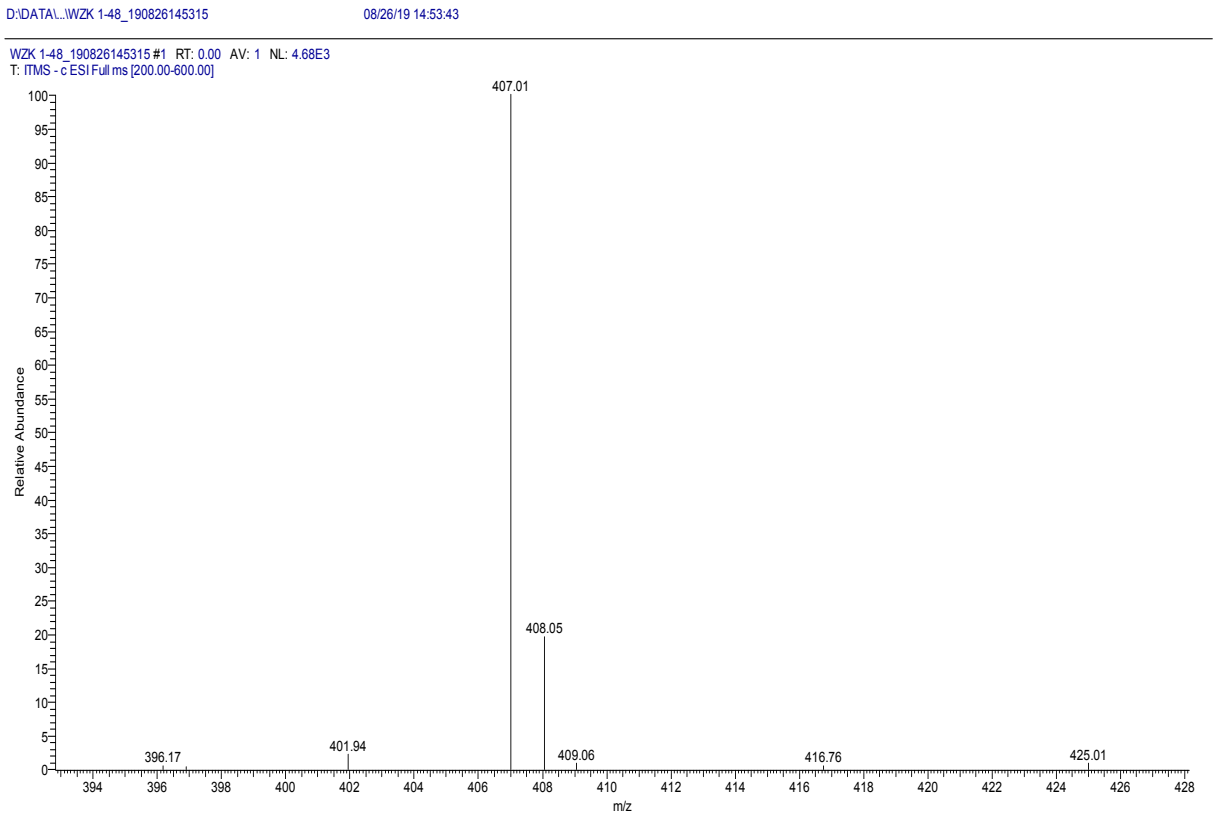

Fig. S39. Negative ESI-MS of compound **10**.

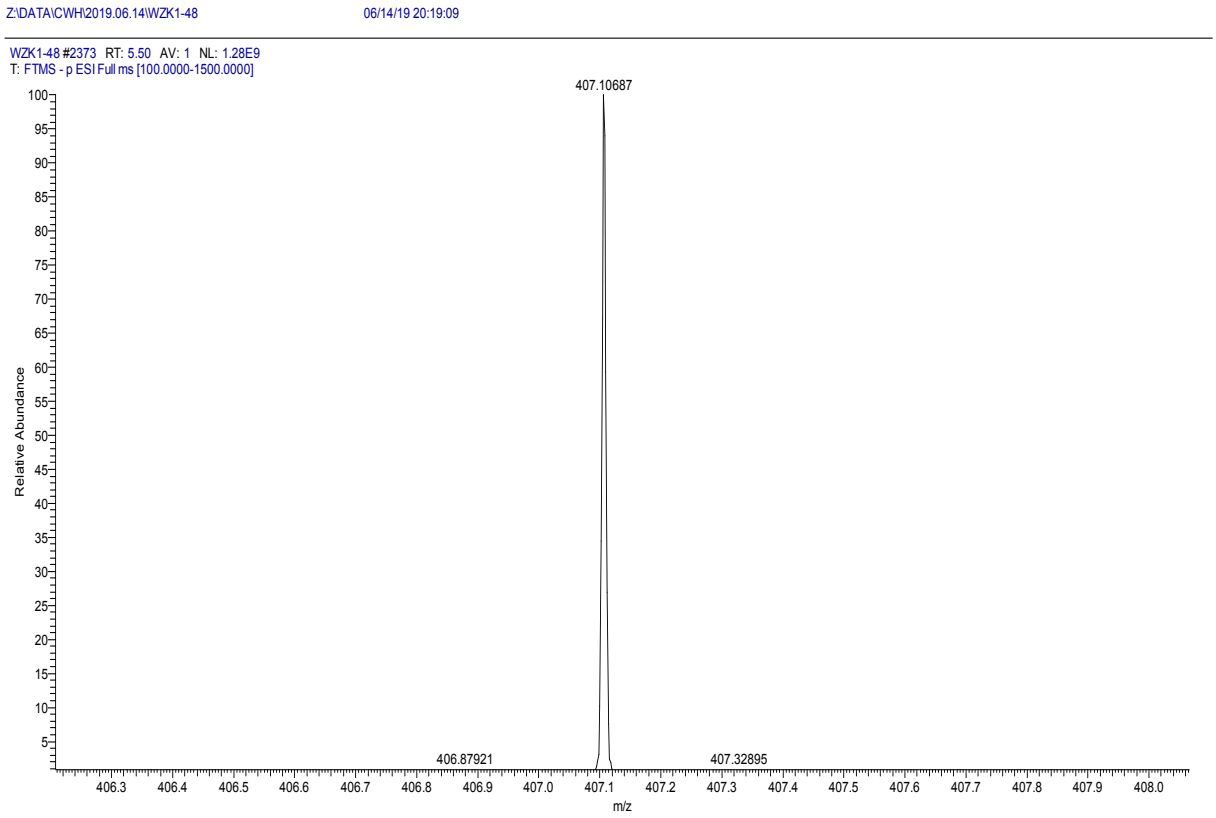

Fig. S40. Negative HR-ESI-MS of compound **10**.

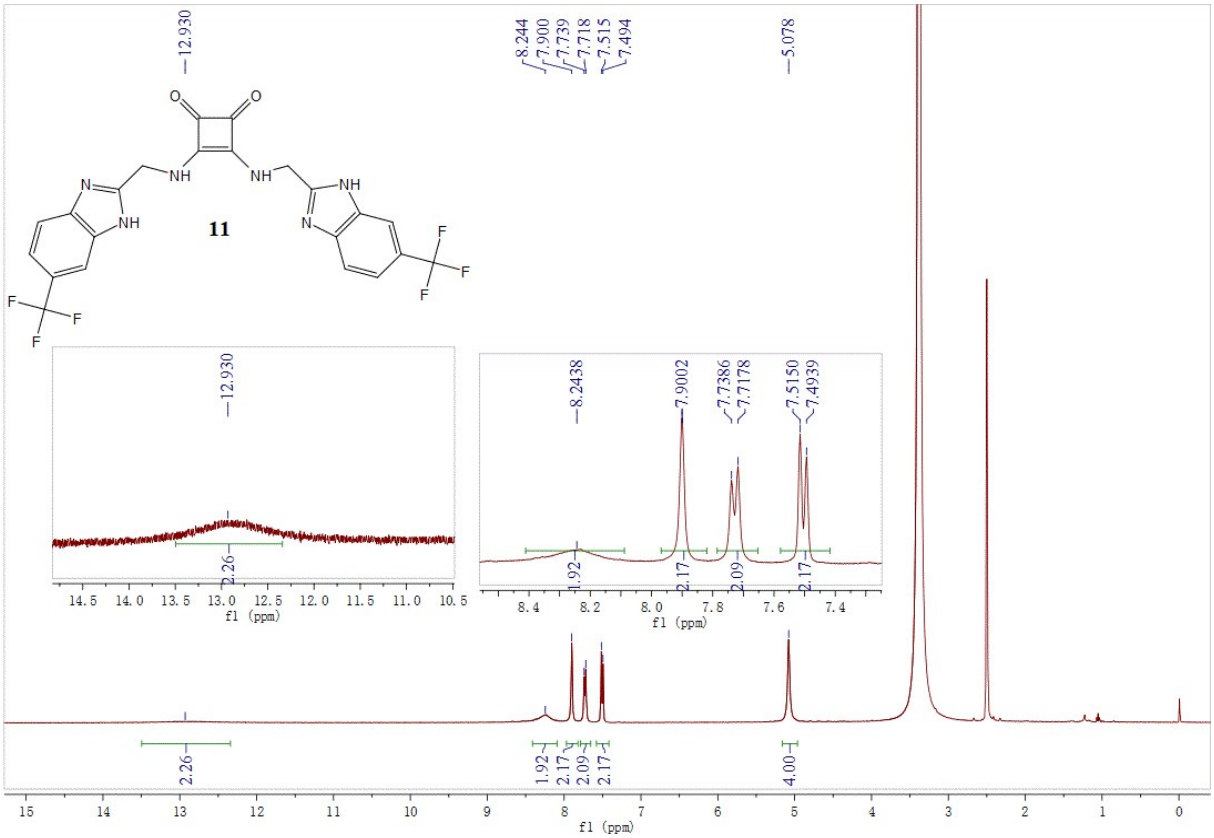

Fig. S41. ^{1}H NMR (DMSO-d_6, 400 MHz) of compound **11**.

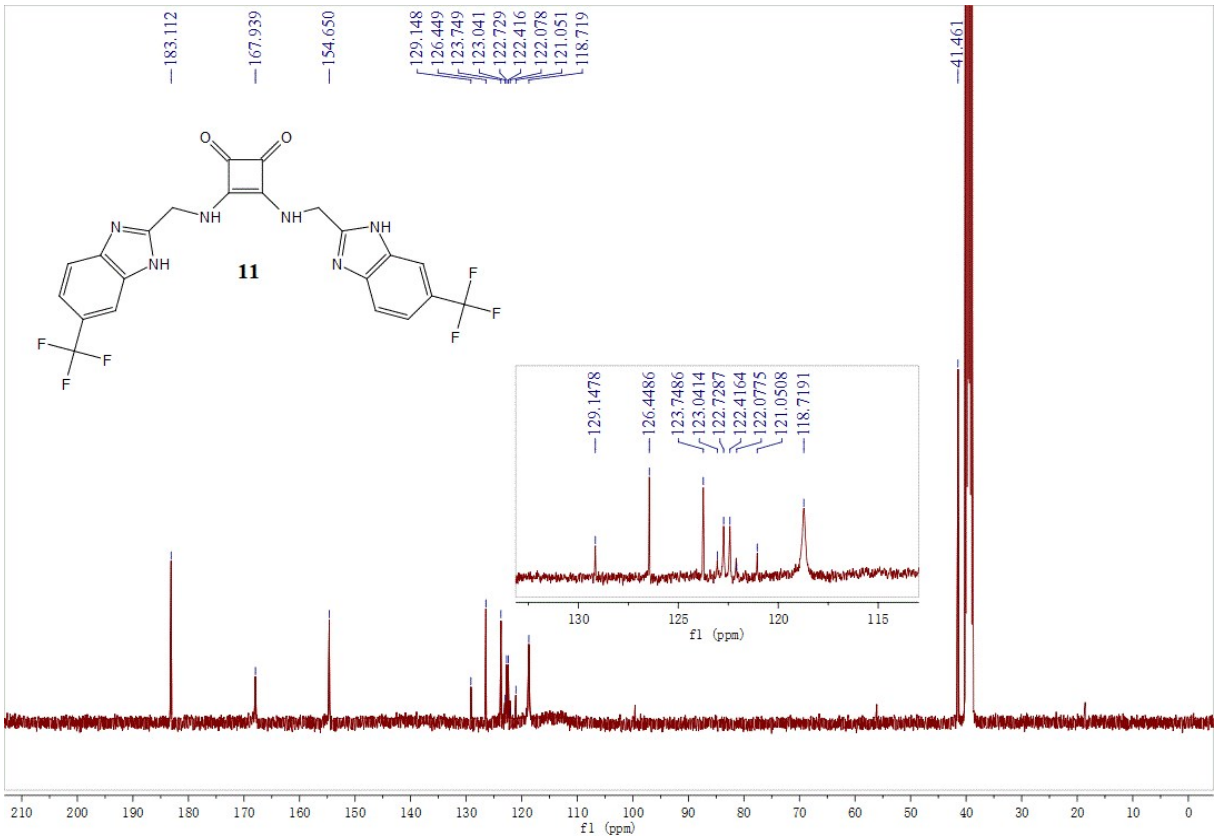

Fig. S42. ^{13}C NMR (DMSO-d_6, 125 MHz) of compound **11**.

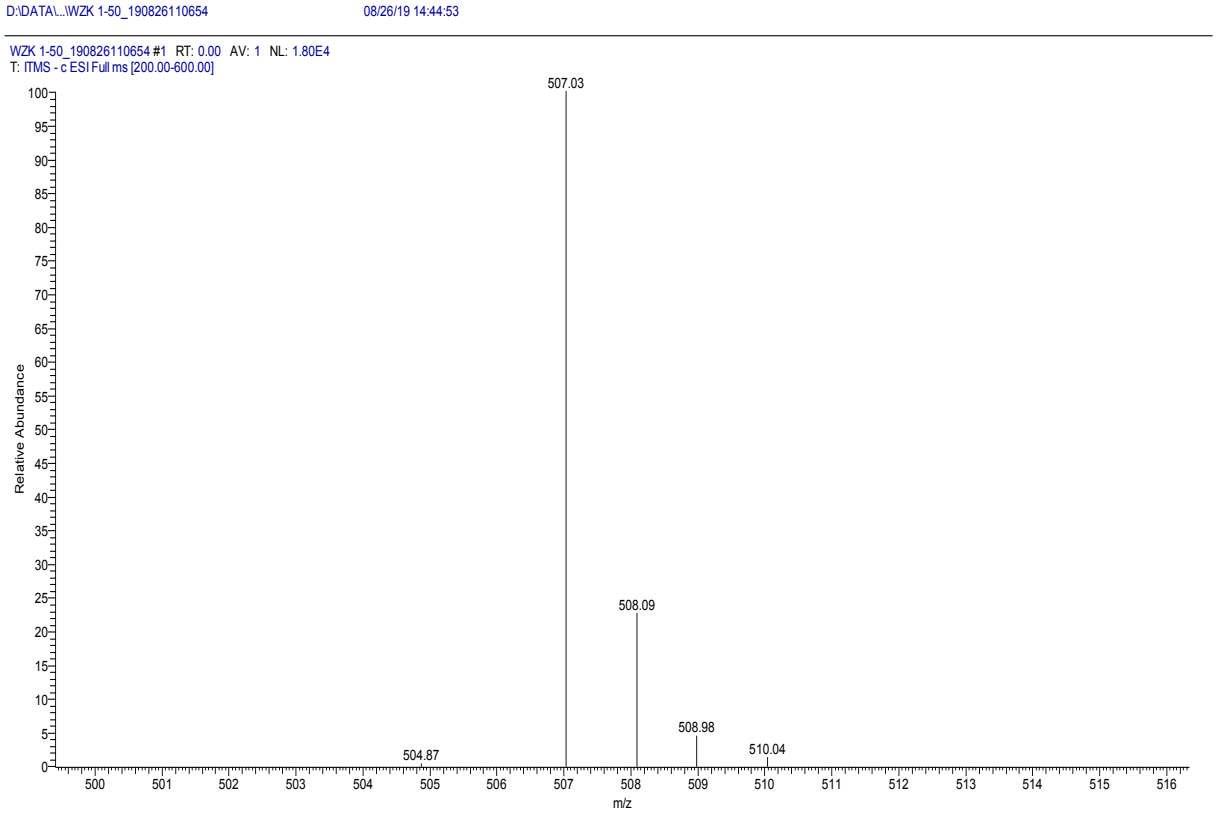

Fig. S43. Negative ESI-MS of compound **11**.

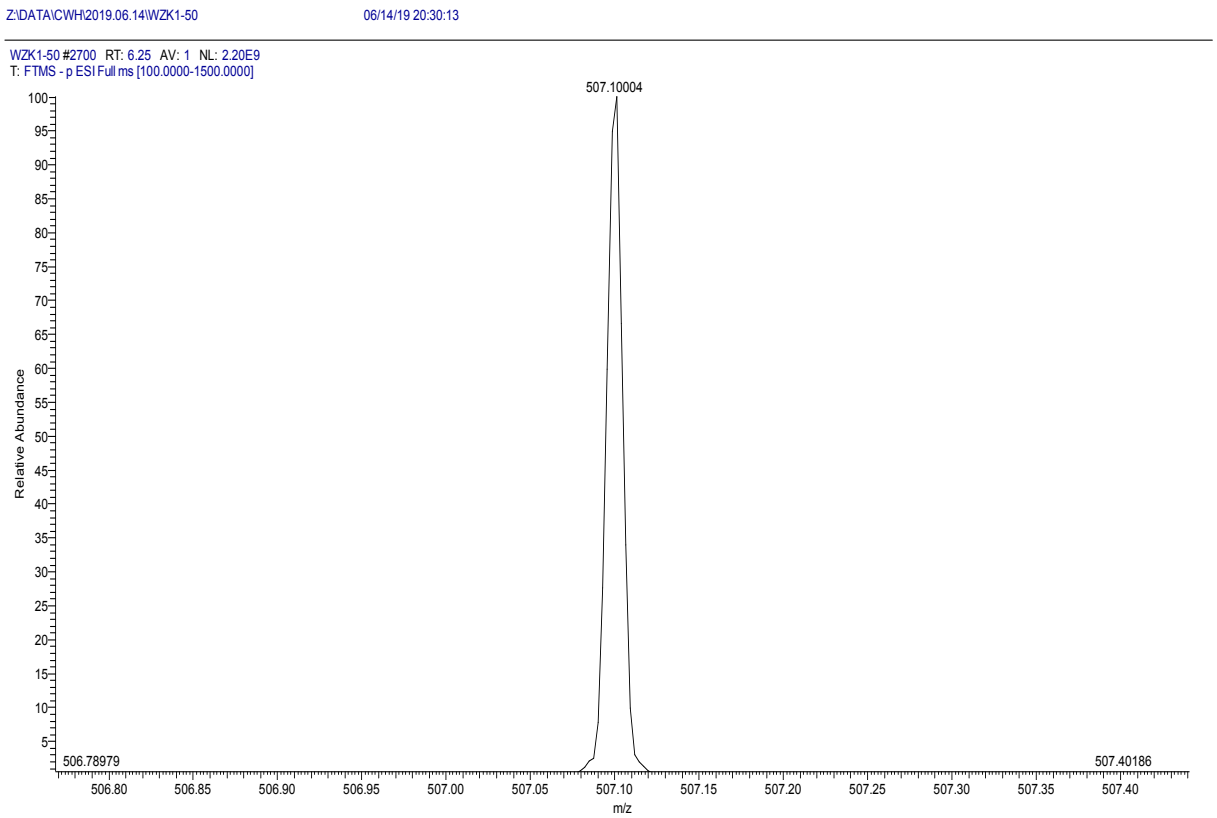

Fig. S44. Negative HR-ESI-MS of compound **11**.

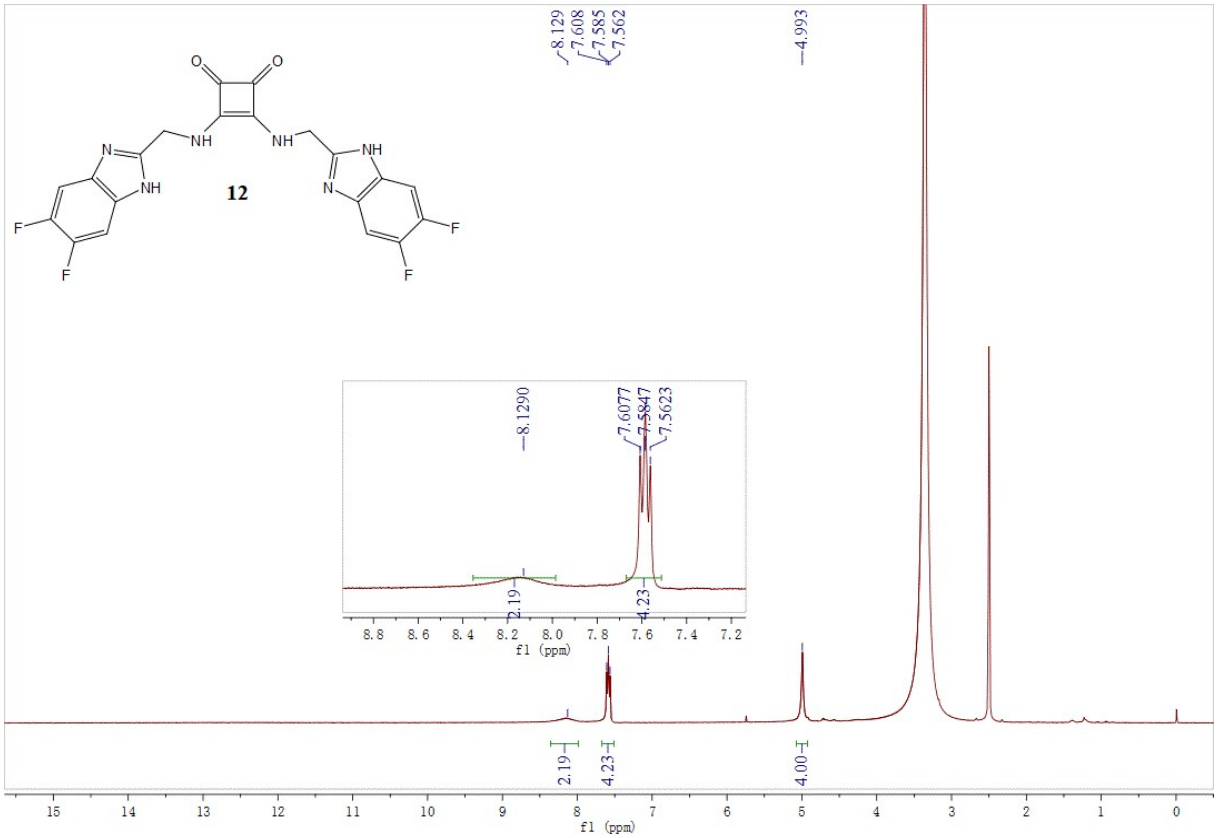

Fig. S45. ^{1}H NMR (DMSO-d_6, 400 MHz) of compound **12**.

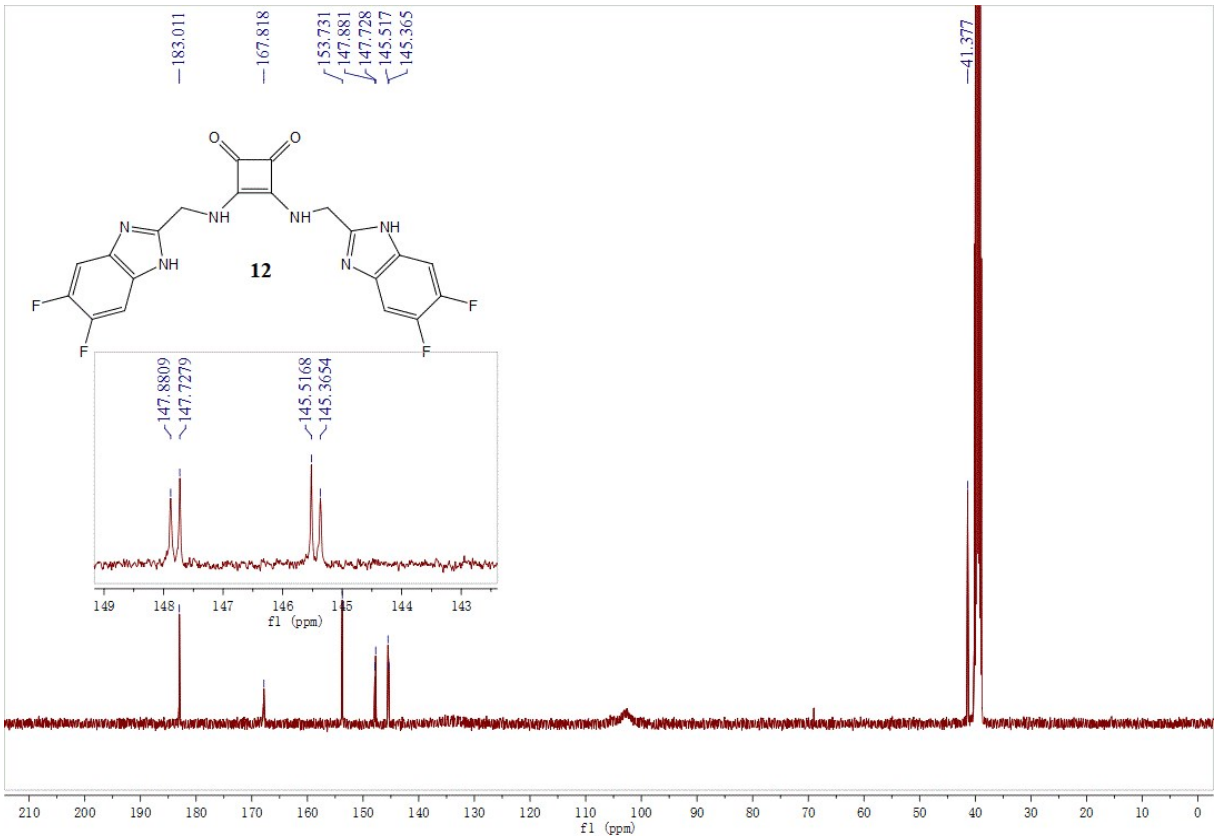

Fig. S46. ^{13}C NMR (DMSO-d_6, 125 MHz) of compound **12**.

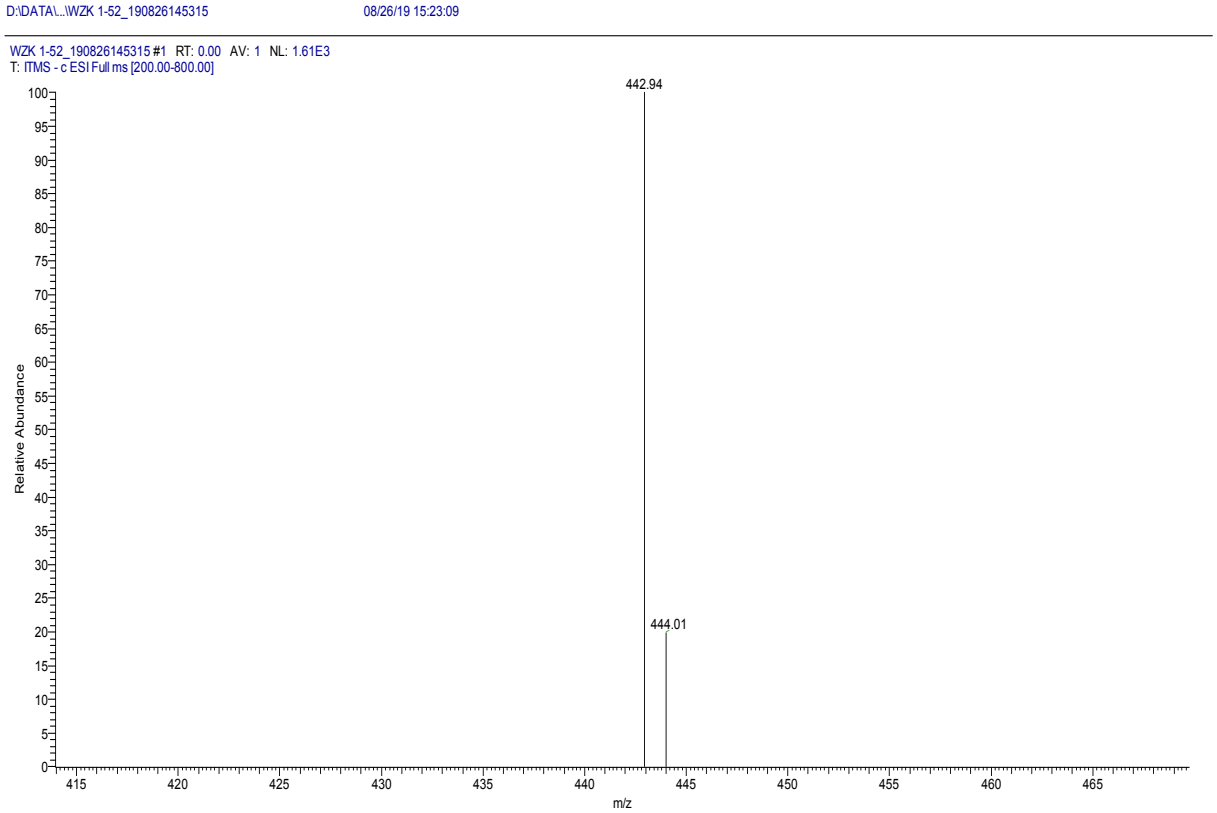

Fig. S47. Negative ESI-MS of compound **12**.

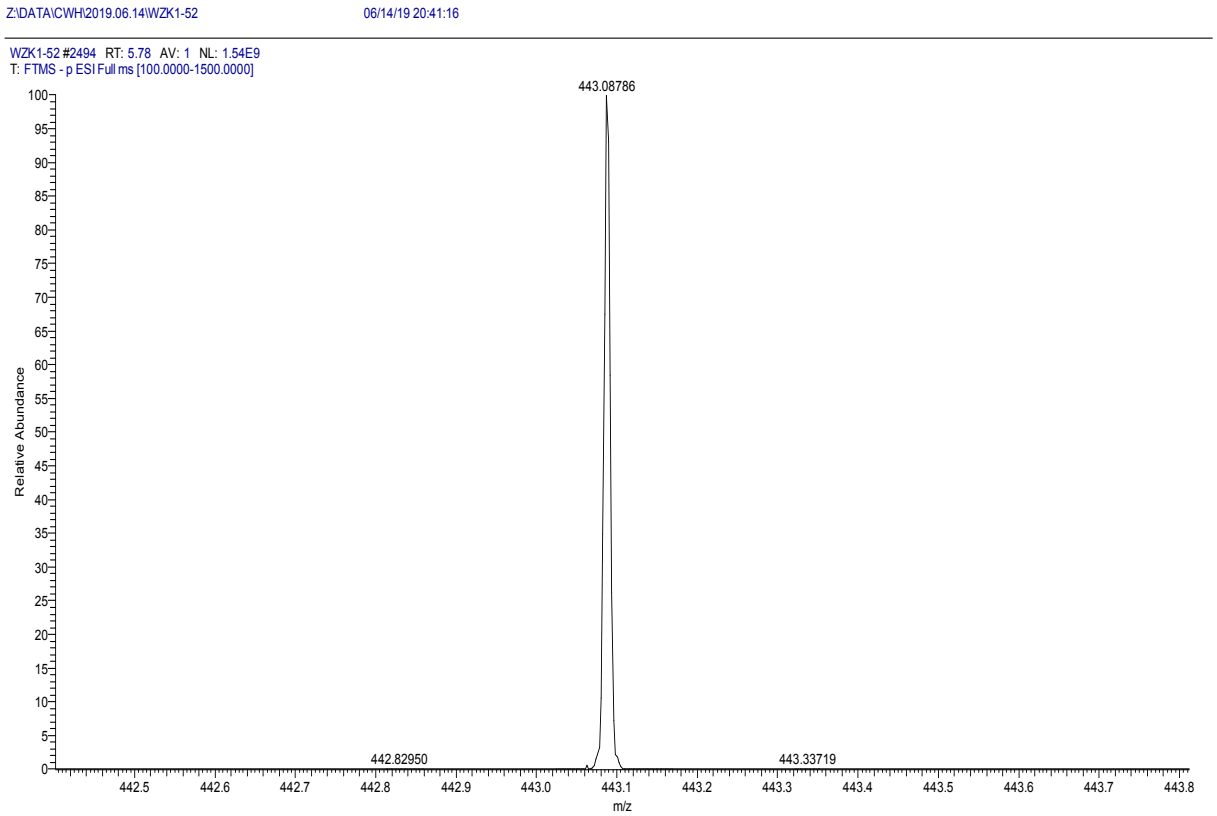

Fig. S48. Negative HR-ESI-MS of compound **12**.

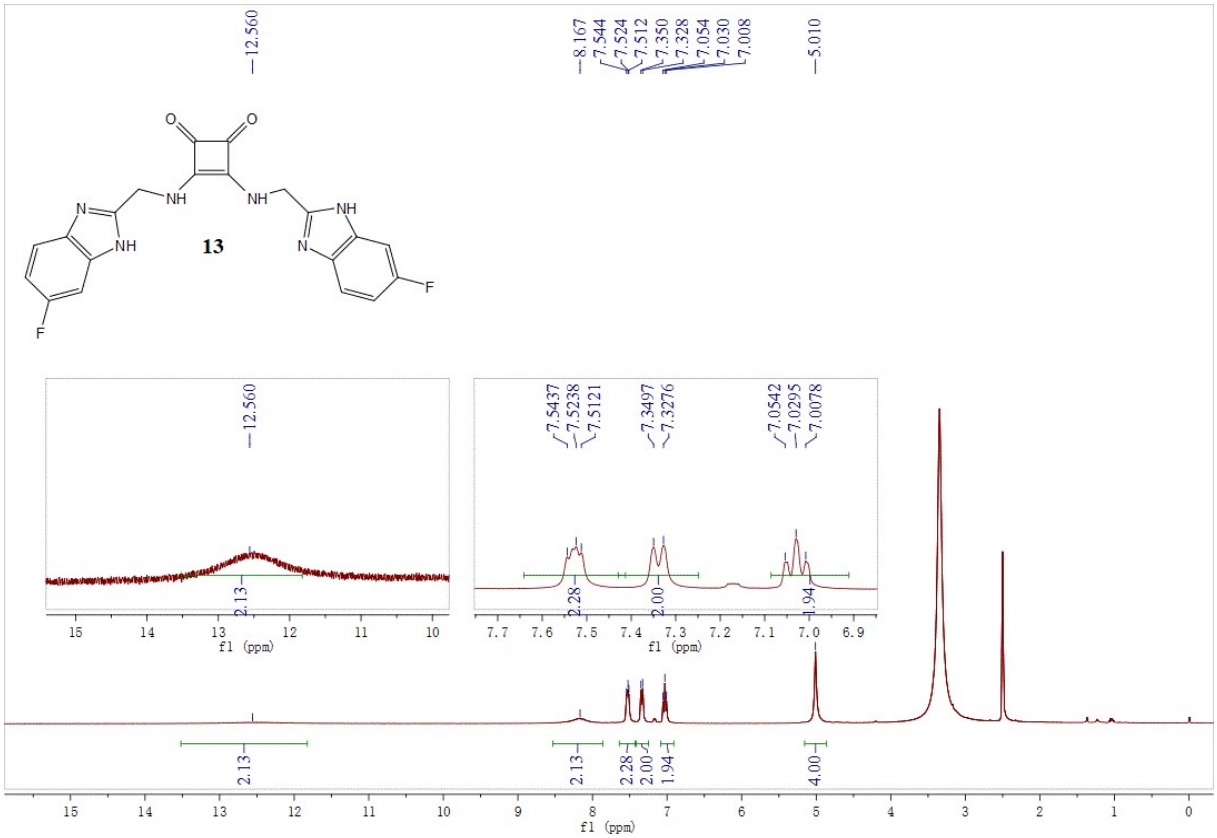

Fig. S49. ^{1}H NMR (DMSO-d_6, 400 MHz) of compound **13**.

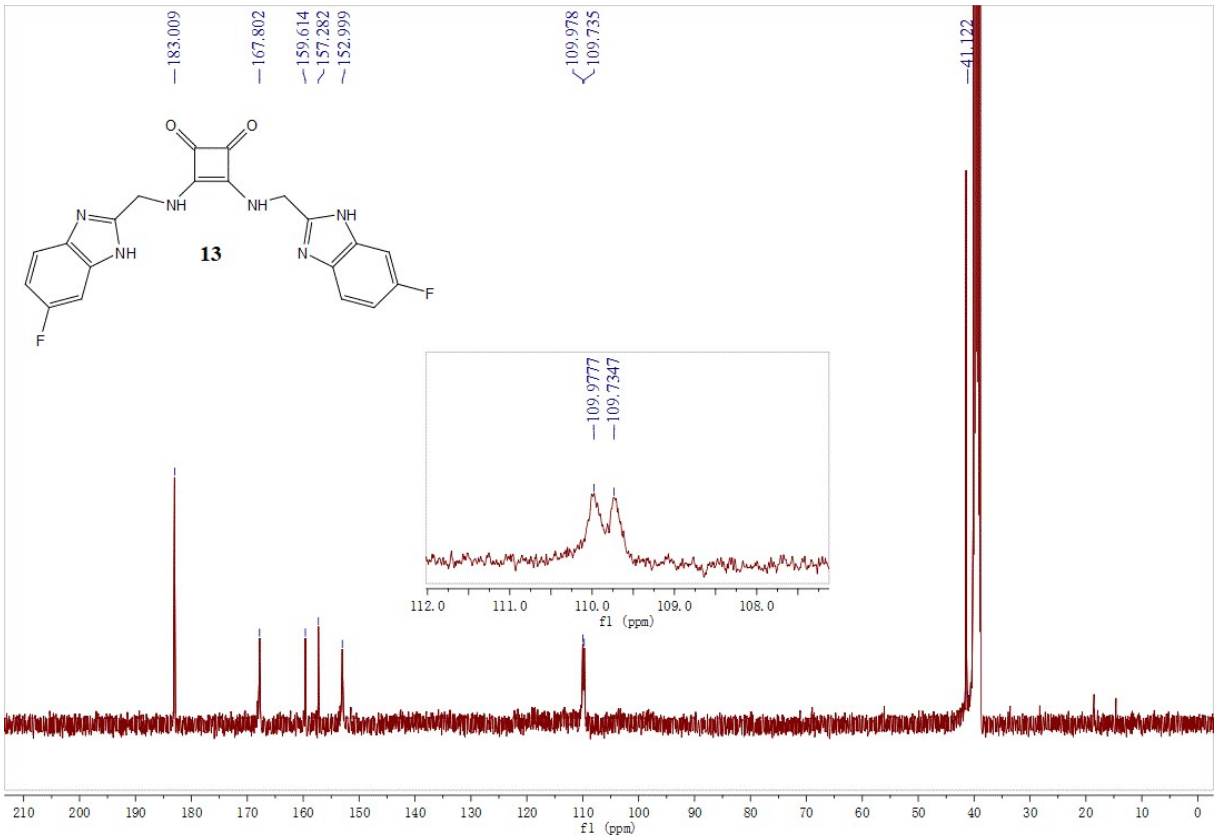

Fig. S50. ^{13}C NMR (DMSO-d_6, 125 MHz) of compound **13**.

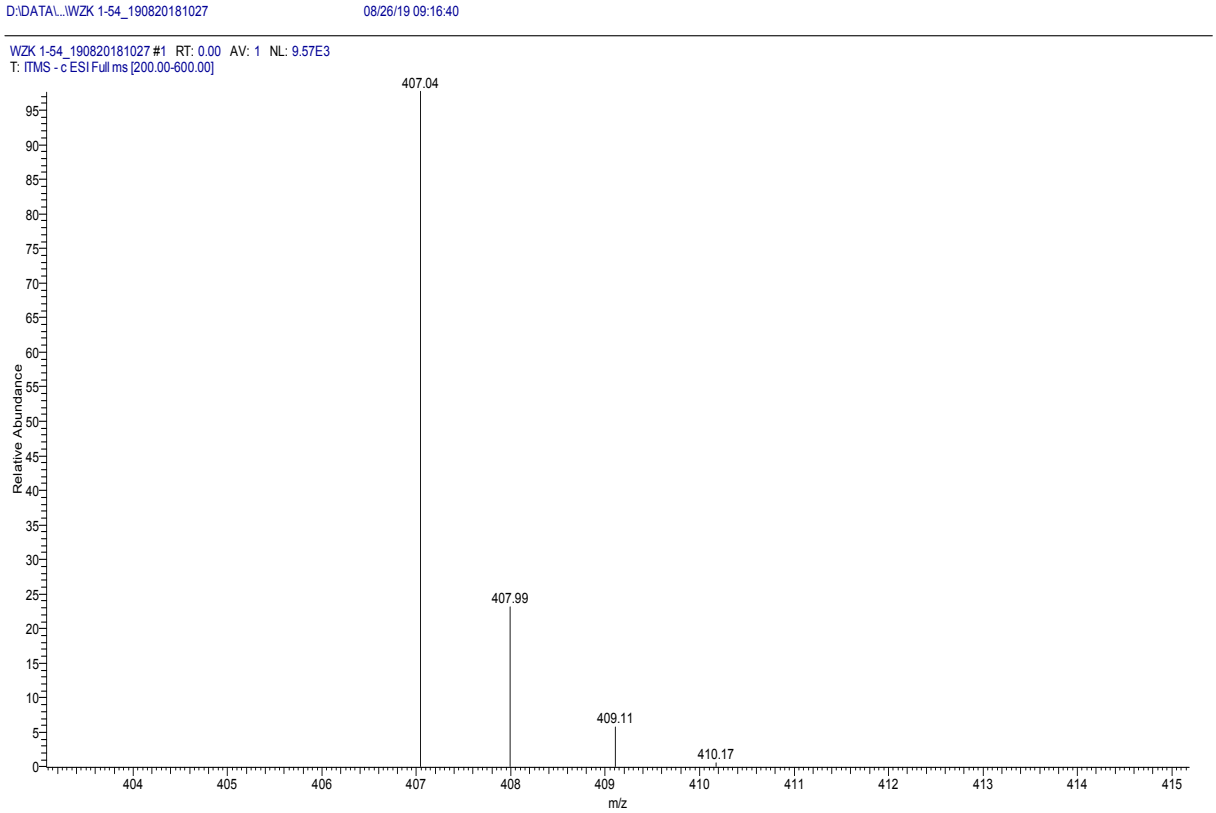

Fig. S51. Negative ESI-MS of compound **13**.

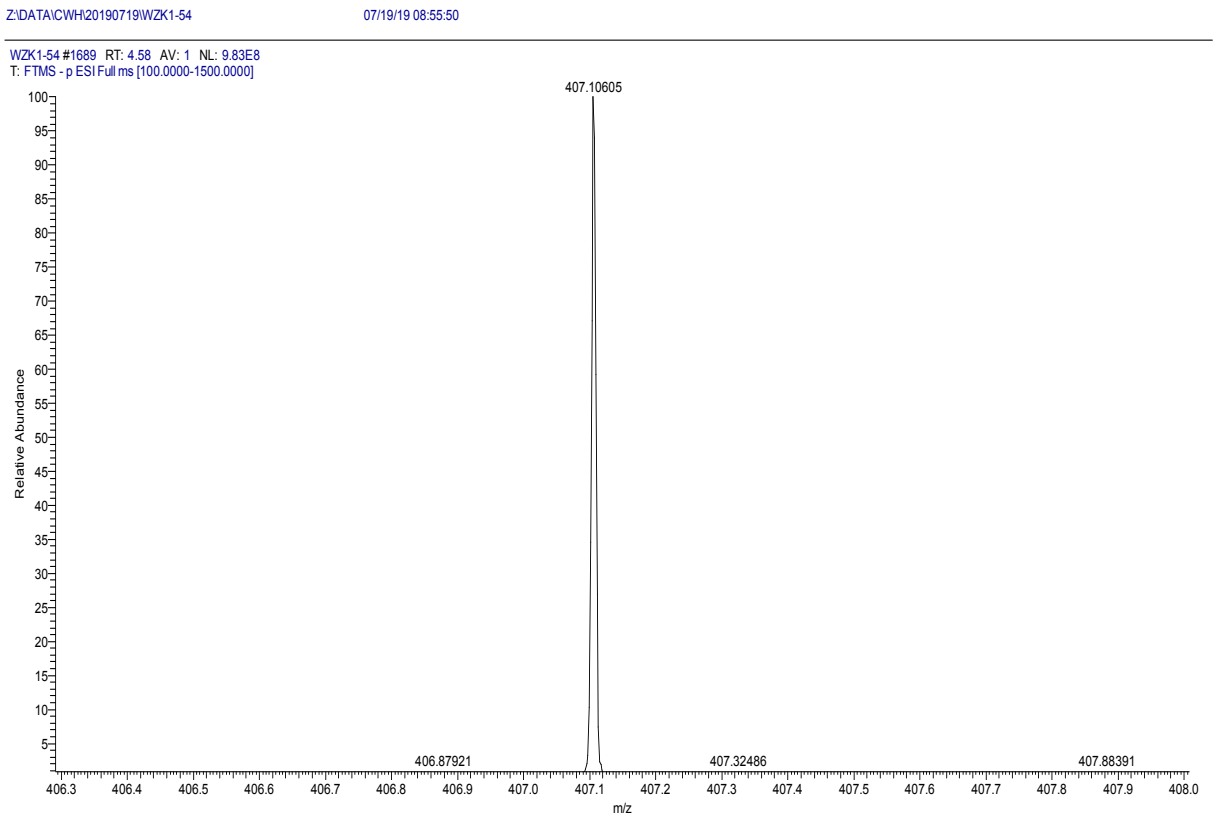

Fig. S52. Negative HR-ESI-MS of compound **13**.

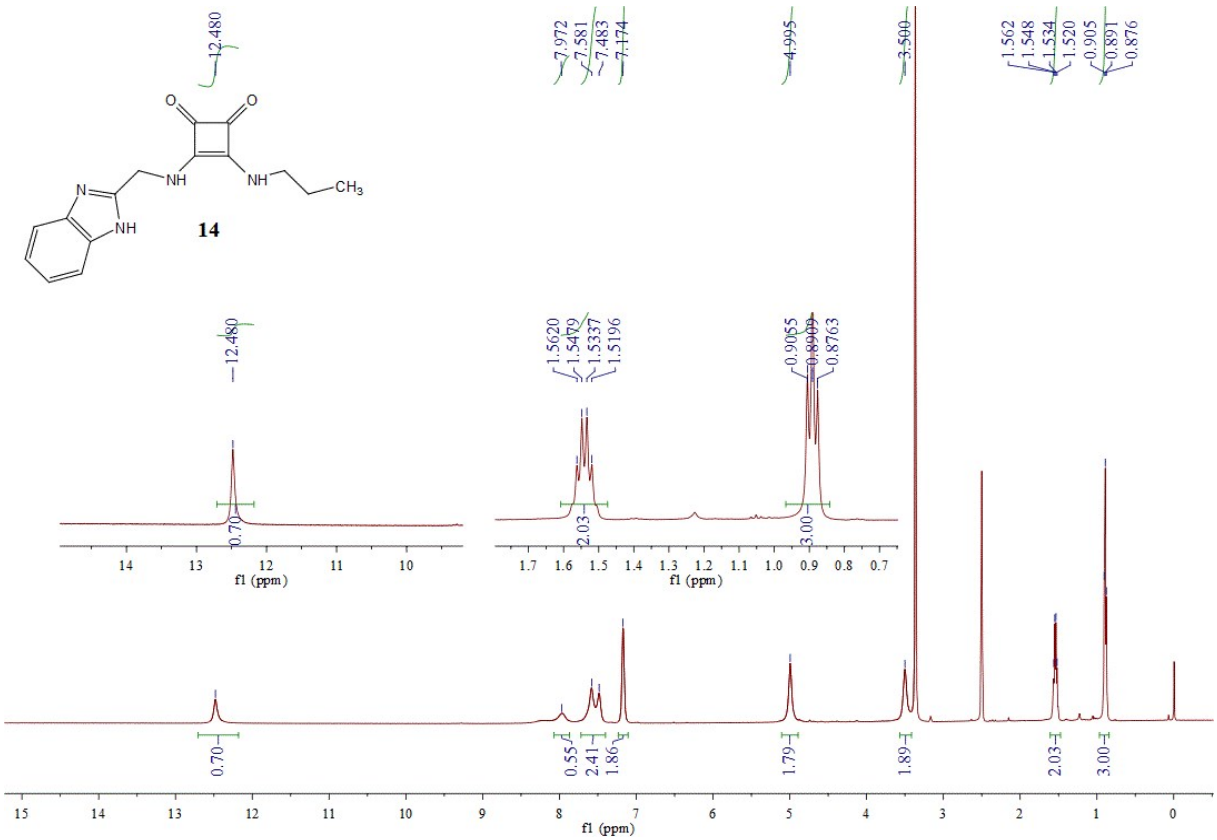

Fig. S53. ^{1}H NMR (DMSO-d_6, 500 MHz) of compound **14**.

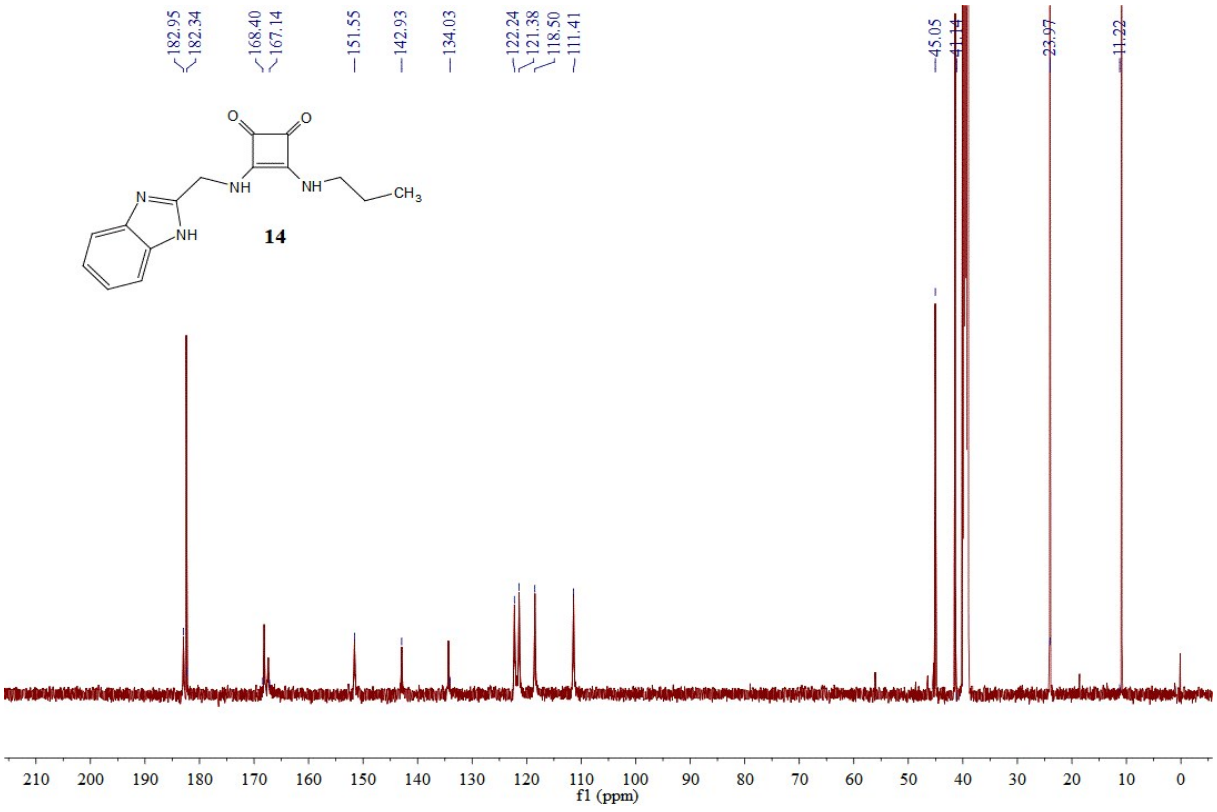

Fig. S54. ^{13}C NMR (DMSO-d_6, 125 MHz) of compound **14**.

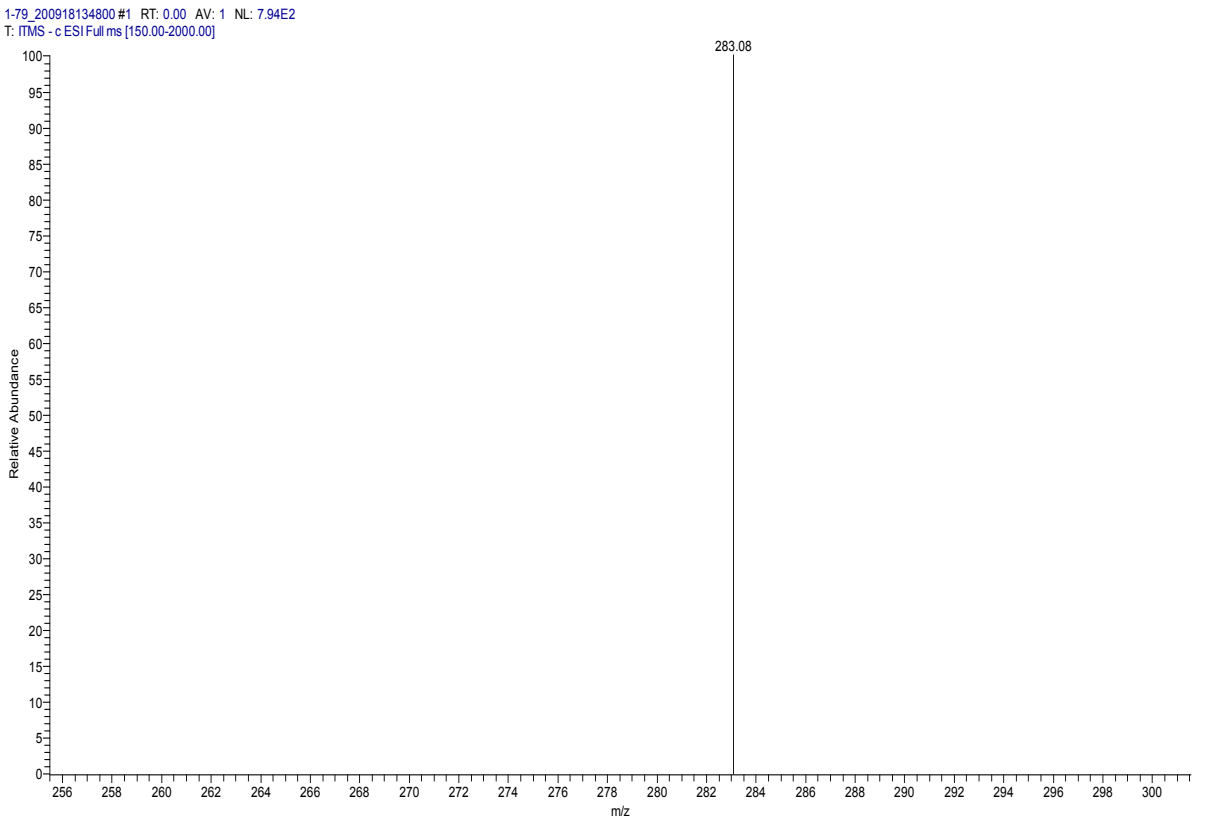

Fig. S55. Negative ESI-MS of compound **14**.

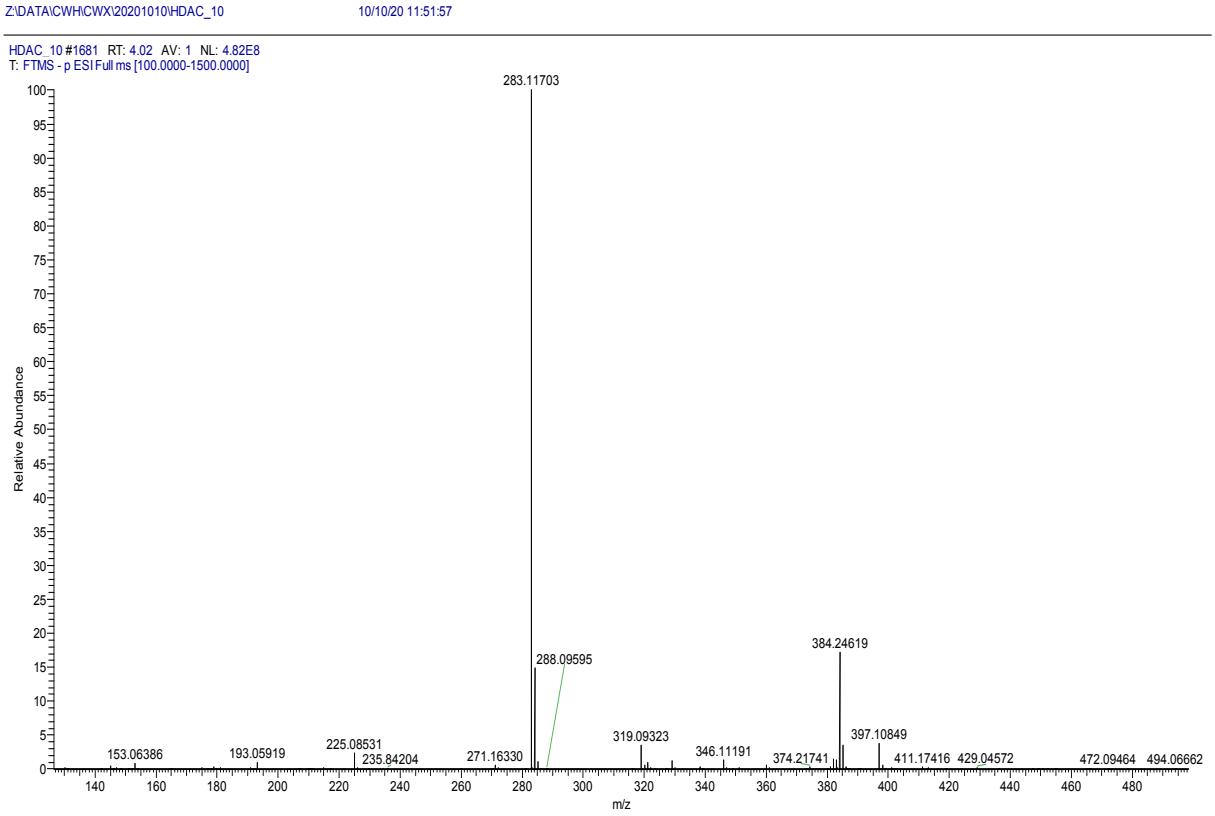

Fig. S56. Negative HR-ESI-MS of compound **14**.

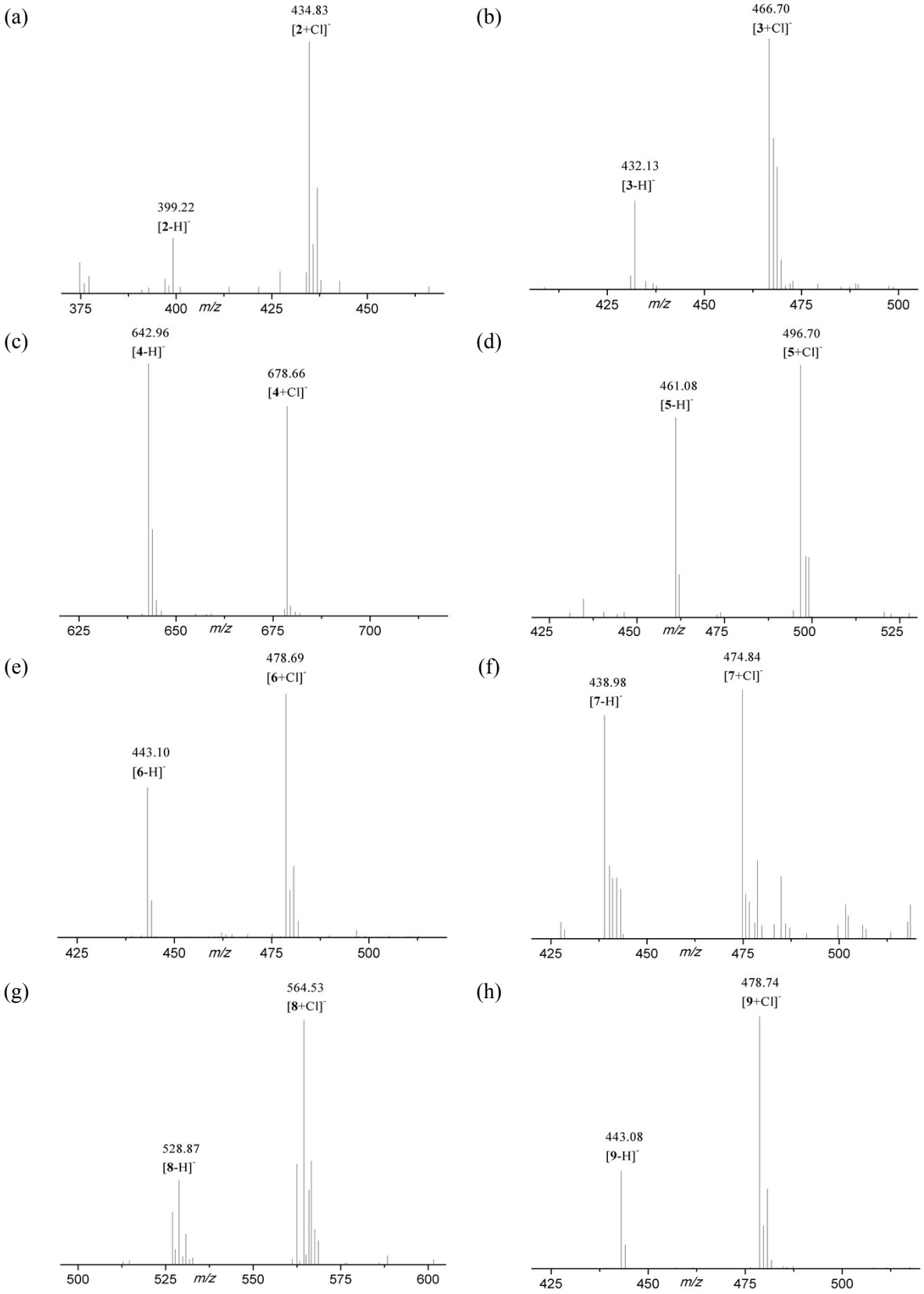

Fig. S57. Negative ESI MS spectra of compounds (a) **2**, (b) **3**, (c) **4**, (d) **5**, (e) **6**, (f) **7**, (g) **8** and (h) **9** (1.0×10^{-3} M) mixed with TBACl (1.5×10^{-2} M) in 4:1 CH_3CN-DMSO.

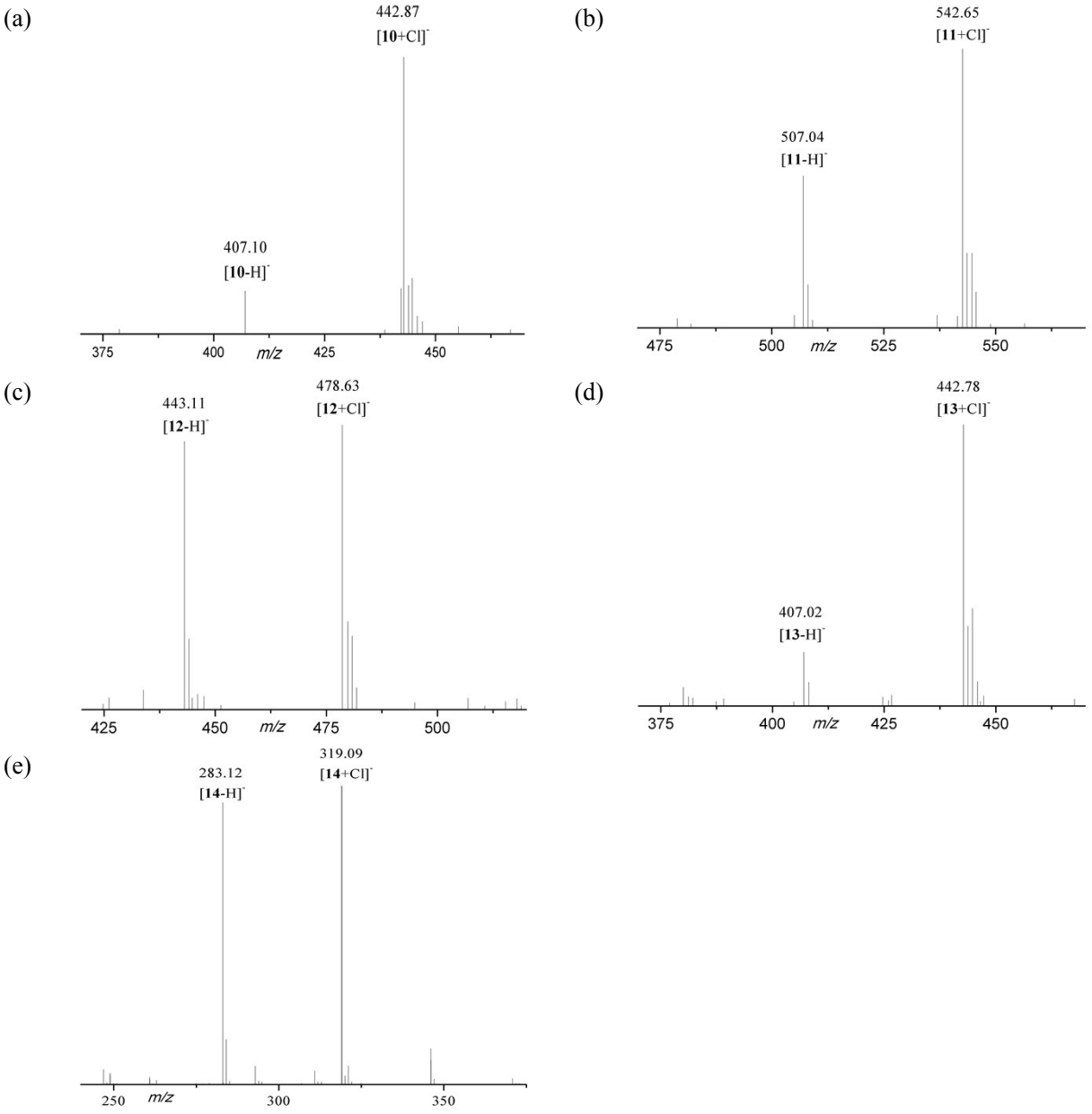

Fig. S58. Negative ESI MS spectra of compounds (a) **10**, (b) **11**, (c) **12**, (d) **13** and (e) **14** (1.0×10^{-3} M) mixed with TBACl (1.5×10^{-2} M) in 4:1 CH_3CN-DMSO.

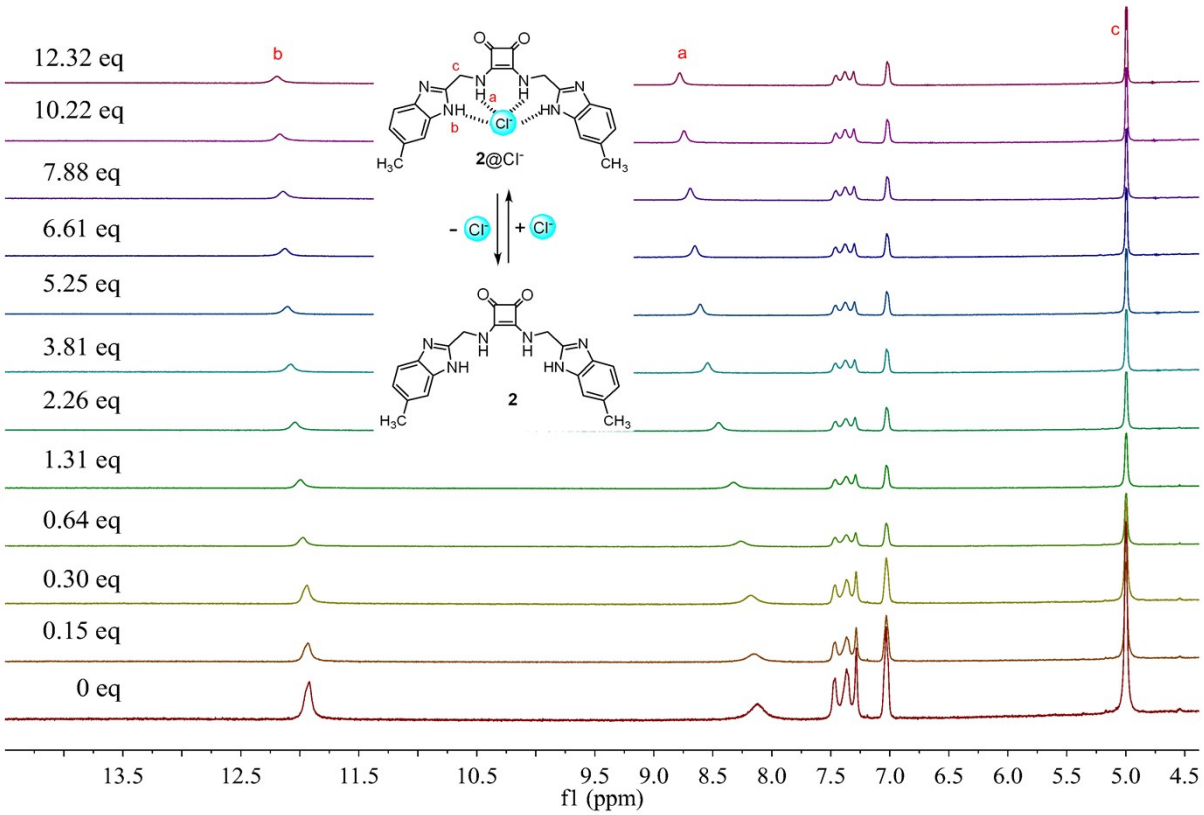

Fig. S59. ^{1}H NMR spectra (4:1 CD_3CN-DMSO-d_6, 500 MHz) of compound **2** (1.0×10^{-3} M) in the presence of TBACl of varying concentrations.

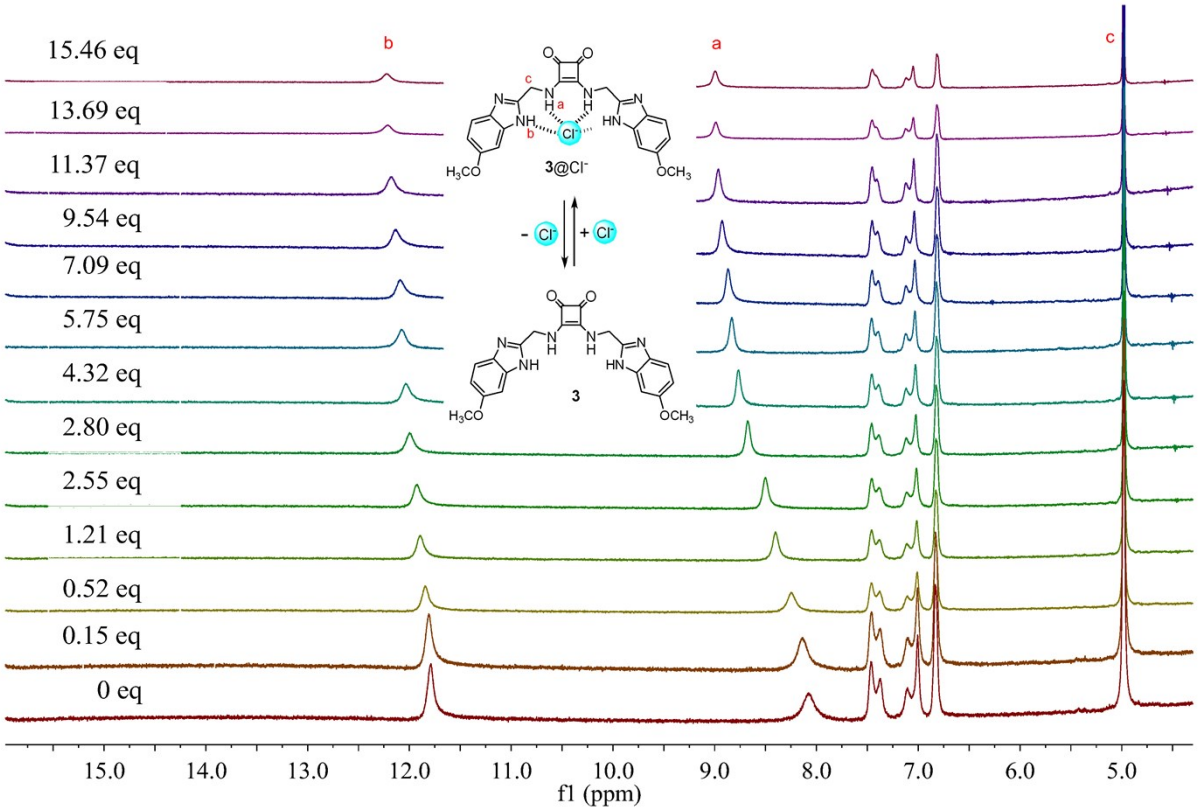

Fig. S60. ^{1}H NMR spectra (4:1 CD_3CN-DMSO-d_6, 500 MHz) of compound **3** (1.0×10^{-3} M) in the presence of TBACl of varying concentrations.

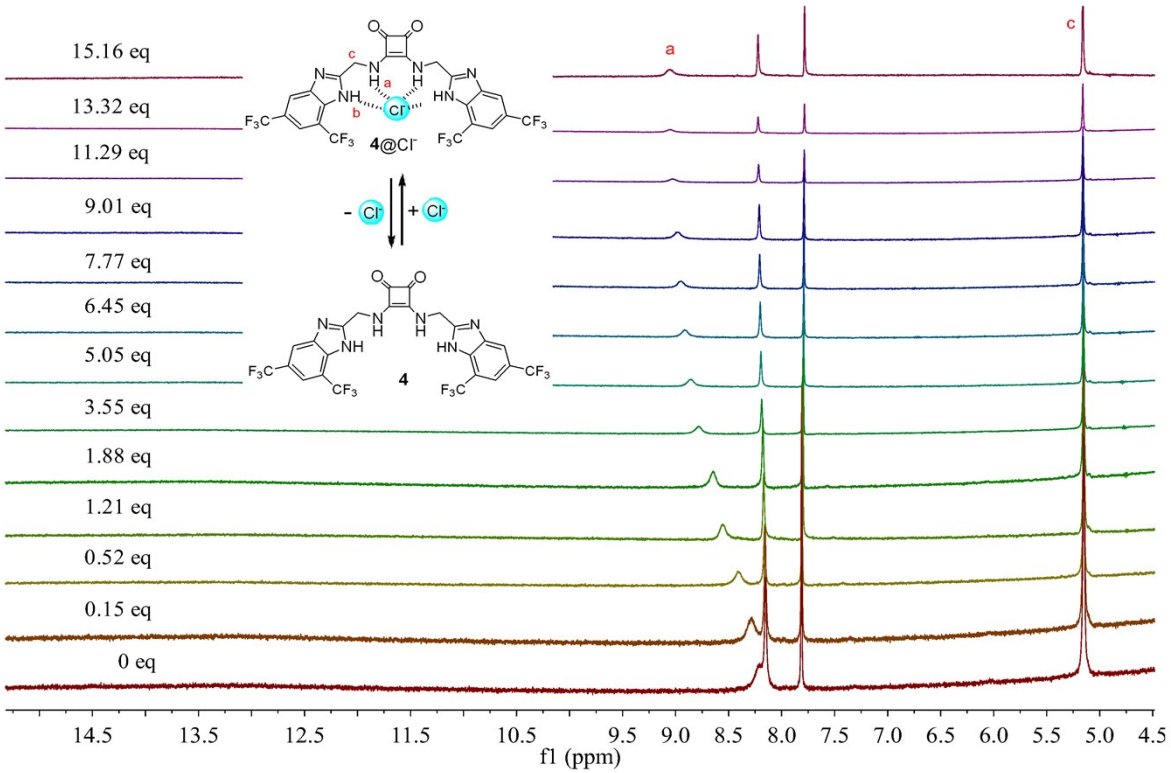

Fig. S61. ^{1}H NMR spectra (4:1 CD_3CN-DMSO-d_6, 500 MHz) of compound **4** (1.0×10^{-3} M) in the presence of TBACl of varying concentrations.

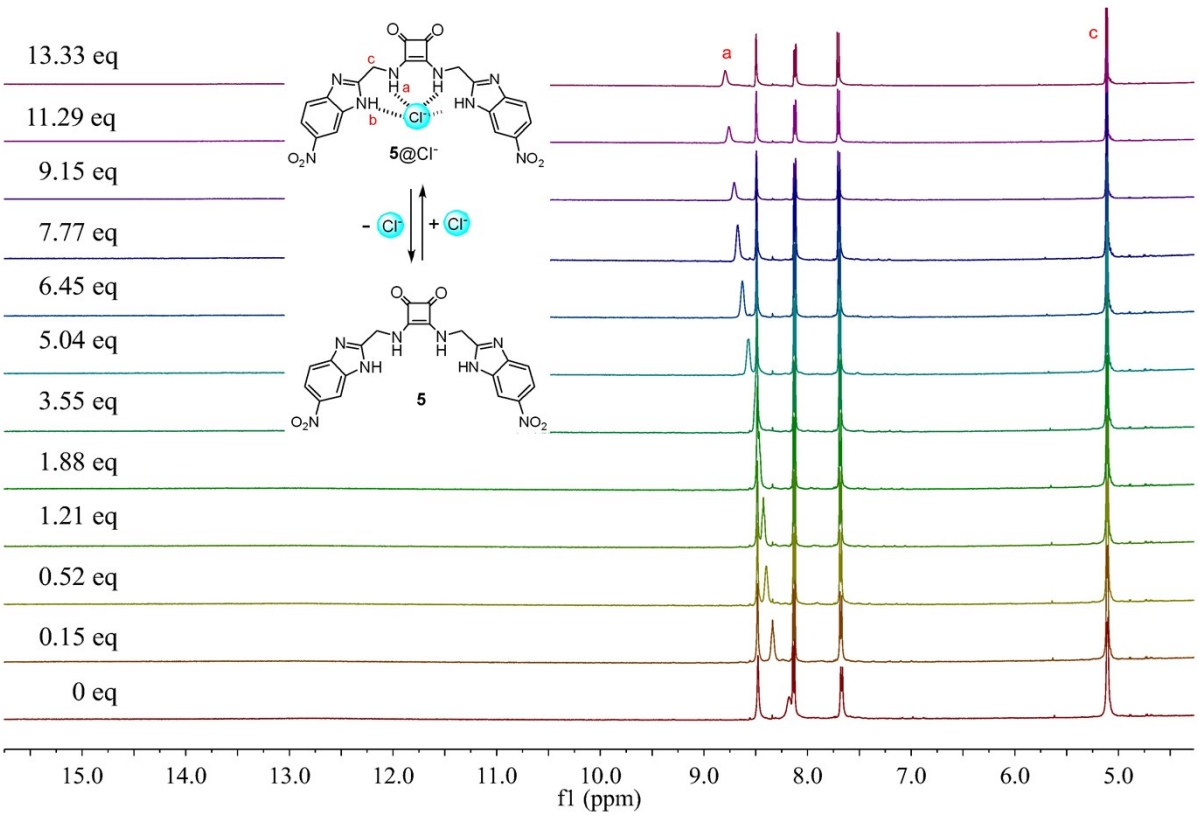

Fig. S62. ^{1}H NMR spectra (4:1 CD_3CN-DMSO-d_6, 500 MHz) of compound **5** (1.0×10^{-3} M) in the presence of TBACl of varying concentrations.

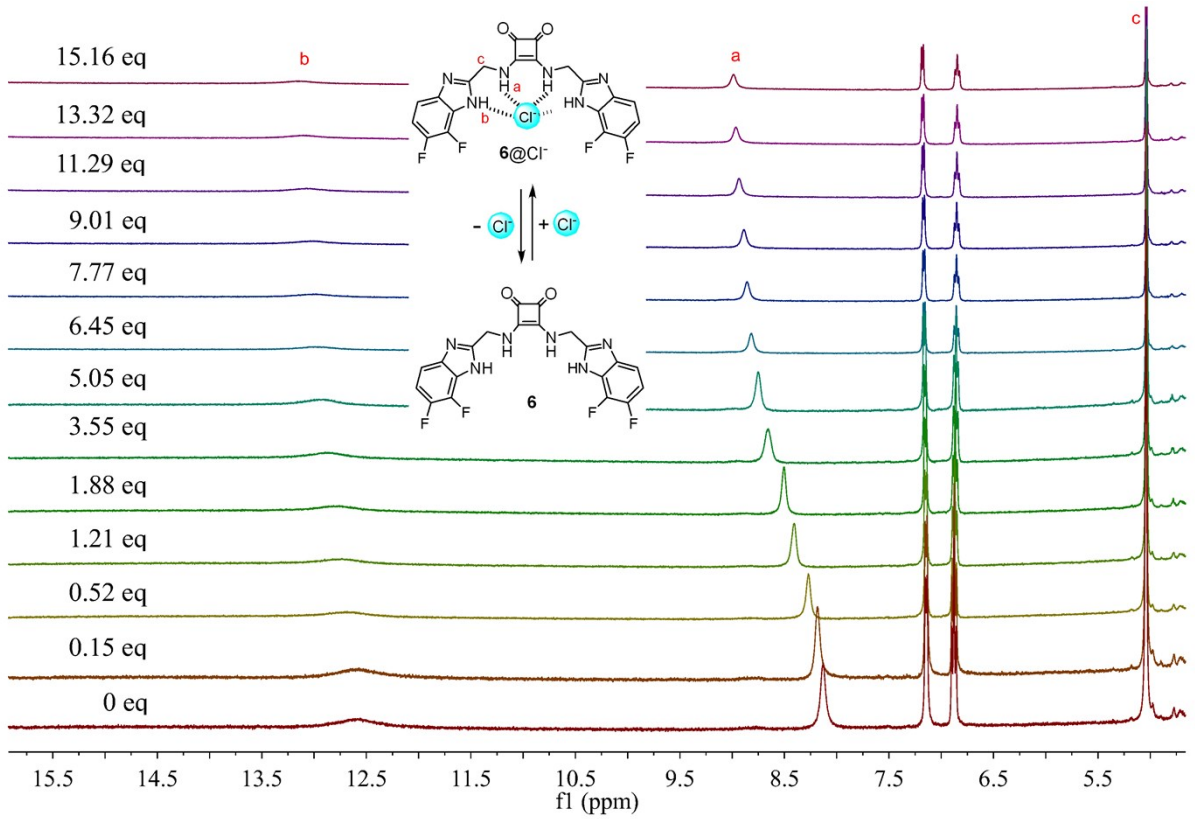

Fig. S63. ^{1}H NMR spectra (4:1 CD_3CN-DMSO-d_6, 500 MHz) of compound **6** (1.0×10^{-3} M) in the presence of TBACl of varying concentrations.

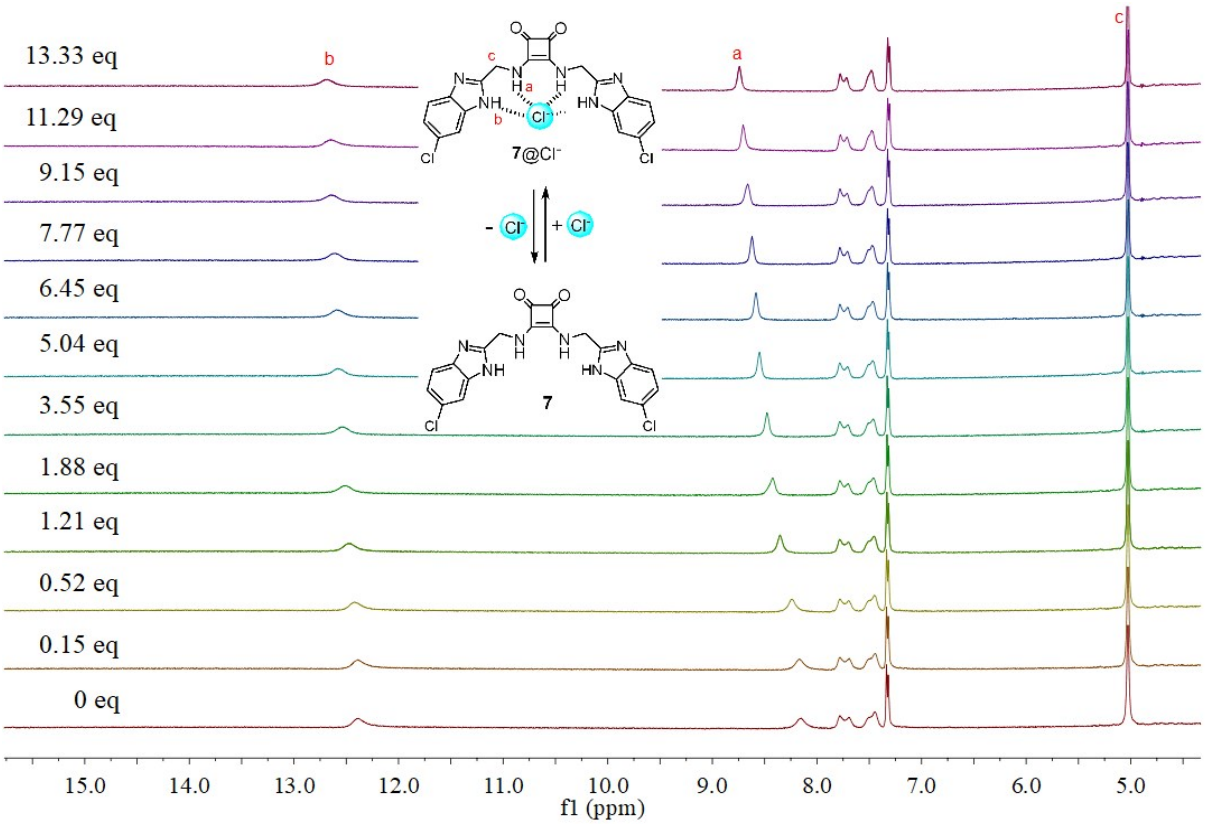

Fig. S64. ^{1}H NMR spectra (4:1 CD_3CN-DMSO-d_6, 500 MHz) of compound **7** (1.0×10^{-3} M) in the presence of TBACl of varying concentrations.

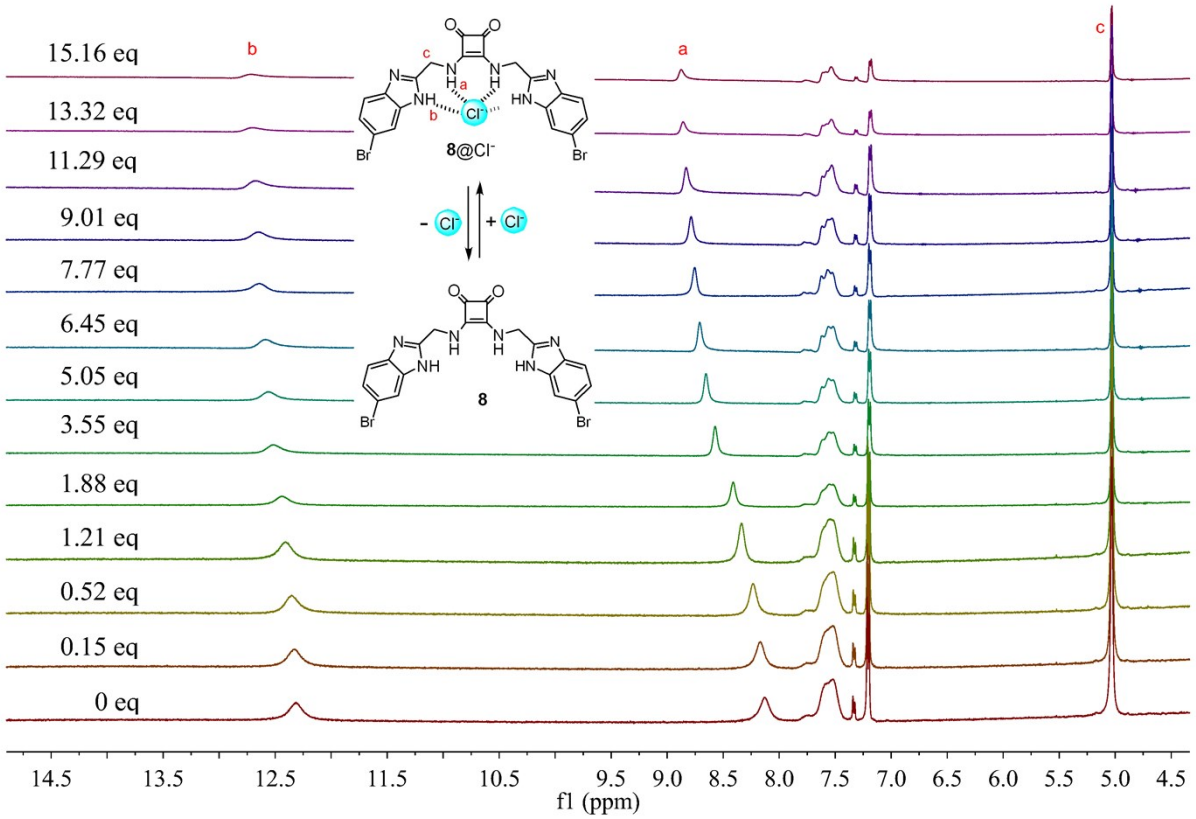

Fig. S65. ^{1}H NMR spectra (4:1 CD_3CN-DMSO-d_6, 500 MHz) of compound **8** (1.0×10^{-3} M) in the presence of TBACl of varying concentrations.

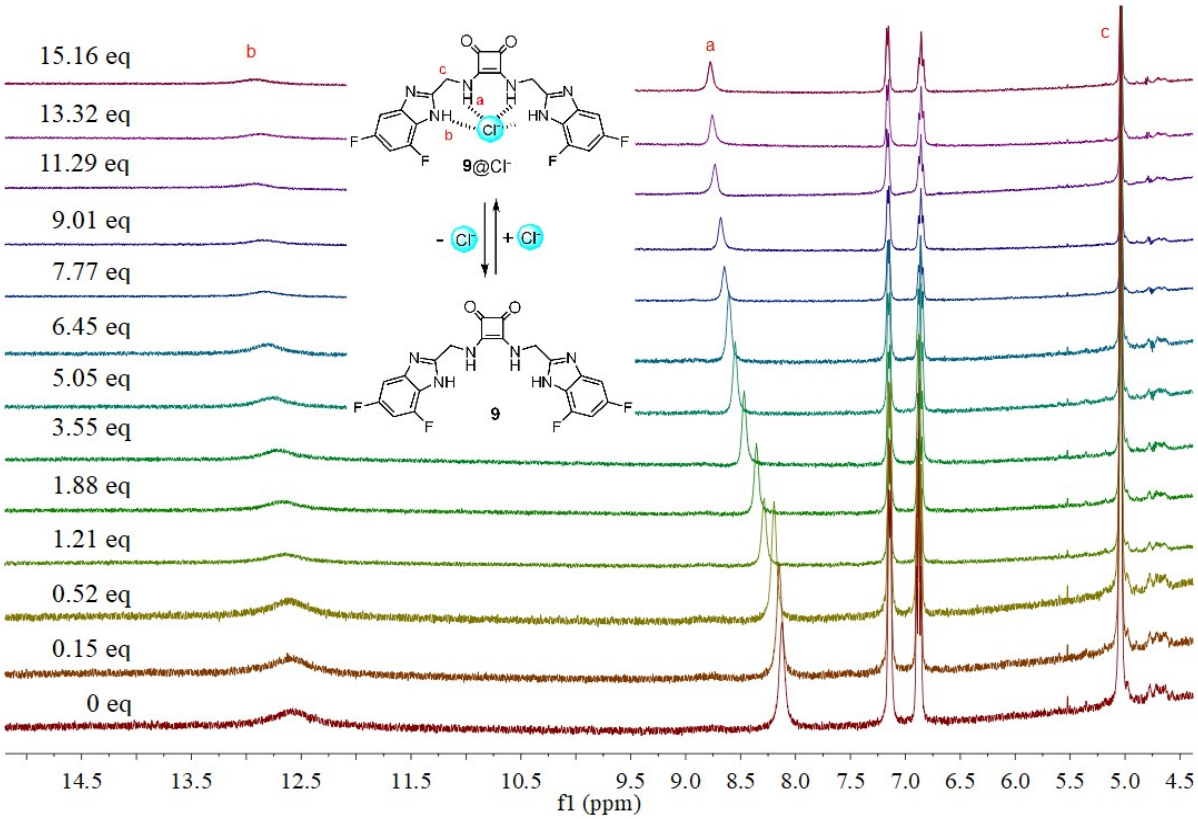

Fig. S66. ^{1}H NMR spectra (4:1 CD_3CN-DMSO-d_6, 500 MHz) of compound **9** (1.0×10^{-3} M) in the presence of TBACl of varying concentrations.

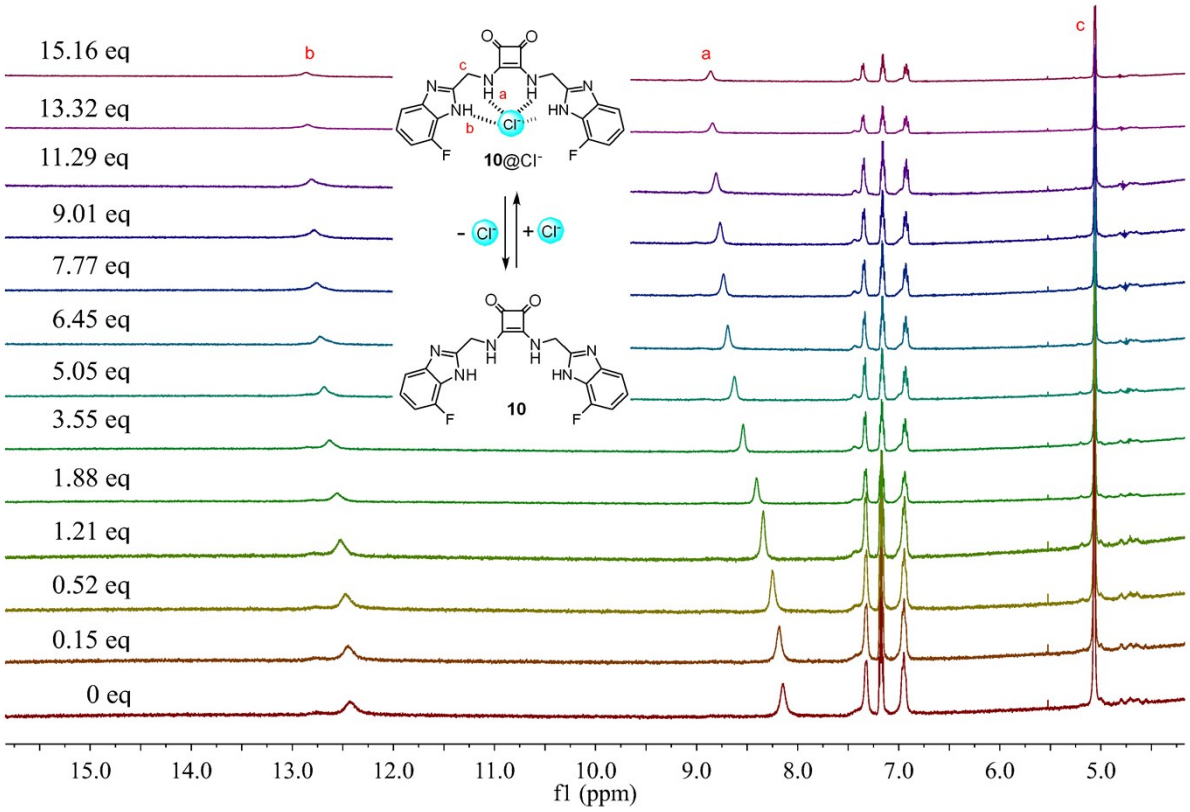

Fig. S67. ^{1}H NMR spectra (4:1 CD_3CN-DMSO-d_6, 500 MHz) of compound **10** (1.0×10^{-3} M) in the presence of TBACl of varying concentrations.

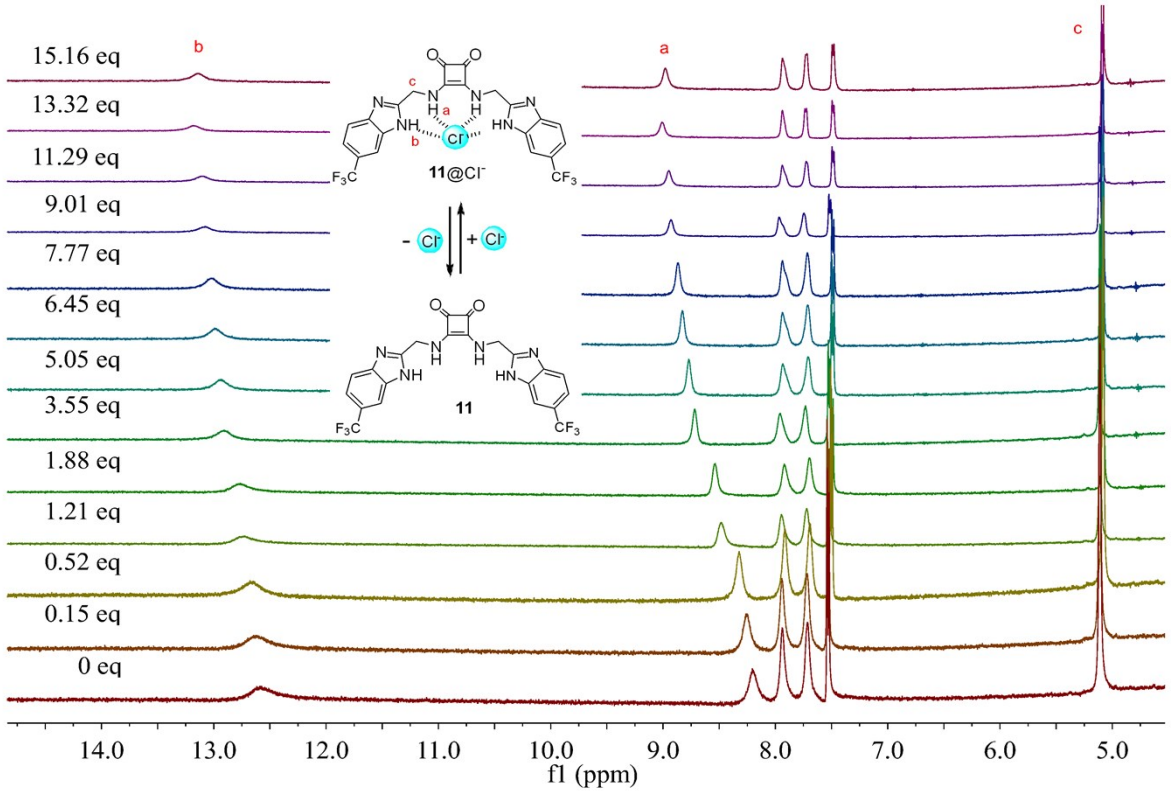

Fig. S68. ^{1}H NMR spectra (4:1 CD_3CN-DMSO-d_6, 500 MHz) of compound **11** (1.0×10^{-3} M) in the presence of TBACl of varying concentrations.

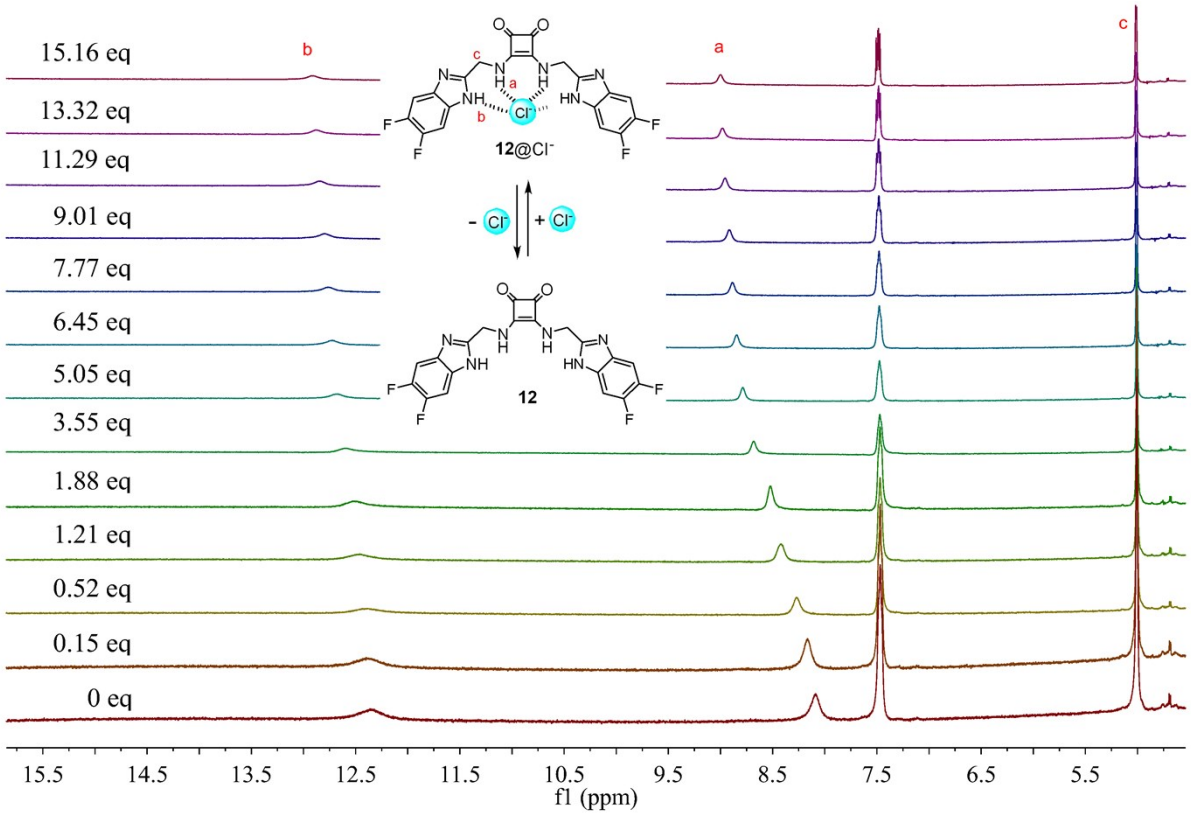

Fig. S69. ^{1}H NMR spectra (4:1 CD_3CN-DMSO-d_6, 500 MHz) of compound **12** (1.0×10^{-3} M) in the presence of TBACl of varying concentrations.

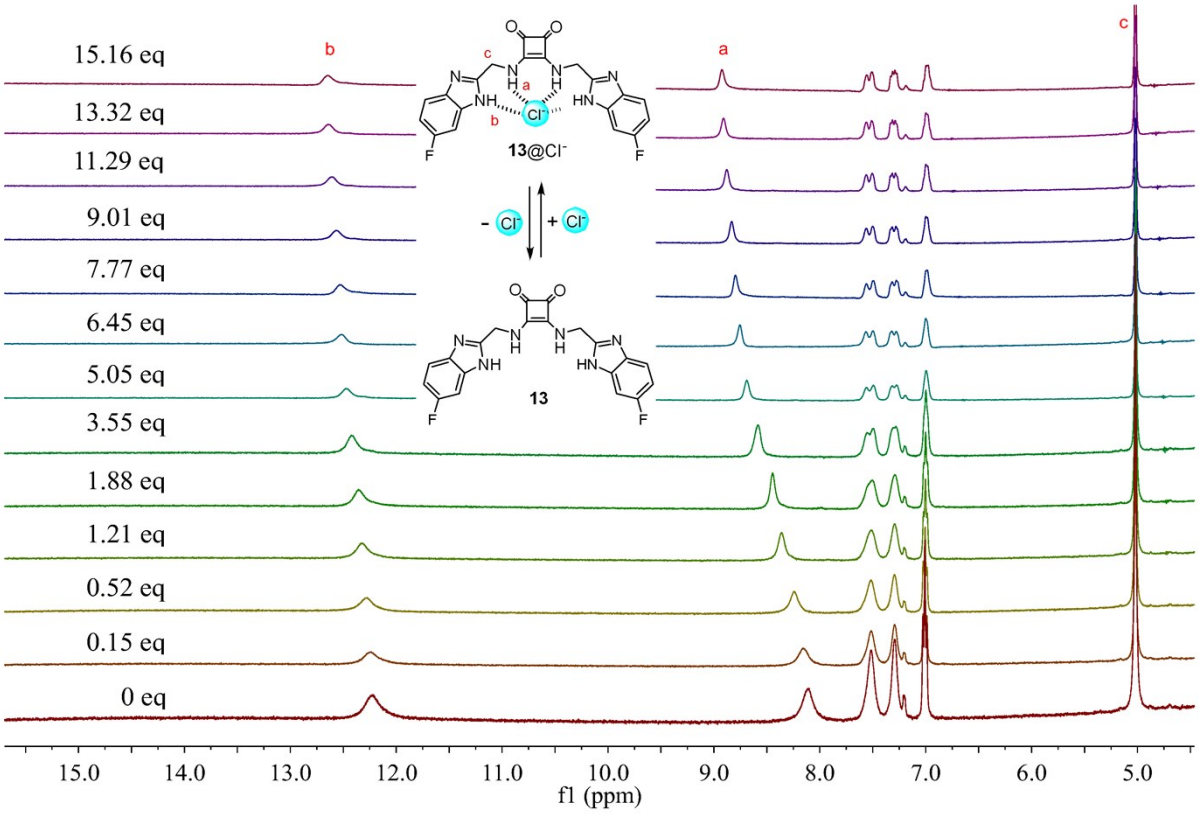

Fig. S70. ^{1}H NMR spectra (4:1 CD_3CN-DMSO-d_6, 500 MHz) of compound **13** (1.0×10^{-3} M) in the presence of TBACl of varying concentrations.

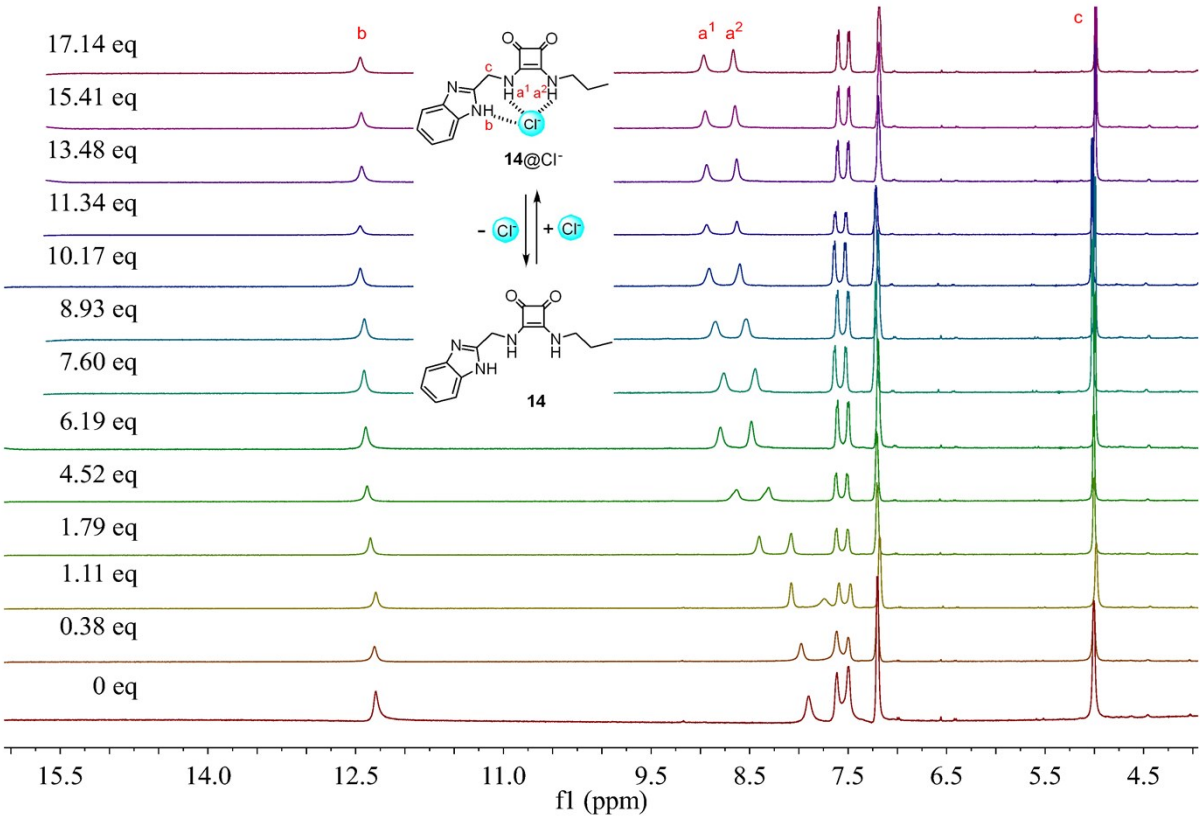

Fig. S71. ^{1}H NMR spectra (4:1 CD_3CN-DMSO-d_6, 500 MHz) of compound **14** (1.0×10^{-3} M) in the presence of TBACl of varying concentrations.

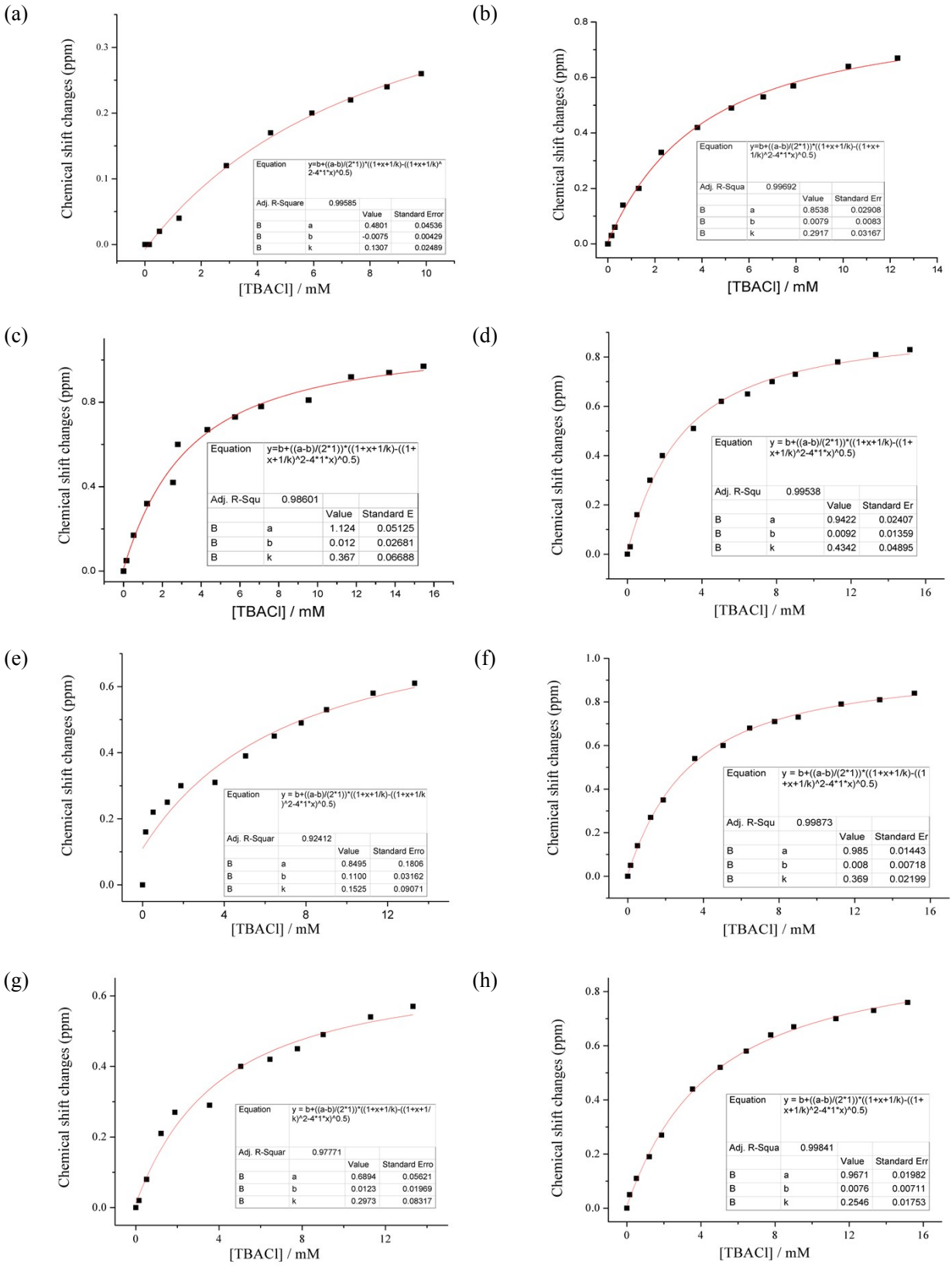

Fig. S72. Fitting binding isotherms of compounds (a) **1**, (b) **2**, (c) **3**, (d) **4**, (e) **5**, (f) **6**, (g) **7** and (h) **8** (1.0×10^{-3} M) showing the changes in chemical shifts for the squaramido NHs, fitted to the 1:1 binding model.

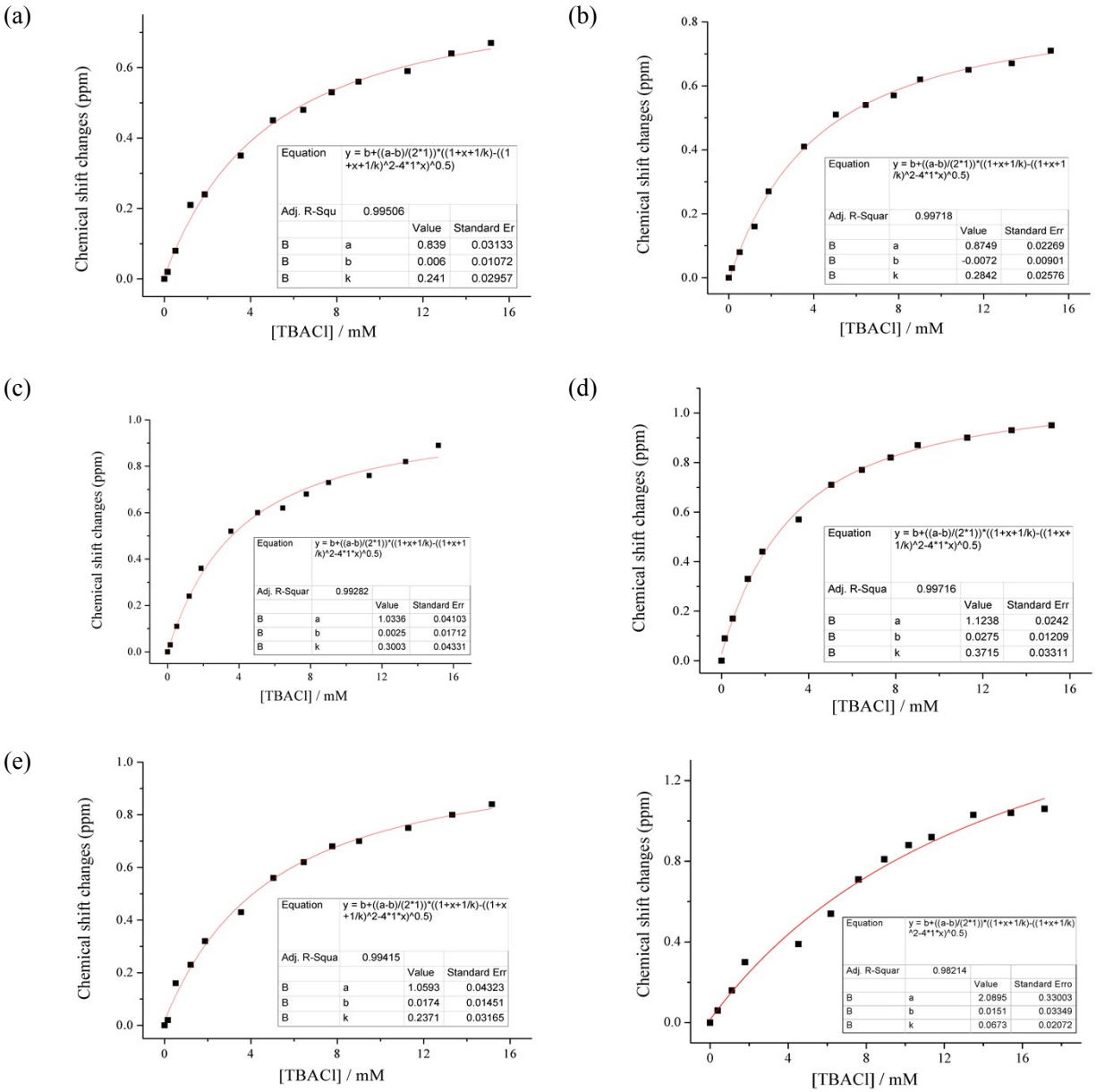

Fig. S73. Fitting binding isotherms of compounds (a) **9**, (b) **10**, (c) **11**, (d) **12**, (e) **13** and (f) **14** (1.0×10^{-3} M) showing the changes in chemical shifts for the squaramido NHs, fitted to the 1:1 binding model.

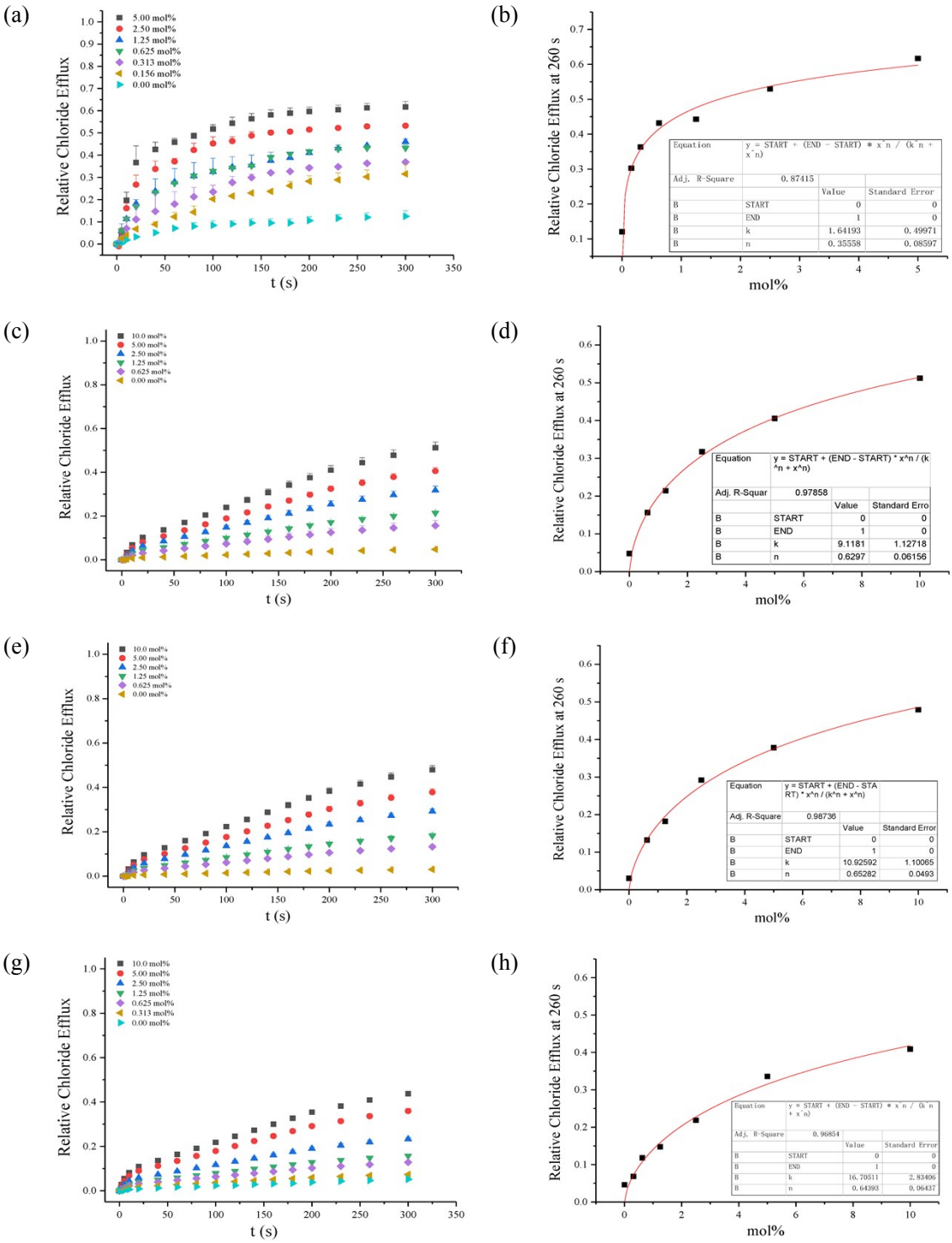

Fig. S74. (a, c, e, g) Typical plots of the chloride efflux against time in the presence of compound **1** of varying concentrations at pH 4.0 (a), 5.0 (c), 6.0 (e) and 7.0 (g). (b, d, f, h) Dose-response plots of the relative chloride efflux at 260 s *versus* the mol% concentrations of compound **1** in EYPC liposomes at pH 4.0 (b), 5.0 (d), 6.0 (f) and 7.0 (h).

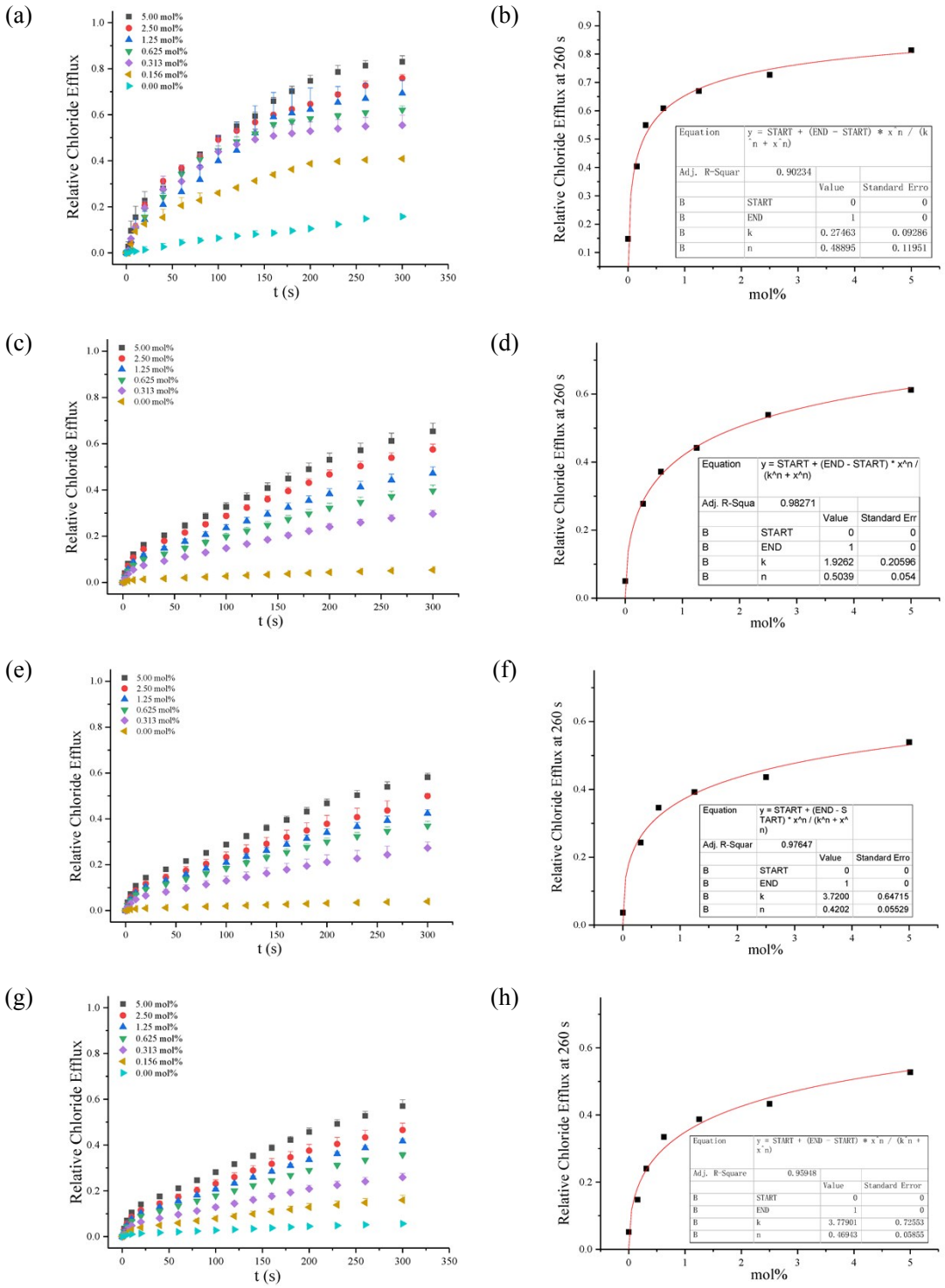

Fig. S75. (a, c, e, g) Typical plots of the chloride efflux against time in the presence of compound **2** of varying concentrations at pH 4.0 (a), 5.0 (c), 6.0 (e) and 7.0 (g). (b, d, f, h) Dose-response plots of the relative chloride efflux at 260 s *versus* the mol% concentrations of compound **2** in EYPC liposomes at pH 4.0 (b), 5.0 (d), 6.0 (f) and 7.0 (h).

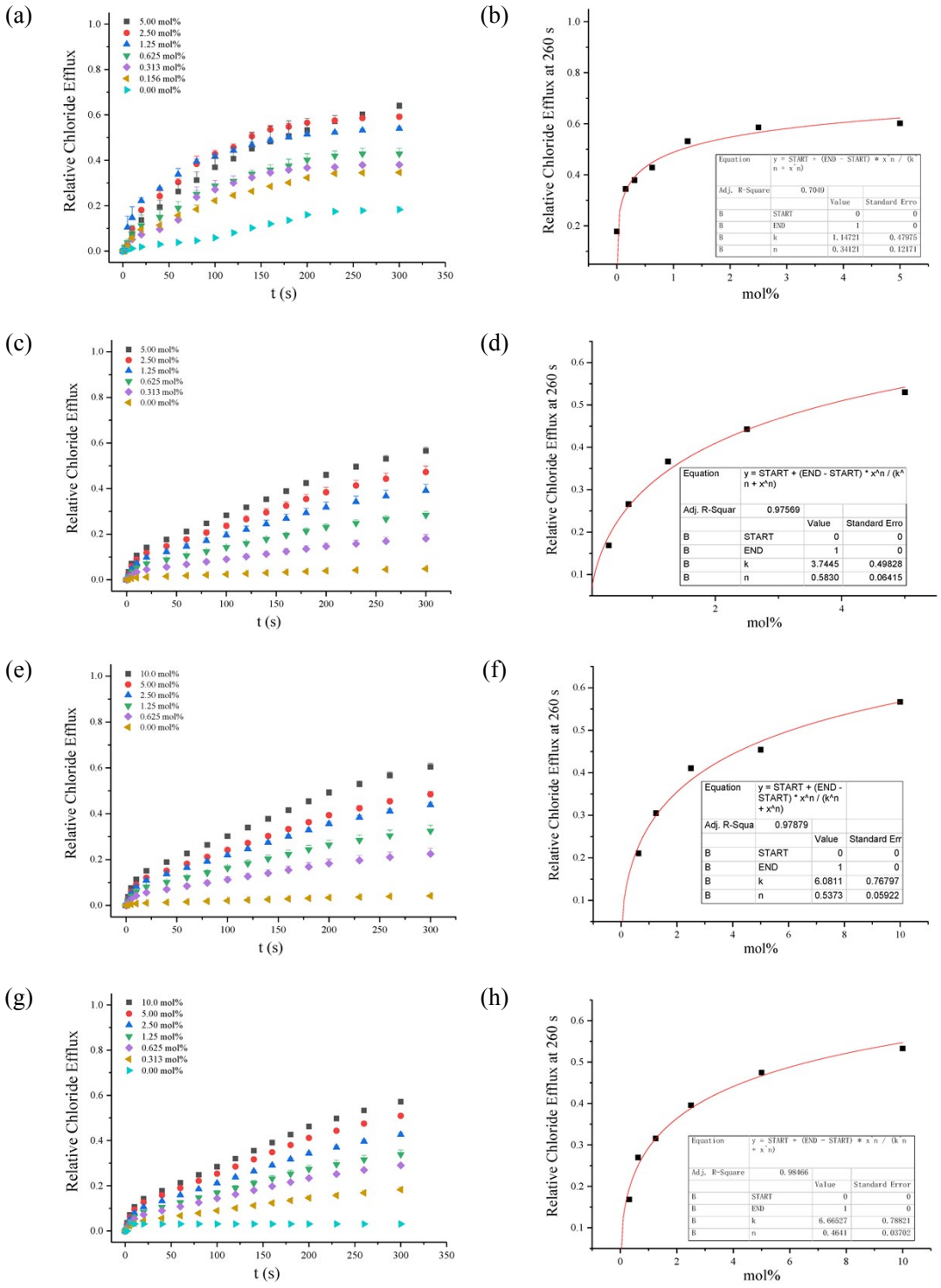

Fig. S76. (a, c, e, g) Typical plots of the chloride efflux against time in the presence of compound **3** of varying concentrations at pH 4.0 (a), 5.0 (c), 6.0 (e) and 7.0 (g). (b, d, f, h) Dose-response plots of the relative chloride efflux at 260 s *versus* the mol% concentrations of compound **3** in EYPC liposomes at pH 4.0 (b), 5.0 (d), 6.0 (f) and 7.0 (h).

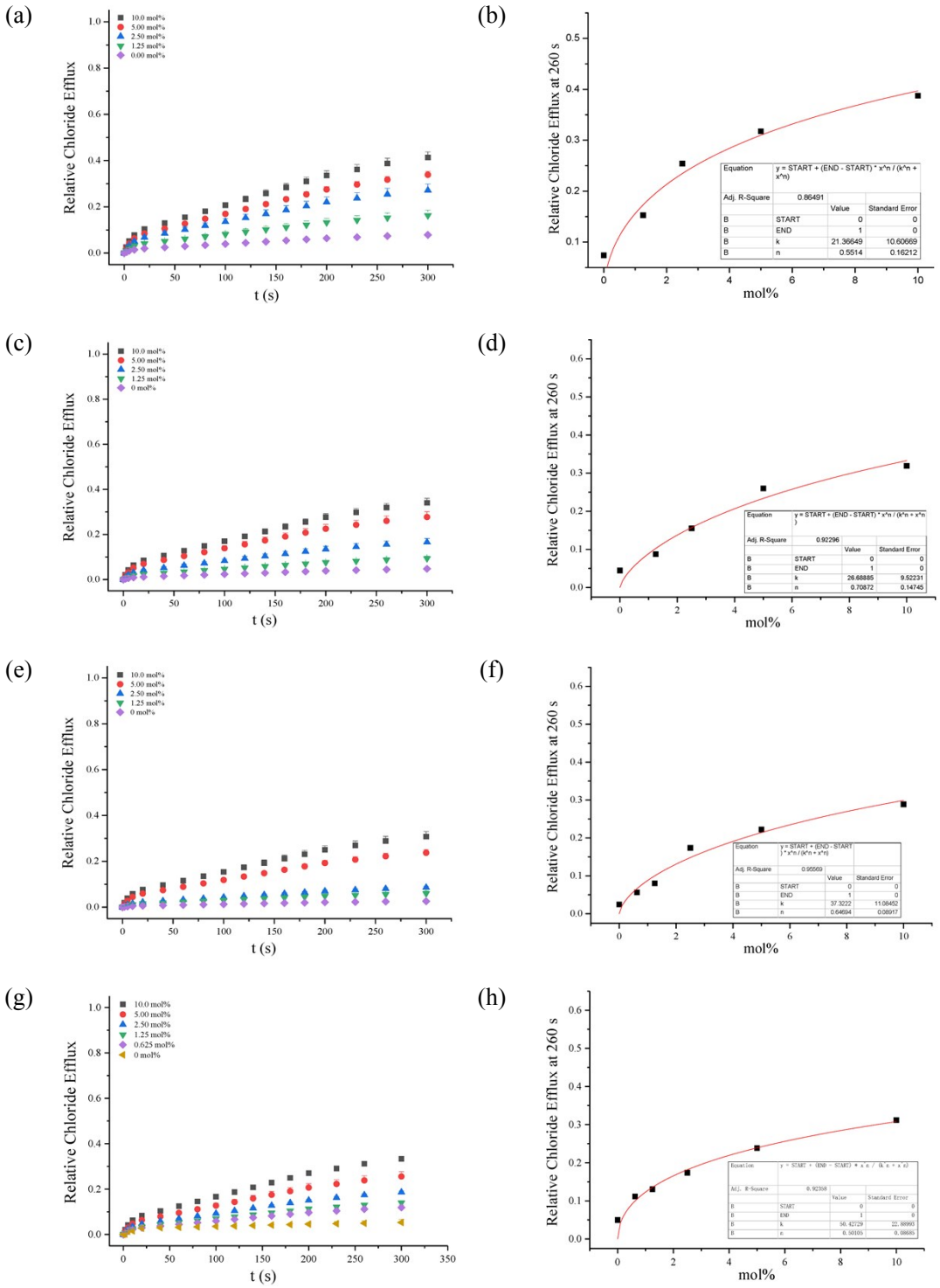

Fig. S77. (a, c, e, g) Typical plots of the chloride efflux against time in the presence of compound **4** of varying concentrations at pH 4.0 (a), 5.0 (c), 6.0 (e) and 7.0 (g). (b, d, f, h) Dose-response plots of the relative chloride efflux at 260 s *versus* the mol% concentrations of compound **4** in EYPC liposomes at pH 4.0 (b), 5.0 (d), 6.0 (f) and 7.0 (h).

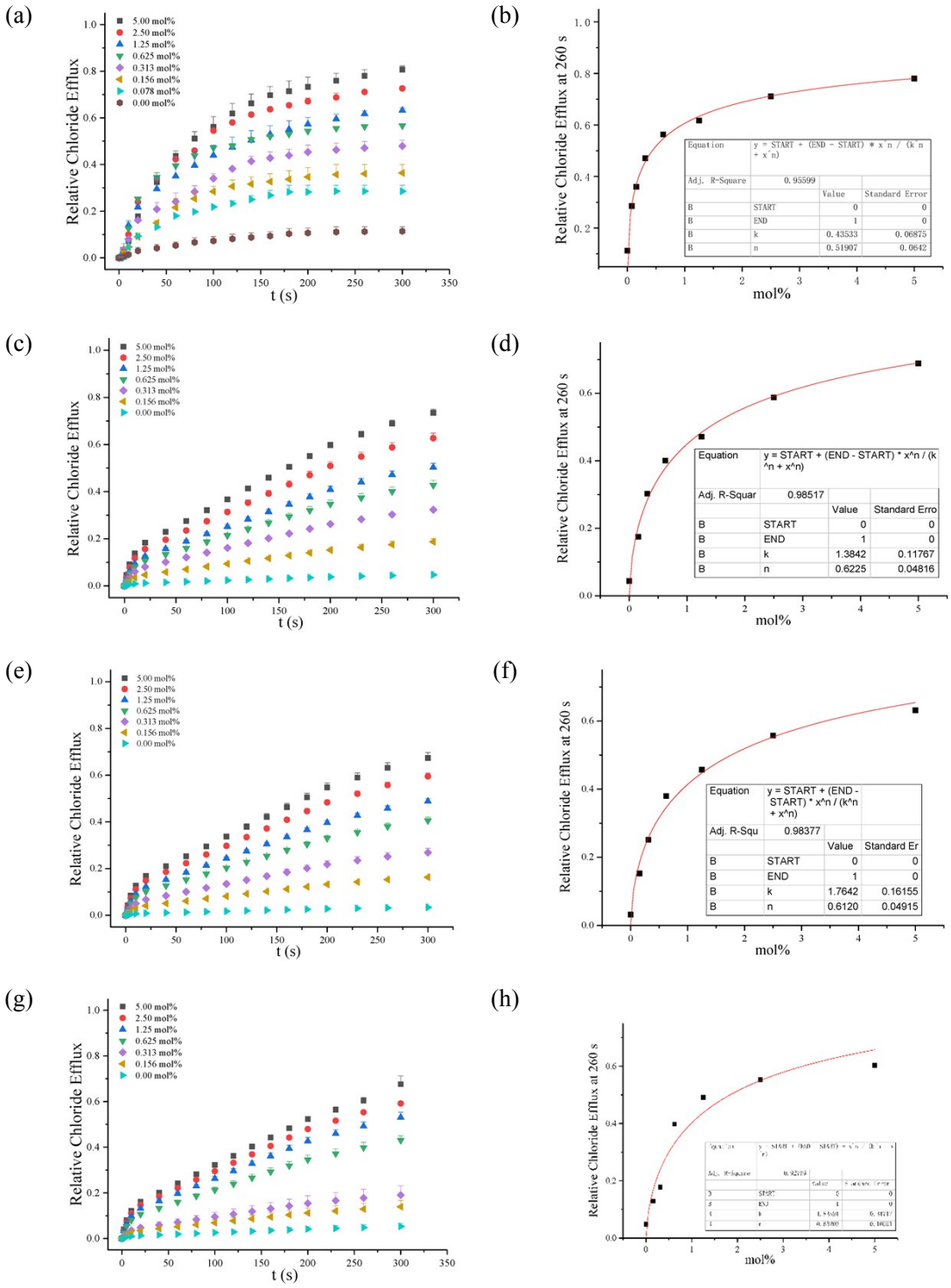

Fig. S78. (a, c, e, g) Typical plots of the chloride efflux against time in the presence of compound **5** of varying concentrations at pH 4.0 (a), 5.0 (c), 6.0 (e) and 7.0 (g). (b, d, f, h) Dose-response plots of the relative chloride efflux at 260 s *versus* the mol% concentrations of compound **5** in EYPC liposomes at pH 4.0 (b), 5.0 (d), 6.0 (f) and 7.0 (h).

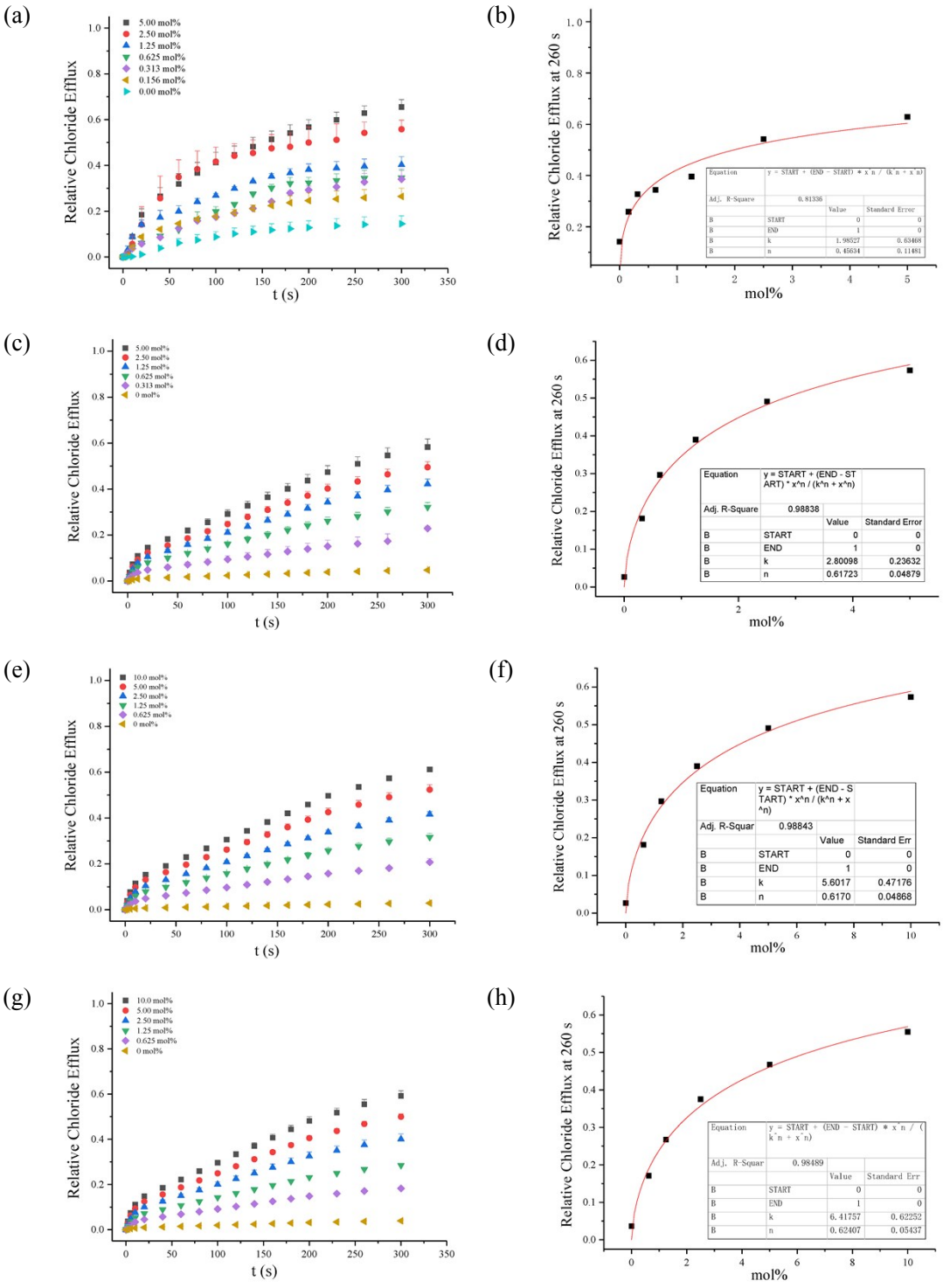

Fig. S79. (a, c, e, g) Typical plots of the chloride efflux against time in the presence of compound **6** of varying concentrations at pH 4.0 (a), 5.0 (c), 6.0 (e) and 7.0 (g). (b, d, f, h) Dose-response plots of the relative chloride efflux at 260 s *versus* the mol% concentrations of compound **6** in EYPC liposomes at pH 4.0 (b), 5.0 (d), 6.0 (f) and 7.0 (h).

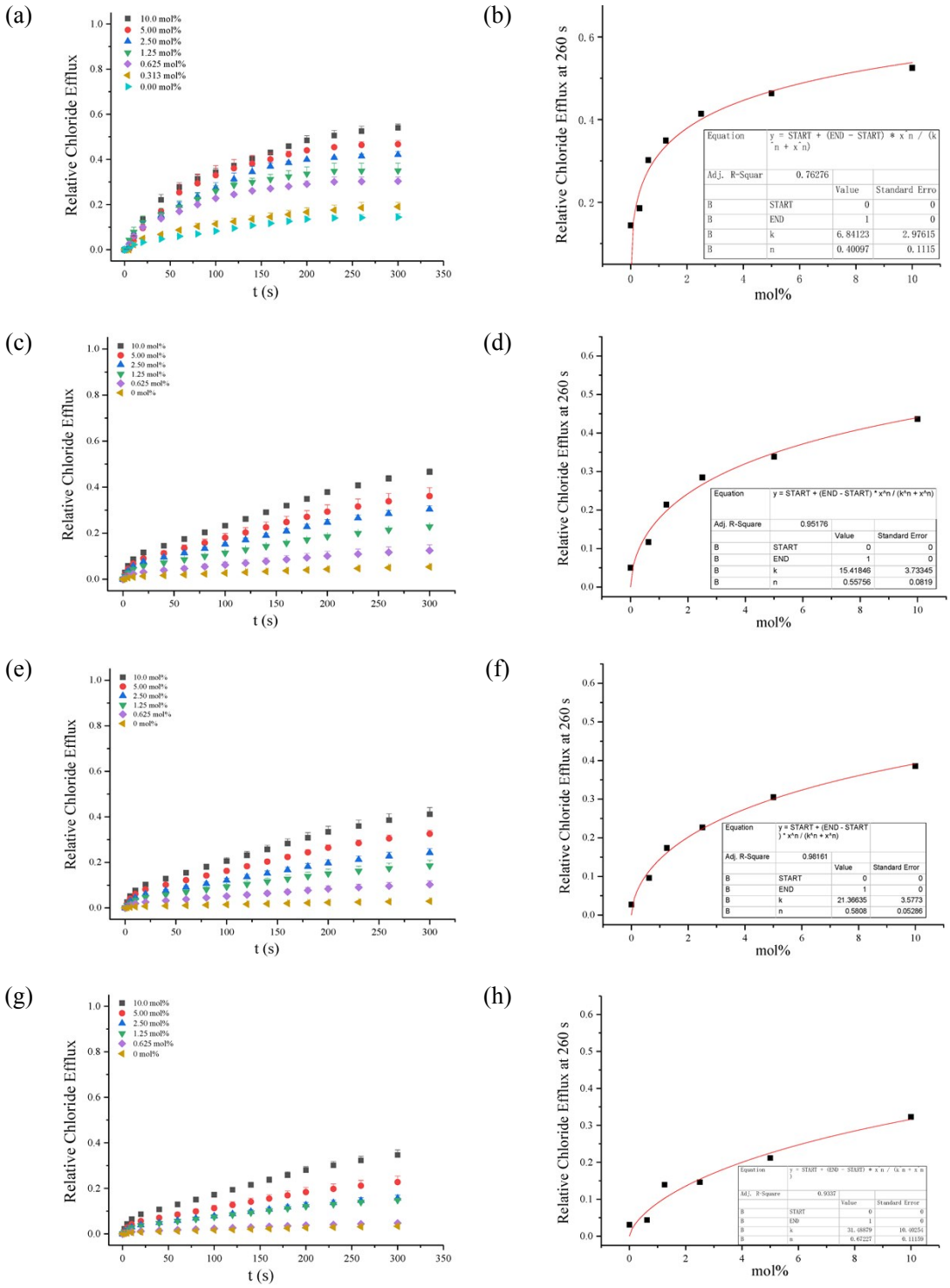

Fig. S80. (a, c, e, g) Typical plots of the chloride efflux against time in the presence of compound **7** of varying concentrations at pH 4.0 (a), 5.0 (c), 6.0 (e) and 7.0 (g). (b, d, f, h) Dose-response plots of the relative chloride efflux at 260 s *versus* the mol% concentrations of compound **7** in EYPC liposomes at pH 4.0 (b), 5.0 (d), 6.0 (f) and 7.0 (h).

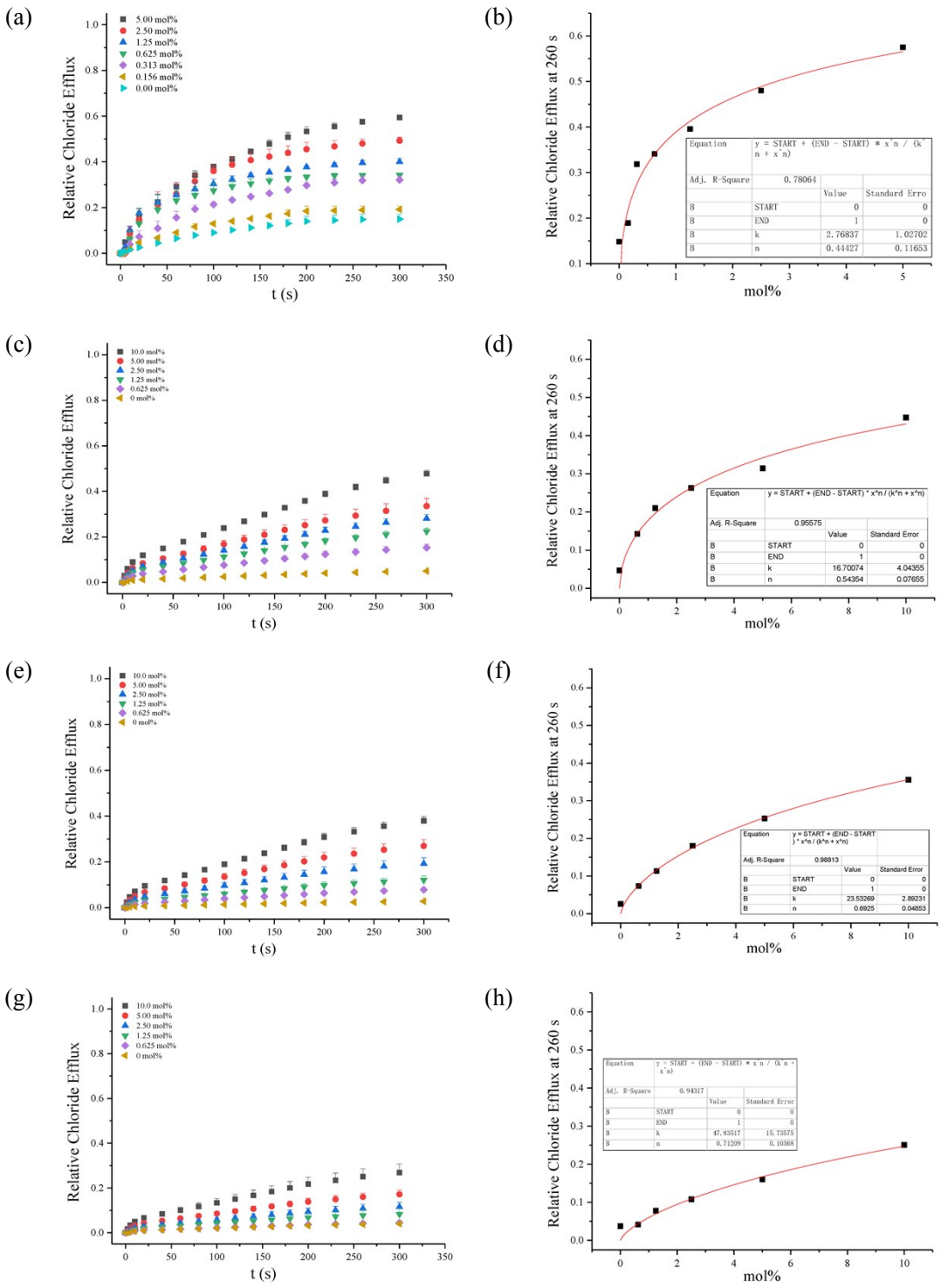

Fig. S81. (a, c, e, g) Typical plots of the chloride efflux against time in the presence of compound **8** of varying concentrations at pH 4.0 (a), 5.0 (c), 6.0 (e) and 7.0 (g). (b, d, f, h) Dose-response plots of the relative chloride efflux at 260 s *versus* the mol% concentrations of compound **8** in EYPC liposomes at pH 4.0 (b), 5.0 (d), 6.0 (f) and 7.0 (h).

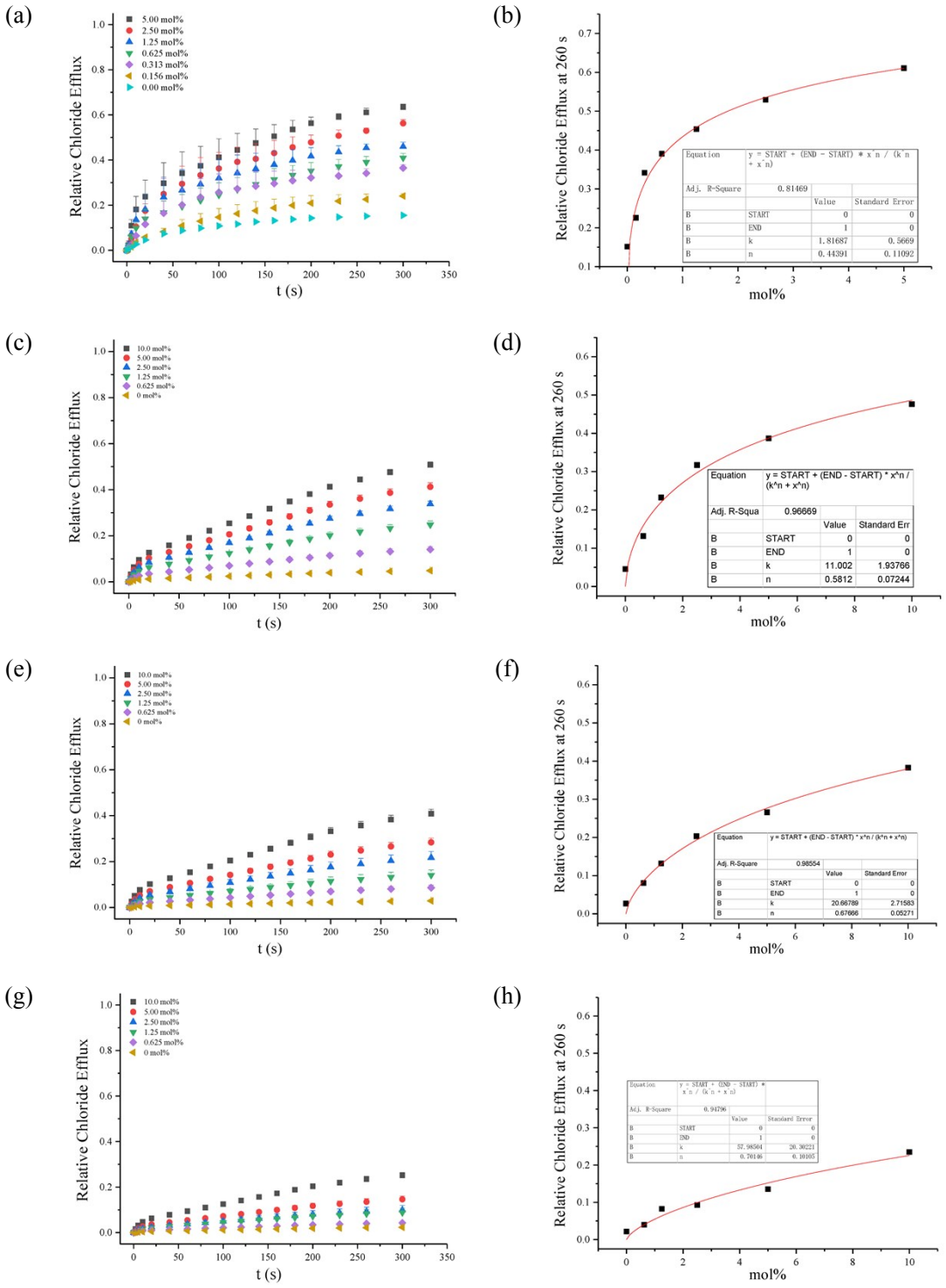

Fig. S82. (a, c, e, g) Typical plots of the chloride efflux against time in the presence of compound **9** of varying concentrations at pH 4.0 (a), 5.0 (c), 6.0 (e) and 7.0 (g). (b, d, f, h) Dose-response plots of the relative chloride efflux at 260 s *versus* the mol% concentrations of compound **9** in EYPC liposomes at pH 4.0 (b), 5.0 (d), 6.0 (f) and 7.0 (h).

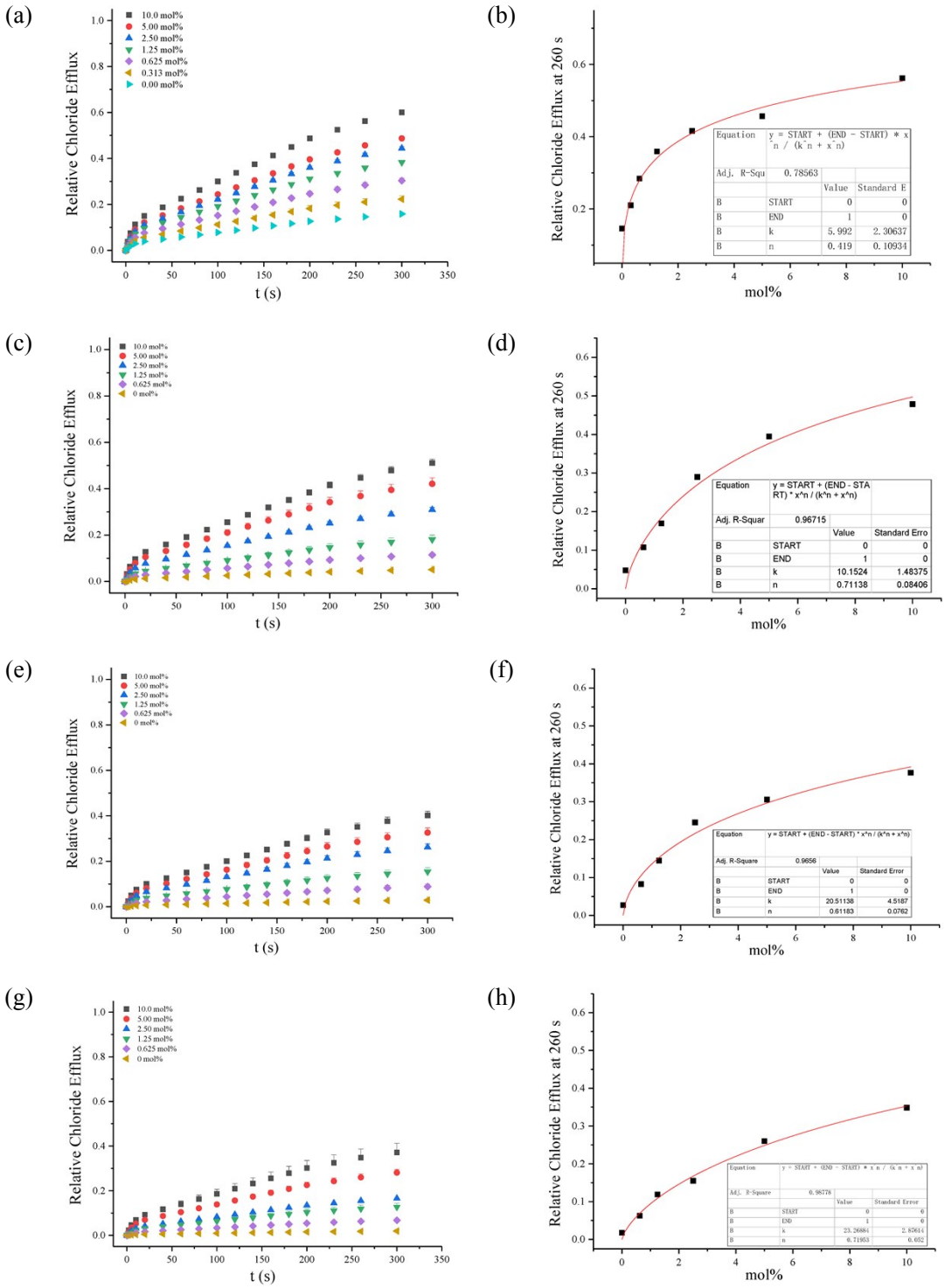

Fig. S83. (a, c, e, g) Typical plots of the chloride efflux against time in the presence of compound **10** of varying concentrations at pH 4.0 (a), 5.0 (c), 6.0 (e) and 7.0 (g). (b, d, f, h) Dose-response plots of the relative chloride efflux at 260 s *versus* the mol% concentrations of compound **10** in EYPC liposomes at pH 4.0 (b), 5.0 (d), 6.0 (f) and 7.0 (h).

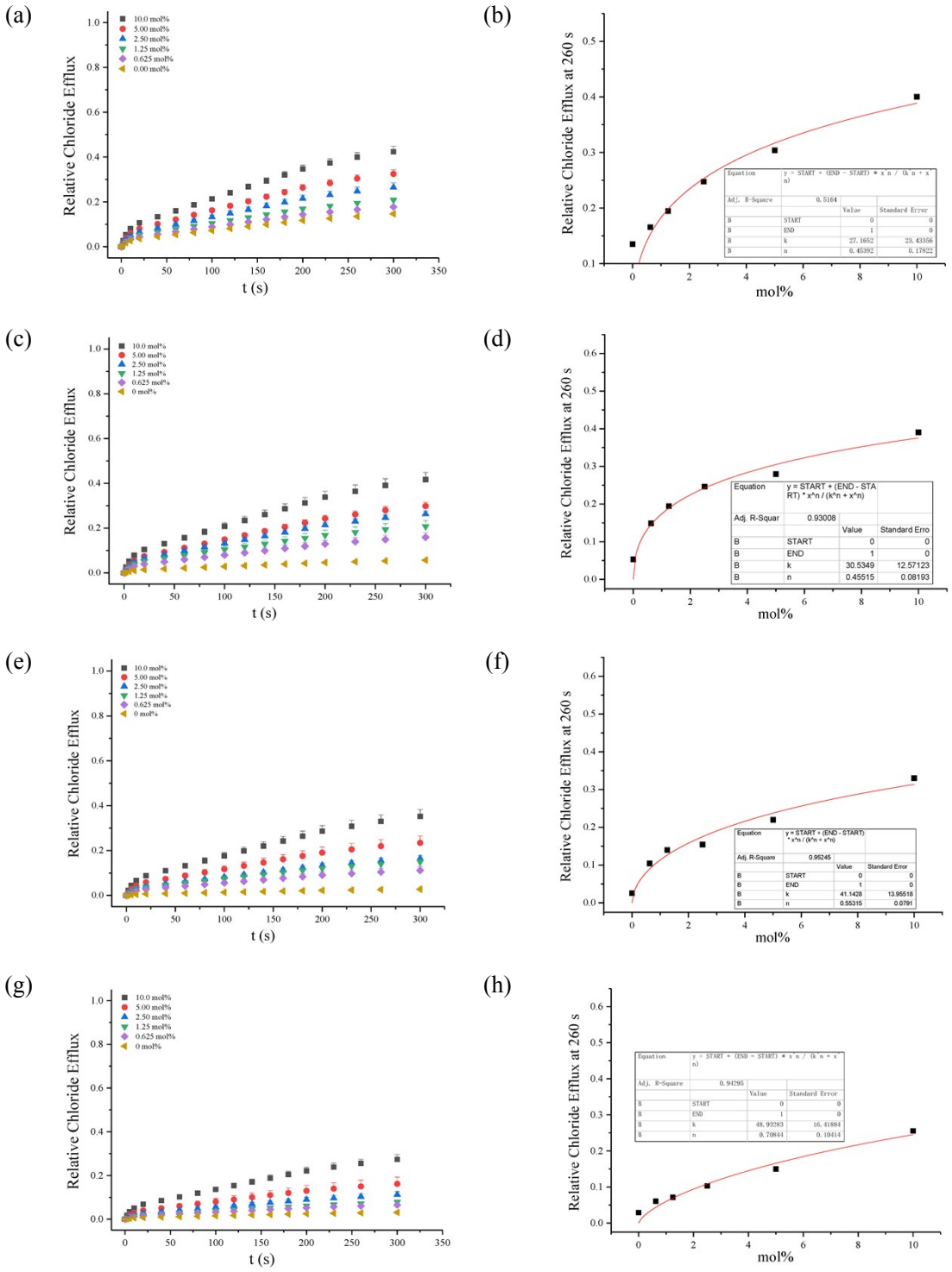

Fig. S84. (a, c, e, g) Typical plots of the chloride efflux against time in the presence of compound **11** of varying concentrations at pH 4.0 (a), 5.0 (c), 6.0 (e) and 7.0 (g). (b, d, f, h) Dose-response plots of the relative chloride efflux at 260 s *versus* the mol% concentrations of compound **11** in EYPC liposomes at pH 4.0 (b), 5.0 (d), 6.0 (f) and 7.0 (h).

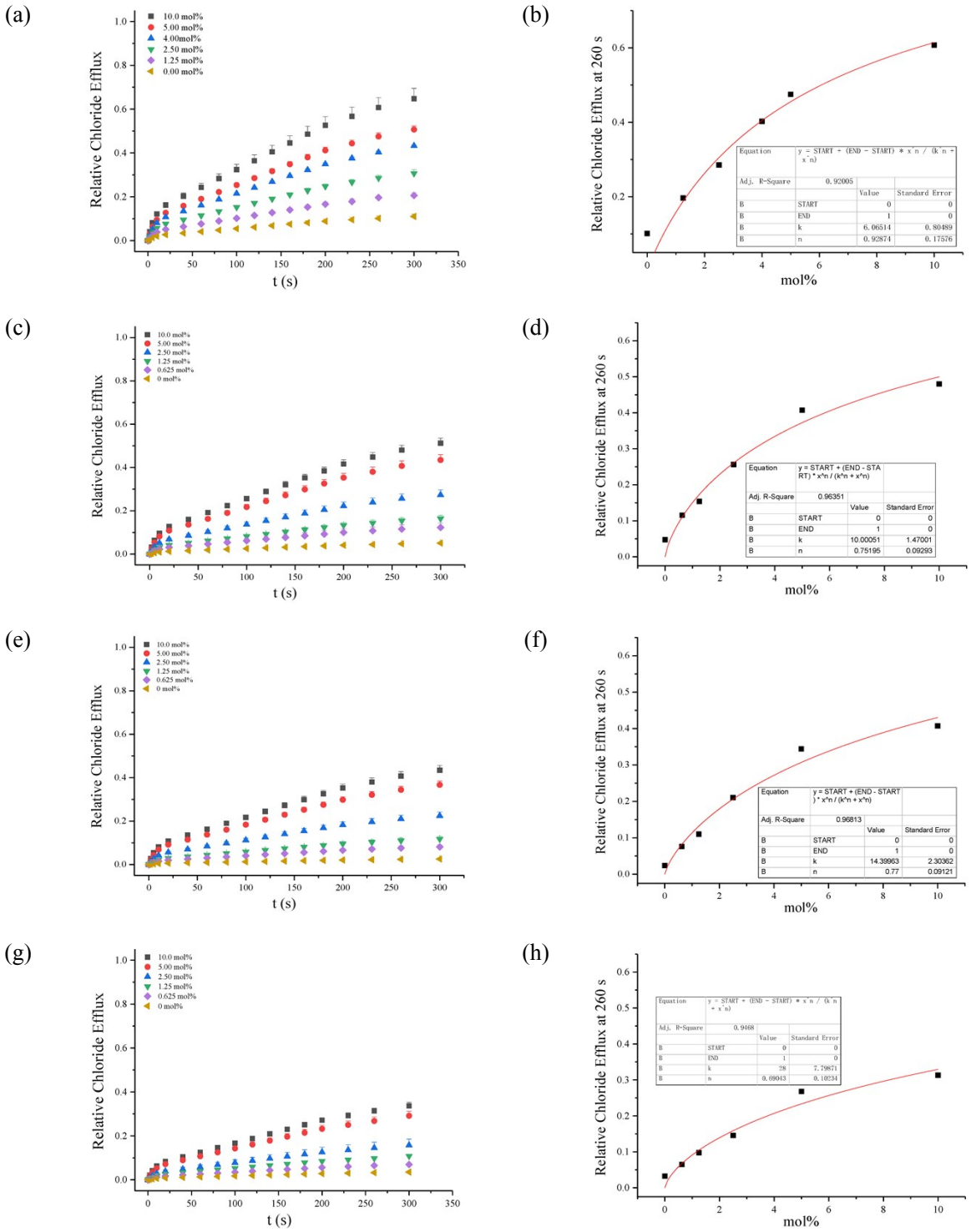

Fig. S85. (a, c, e, g) Typical plots of the chloride efflux against time in the presence of compound **12** of varying concentrations at pH 4.0 (a), 5.0 (c), 6.0 (e) and 7.0 (g). (b, d, f, h) Dose-response plots of the relative chloride efflux at 260 s *versus* the mol% concentrations of compound **12** in EYPC liposomes at pH 4.0 (b), 5.0 (d), 6.0 (f) and 7.0 (h).

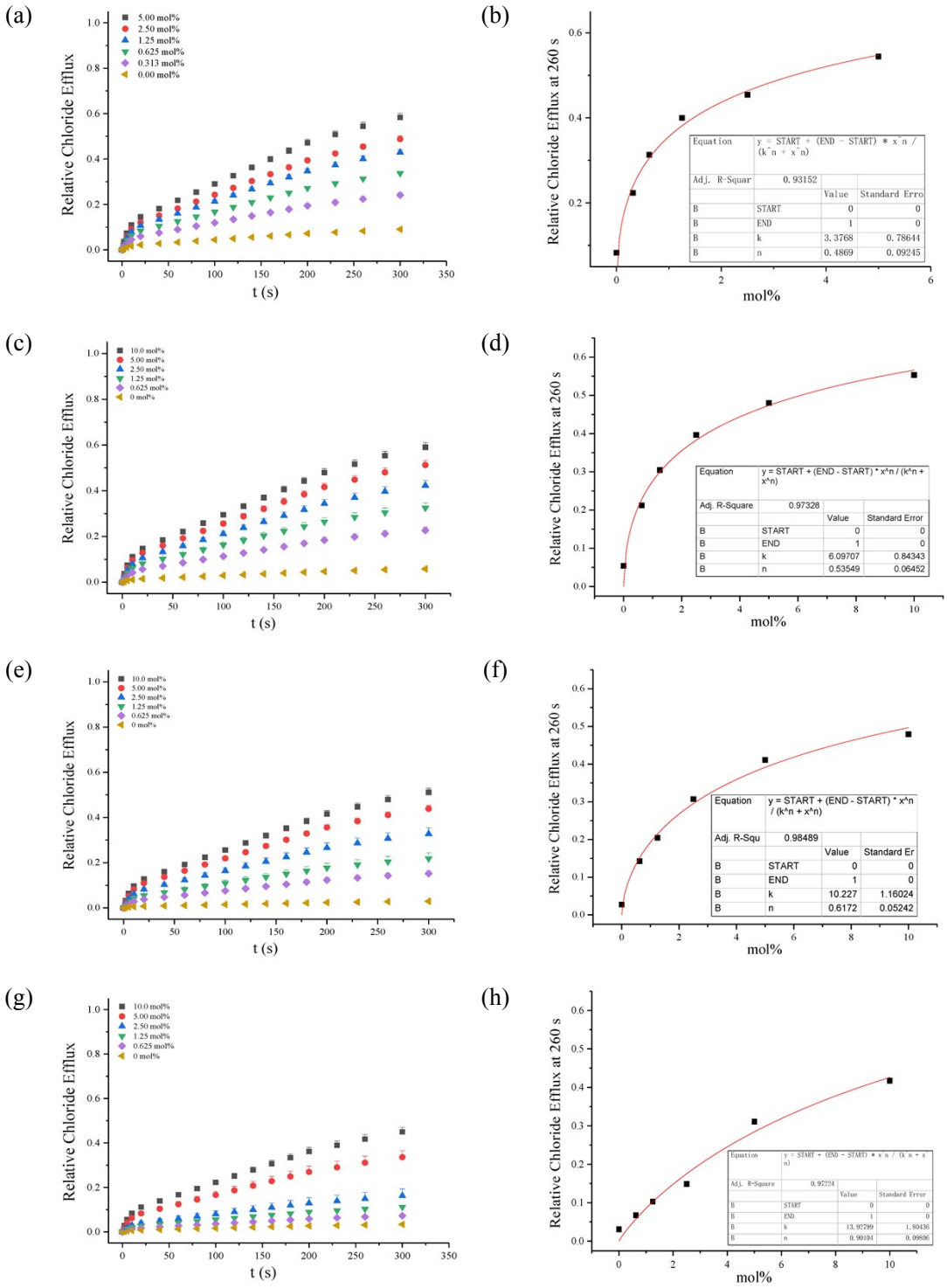

Fig. S86. (a, c, e, g) Typical plots of the chloride efflux against time in the presence of compound **13** of varying concentrations at pH 4.0 (a), 5.0 (c), 6.0 (e) and 7.0 (g). (b, d, f, h) Dose-response plots of the relative chloride efflux at 260 s *versus* the mol% concentrations of compound **13** in EYPC liposomes at pH 4.0 (b), 5.0 (d), 6.0 (f) and 7.0 (h).

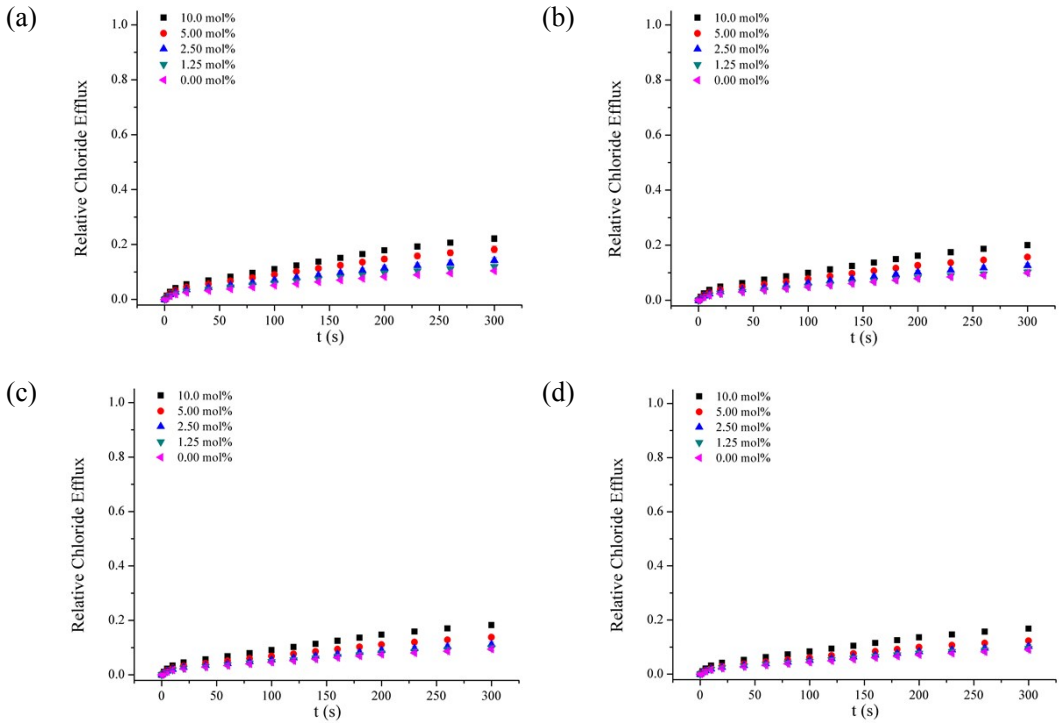

Fig. S87. Typical plots of the chloride efflux against time in the presence of compound **14** of varying concentrations at pH 4.0 (a), 5.0 (b), 6.0 (c) and 7.0 (d).

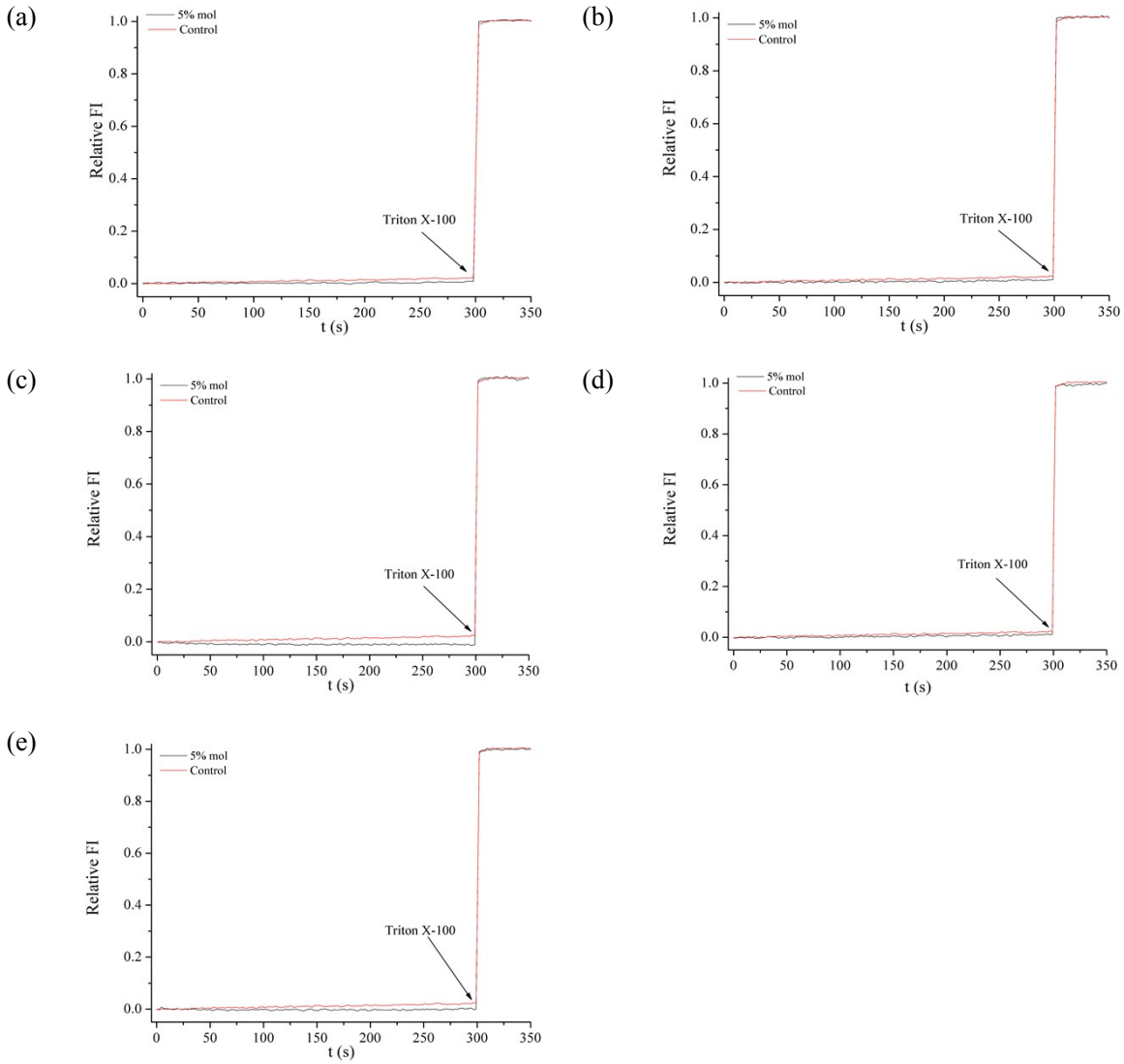

Fig. S88. The relative fluorescence intensity of calcein against time (min) enhanced by 5 mol% of compounds **1** (a), **2** (b), **3** (c), **5** (d) and **6** (e). Experimental conditions: intravesicular 25 mM HEPES, 50 mM NaCl, 100 mM calcein, pH 7.4 and extravesicular 25 mM HEPES, 50 mM NaCl, pH 7.4.

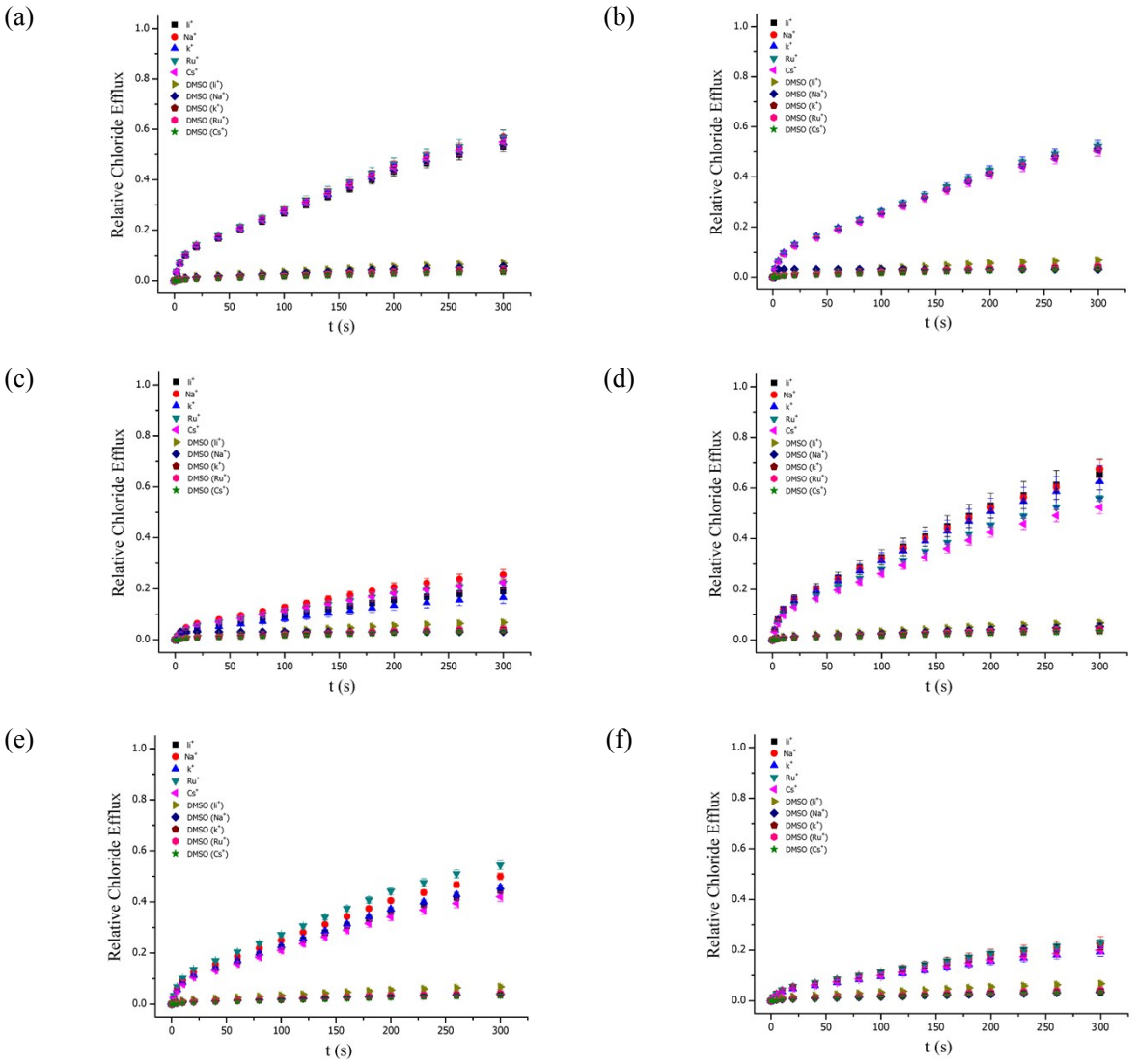

Fig. S89. The relative efflux of chloride anions over time in the presence of different cations, enhanced by 5 mol% of compounds **2** (a), **3** (b), **4** (c), **5** (d), **6** (e) and **7** (f).

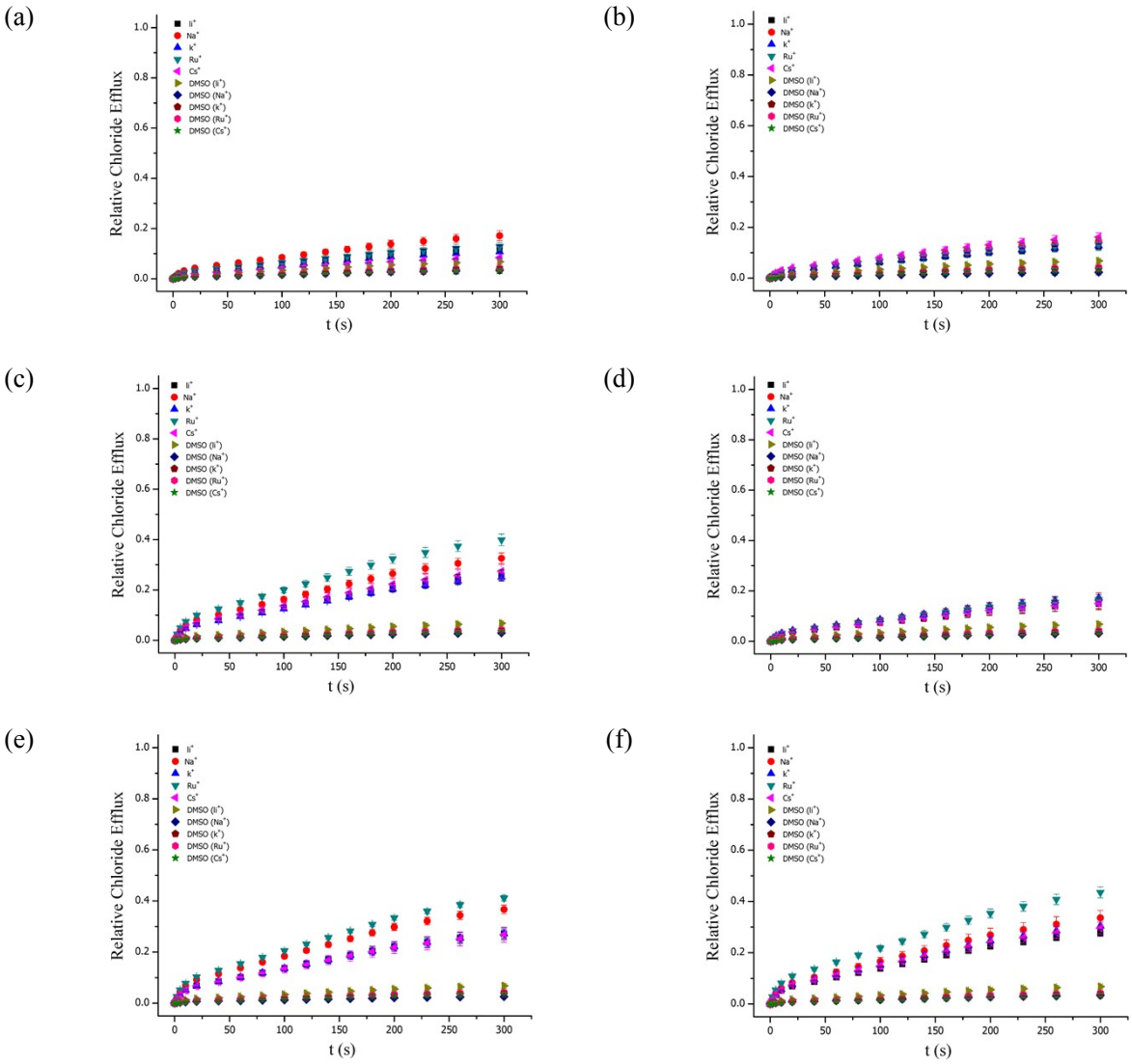

Fig. S90. The relative efflux of chloride anions over time in the presence of different cations, enhanced by 5 mol% of compounds **8** (a), **9** (b), **10** (c), **11** (d), **12** (e) and **13** (f).

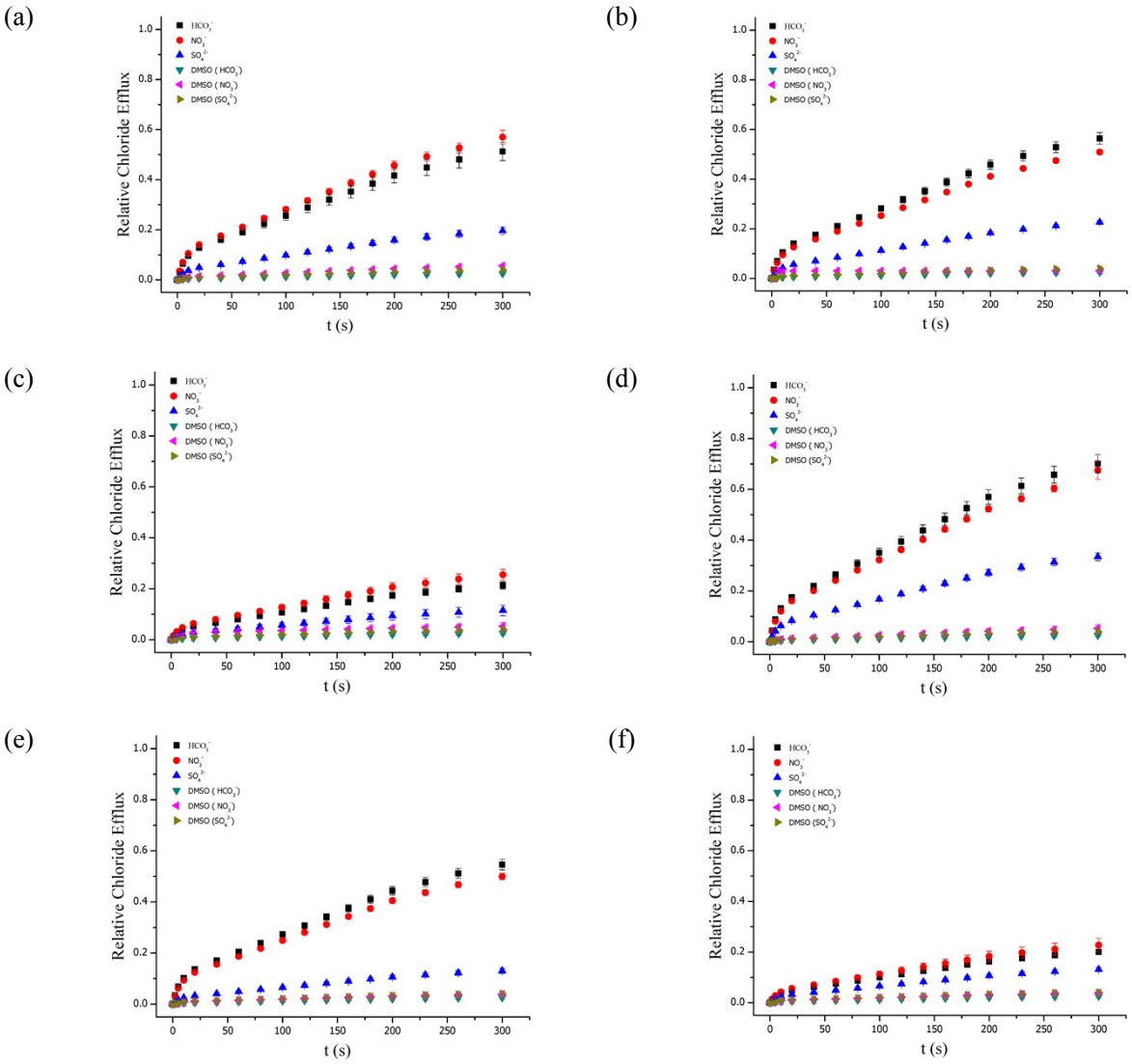

Fig. S91. The relative efflux of chloride anions over time in the presence of different anions, enhanced by 5 mol% of compounds **2** (a), **3** (b), **4** (c), **5** (d), **6** (e) and **7** (f).

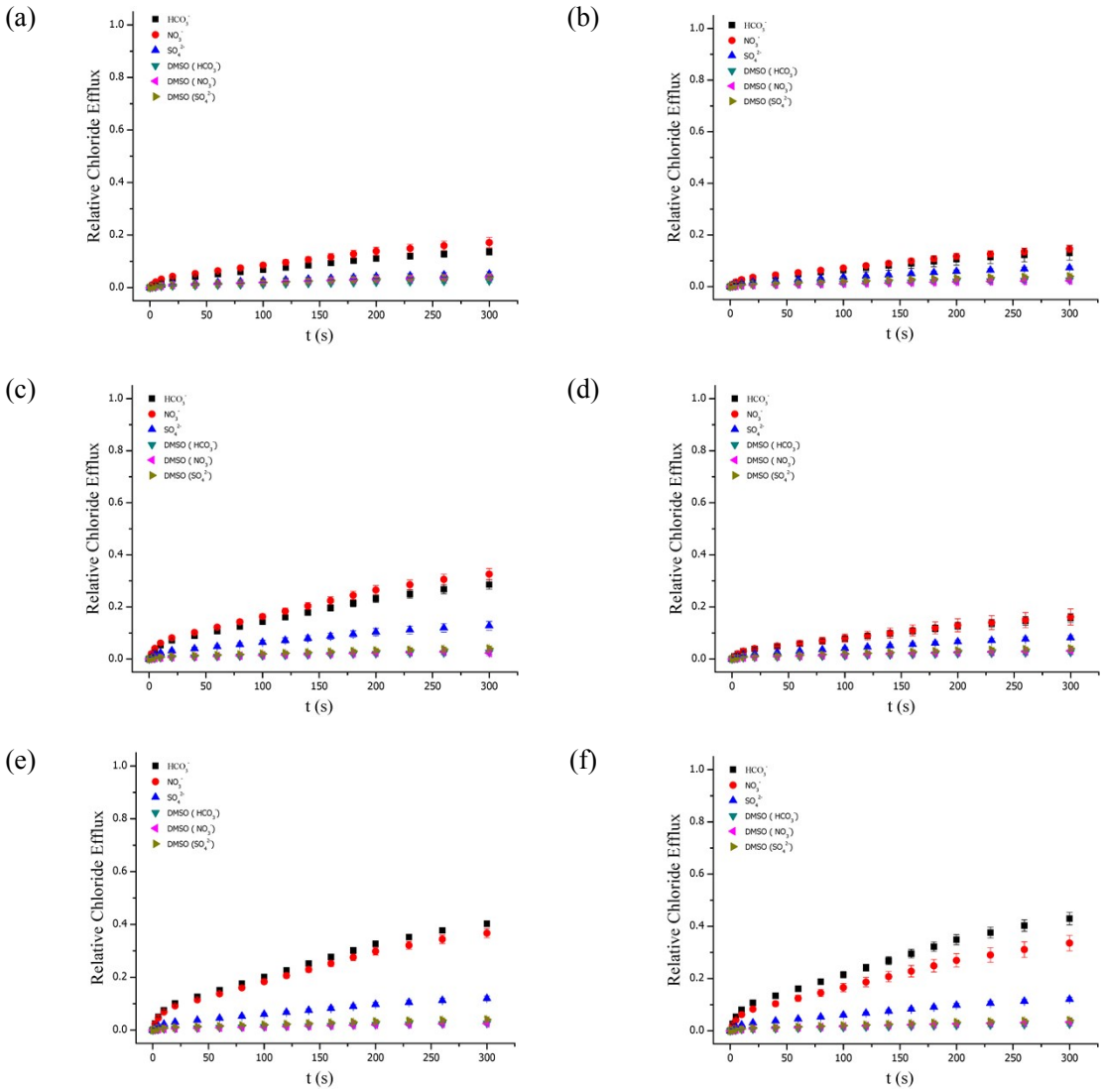

Fig. S92. The relative efflux of chloride anions over time in the presence of different anions, enhanced by 5 mol% of compounds **8** (a), **9** (b), **10** (c), **11** (d), **12** (e) and **13** (f).

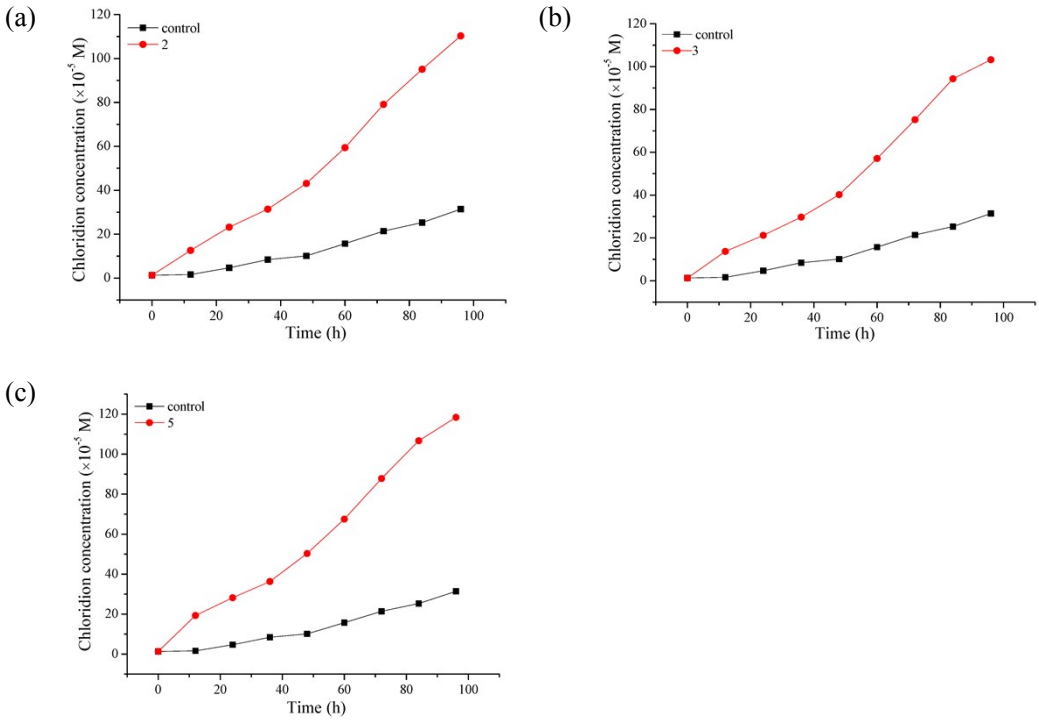

Fig. S93. Chloride transport across a bulky nitrobenzene membrane, promoted by 1.0 mM of compounds **2** (a), **3** (b), **5** (c) and detected by a chloride ion selective electrode in the receiving aqueous phase of U-tube, under the conditions of 500 mM $NaNO_3$ (25 mM HEPES, pH 7.0) for the U-tube chloride receiver, 500 mM NaCl (25 mM HEPES, pH 7.0) for the U-tube chloride donor and 2 mM $TBAPF_6$ in the nitrobenzene organic phase.

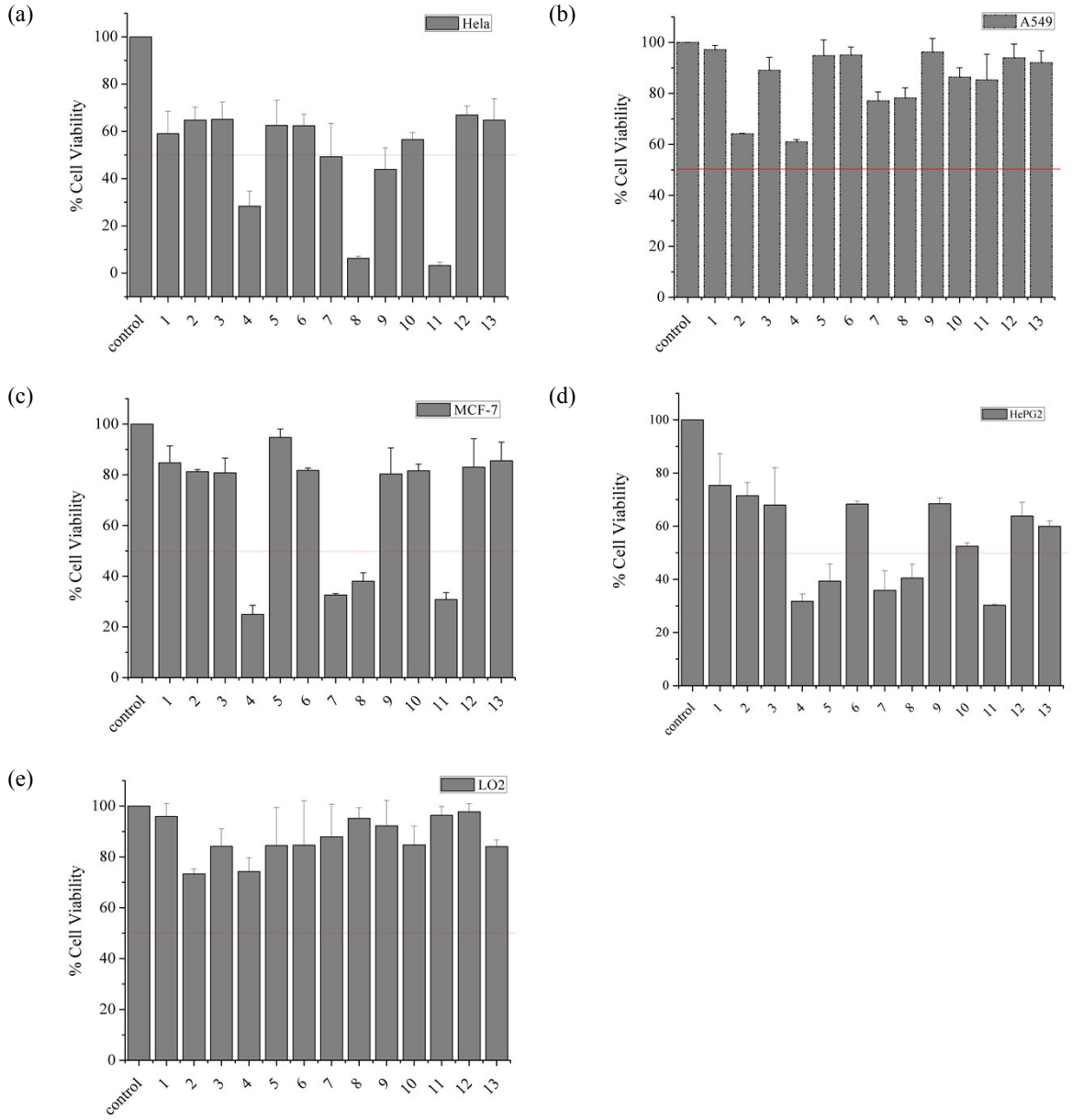

Fig. S94. Cell viability of compounds **1-13** (50 μM) toward (a) HeLa, (b) A549, (c) MCF-7, (d) HepG2 and (e) LO2 cell lines for 48 h.

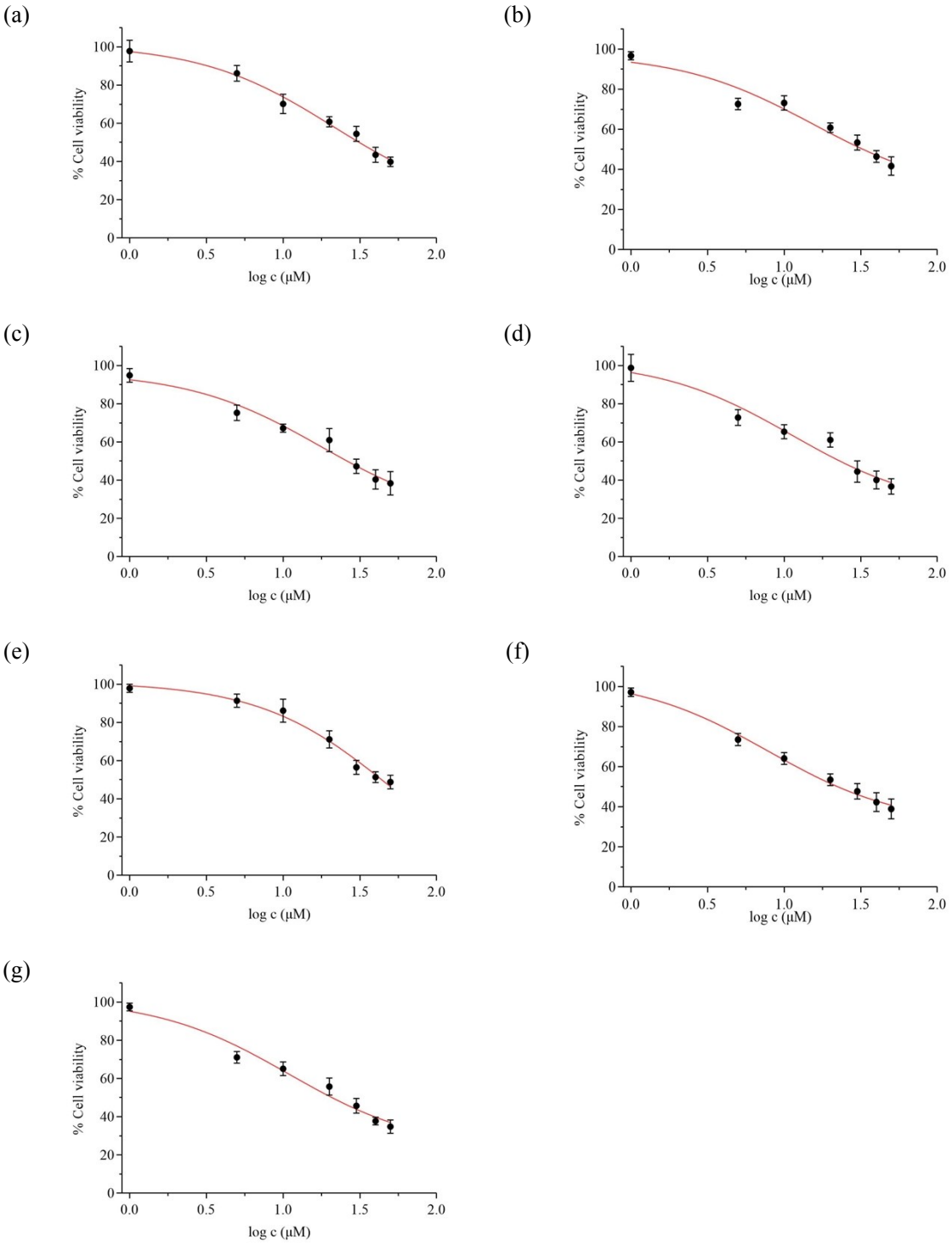

Fig. S95. Typical dose-cell viability curves for (a, e) HeLa, (b, f) MCF-7 and (c, d, g) HepG2 cells treated with varying doses of compounds **4** (a, b, c), **5** (d) and **7** (e, f, g).

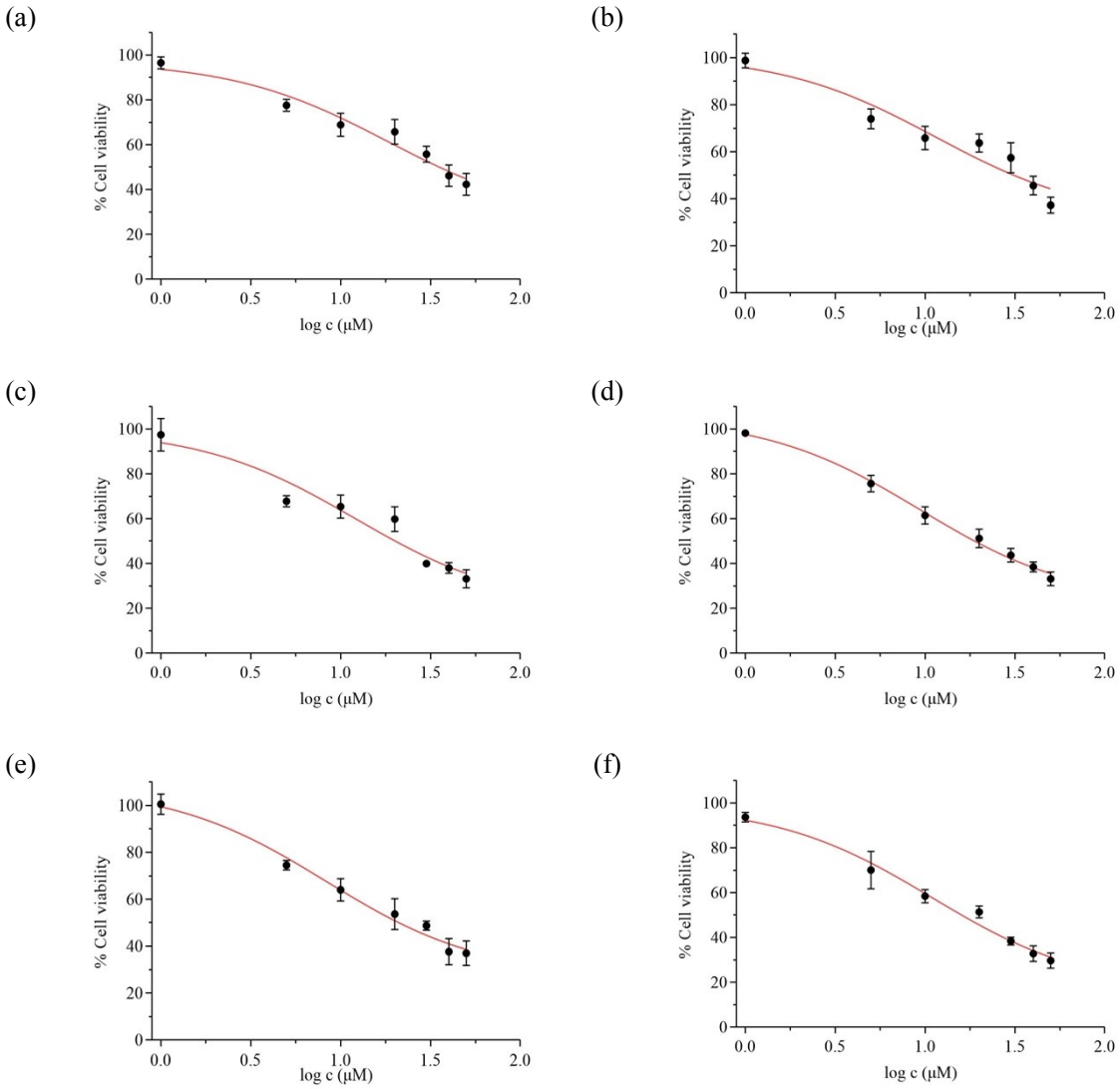

Fig. S96. Typical dose-cell viability curves for (a, d) HeLa, (b, e) MCF-7 and (c, f) HepG2 cells treated with varying doses of compounds **8** (a, b, c) and **11** (d, e, f).